EXAMINATION OF THE DECOMPOSITION PATHWAYS OF THE COMPLEX BOROHYDRIDES AND THE IMPLICATIONS FOR HYDROGEN STORAGE

A DISSERTATION SUBMITTED TO THE GRADUATE DIVISON OF THE UNIVERSITY OF HAWAI`I AT MĀNOA IN PARTIAL FULFILLMENT OF THE REQUIREMENTS FOR THE DEGREE OF

DOCTOR OF PHILOSOPHY

IN

CHEMISTRY

MAY 2013

By

Marina Chong

Dissertation Committee:

Craig Jensen, Chairperson
Marcus Tius
Thomas Hemscheidt
Philip Williams
Tom Apple

ProQuest LLC.
789 East Eisenhower Parkway
P.O. Box 1346
Ann Arbor, MI 48106 - 1346

ACKNOWLEDGEMENTS

I would like to thank all contributors to my dissertation work including Dr. T. Autry of PNNL for collaborative work on the $Mg(BH_4)_2$ dehydrogenation studies, Dr. S. Orimo and members of his research group at Tohoku University for allowing me the opportunity to collect DSC data at his (wonderfully pristine and well-maintained) laboratory, Dr. E. Callini at EMPA for providing the *in situ* TG-IR data, and Junzhi Yang for the collaborative studies on the $Mg(BH_4)_2$/LiH composite. Additional thanks goes to Dr. T. Humphries, Keelie Humphries, Dr. D. Brayton, and Paul Beaumont for the editing assistance. I would also like to acknowledge Dr. W. Niemczura and Wes Yoshida for all their invaluable help with the NMR analyses. Finally, I need to thank my parents who have supported me no matter what choices I have made and I especially must thank them for taking care of Wallace who, I admit, is not the easiest dog to foster.

ABSTRACT

The impending problems associated with the continued use of petroleum as a primary energy source has motivated efforts to find renewable alternatives. Hydrogen is an especially attractive possibility as its role as an electron donor in polymer electrolyte fuel cells only releases water as a byproduct. The development of a practical method to store hydrogen on board mobile vehicles is a huge challenge and many techniques have been considered. Solid state storage by chemisorption is an ideal way to minimize the volume and weight of the storage container but the viability of such a method is dependent on finding a material that has a suitable gravimetric hydrogen density. The complex hydrides have emerged at the forefront due to their high hydrogen content and the borohydrides in particular are considered to have great potential for cycling hydrogen. Intense research efforts over recent years have assisted in elucidating the thermodynamic and kinetic controls on the dehydrogenation pathways of the borohydrides. Within this class of complex hydrides, magnesium borohydride ($Mg(BH_4)_2$) may have the appropriate characteristics to reversibly store hydrogen. The studies presented in this dissertation were aimed at understanding the mechanism behind the solid state decomposition of $Mg(BH_4)_2$ and evaluating the potential for hydrogen storage under moderate reaction conditions. Similar experiments were conducted for bimetallic borohydrides consisting of a Group I metal and a volatile transition metal. These complexes show interesting modifications to their thermodynamic properties arising from the incorporation of two metal cations with different stabilities. Nuclear magnetic resonance (NMR) spectroscopy was the primary characterization tool for these

experiments in combination with other spectroscopic, diffraction, and calorimetric techniques.

TABLE OF CONTENTS

LIST OF TABLES

LIST OF FIGURES

CHAPTER 1 INTRODUCTION

1.1 *The Energy Issue from Economical and Environmental Viewpoints*

One of the most notable achievements in the history of human civilization is the extraction of energy from inanimate materials. This accomplishment has allowed us to continue developing new technologies and pursue new frontiers in all areas of research. Our dependency on having energy sources readily at hand, however, has reached a critical point where the continuation of this luxury is uncertain. From the time that coal became our primary energy carrier, fuel consumption has steadily increased from $5x10^{12}$ kWh/year in 1860 to $1.2x10^{14}$ kWh/year as of 2004.[1] This growth is heading towards potential disaster as it seems inevitable that energy production will eventually be unable to meet global energy demands.

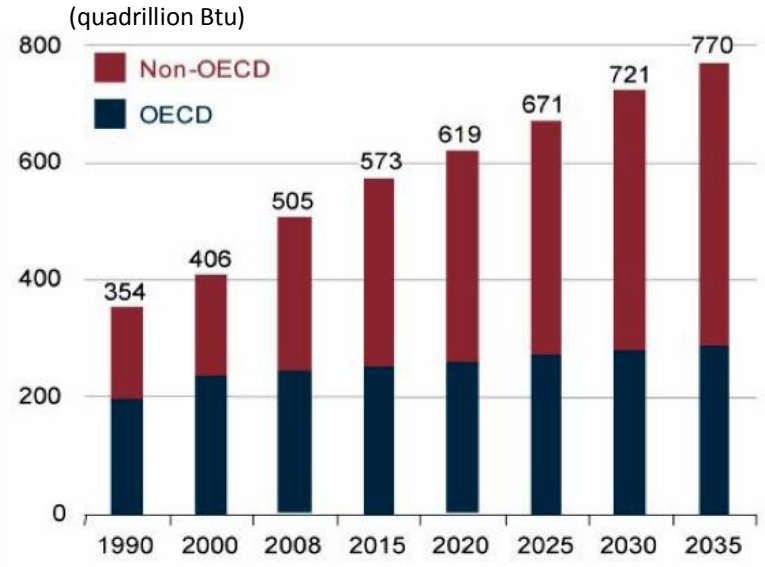

Fig. 1.1 World energy consumption, 1990-2035.[2] OECD = Organization for Economic Cooperation and Development

Data for world energy consumption in Btu from 1990 and projected to 2035 is given in Fig. 1.1.[2] The escalating demands for energy production arises from both population growth and the continued industrialization of formerly underdeveloped countries. In fact, while the number of human beings on the planet has increased six-fold, energy consumption has disproportionately increased by a factor of 80.[3] Considering that the energy is primarily obtained through the burning of fossil fuels, this rate of consumption cannot be sustained, particularly when the energy source is finite.

In addition to the concern over how long the fossil fuel supply can be expected to last, there is a growing movement to reduce our dependency on petroleum in order to control how much CO_2 is being released into the atmosphere. Burning fossil fuels produces carbon dioxide, contributing to an increase in the atmosphere of approximately $3x10^{12}$ kg C/year.[4] Since the middle of the 20th century, CO_2 emissions, as depicted in Fig. 1.2[5] (left), have consistently risen as a direct result of fossil fuel usage. The role of CO_2 as a greenhouse gas has also led to increasing global average temperatures (Fig. 1.2, right) which may result in dire environmental consequences.

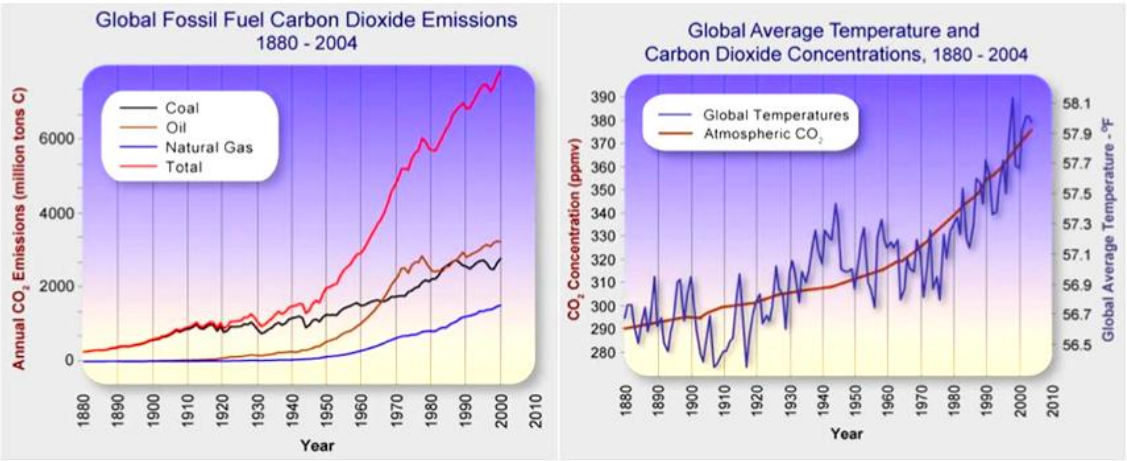

Fig. 1.2 Global CO_2 emissions and average temperature from 1880-2004.[5]

One potentially devastating impact of anthropogenic CO_2 is a disruption of the carbon content in the earth's natural reservoirs. A huge portion (about 98%)[1] of the total CO_2 on earth is found dissolved in ocean waters. Increasing the amount of CO_2 in seawater has the effect of lowering the pH through formation of carbonic acid, which is detrimental to marine life. The concomitant higher global temperature has the added effect of lowering the solubility of carbon dioxide thus reducing the ability of the oceans to act as a CO_2 buffer by absorbing it from the atmosphere. As a result, more CO_2 would be shifted to the atmosphere, intensifying its global warming effects.

There is no simple answer to this problem that has become a widespread source of concern. The need for alternatives to fossil fuels is inevitable, regardless of the debate over how much longer reservoirs can last. In the search for a permanent substitute for petroleum, there are many issues to take into consideration. The replacement must have minimal anthropogenic impact with regards to the release of greenhouse/harmful gases or materials, be a cheap and easily accessible source of energy in order to be attractive to the general public, and be in unlimited supply.

1.2 *Alternatives to Fossil Fuels*

There are several potential alternatives to petroleum that utilize natural resources. Wind, wave, hydro, geothermal and solar power are all renewable energy sources that do not produce any harmful emissions but tend to be geographically limited and thus a means of energy transport must be taken into account. As well, these methods have yet to provide the same energy output as the burning of fossil fuels. Furthermore, these

alternatives are not yet capable of mobilizing vehicles, being only suitable for stationary applications.

Biofuels have received interest in recent years, often relying on agriculturally derived residues such as bio-oil, bio-char, and bio-gas.[6] This may also provide a use for byproducts traditionally viewed as waste such as straw, plant stalks, seeds, fruit and nut shells.[7] When these materials are treated by either anaerobic digesters or undergo pyrolysis, methane or oil is produced. Both products have potential as widely applicable energy sources but CO_2 is still released upon their combustion. Theoretically, biomass consumption should result in a net CO_2 emission of zero since the carbon contained in the biomaterial originated from the atmosphere.[8] The displacement of carbon from a reduced form in vegetation to CO_2 in the atmosphere, however, would occur at a much faster rate than by natural processes. It is difficult to predict what the consequences of such a disruption in the distribution of carbon amongst the Earth's reservoirs may be. It has yet to be determined, as well, if the energy density of such materials can match that of gasoline.

Over time, our primary fuel sources have transitioned from coal (C) to oil (CH_2) to natural gas (CH_4).[1] This shift to higher hydrogen content suggests that hydrogen has a desirable effect on the efficiency of a fuel. Increasing the hydrogen content of a fuel corresponds to lower CO_2 emissions[9] and clearly, hydrogen on its own will not contribute to CO_2 release at all. The potential for hydrogen to provide energy was suggested decades ago[10] and it has now become a serious candidate to replace petroleum based fuels, particulary for mobile applications.

If hydrogen is substituted for petroleum in an internal combustion engine, its capacity to transform mechanical energy to chemical energy is slightly higher than that of petroleum.[11] Alternatively, when acting as an electron source at the anodic half of a polymer electrode membrane fuel cell, its efficiency can double or triple that of combustion.[11] The chemical energy of hydrogen is 143 MJ kg^{-1}, significantly larger than any other known chemical fuel.[11] The successful launch of the Space Shuttle was an effective demonstration of the high energy density as well as the weight advantage of hydrogen over conventional fuels.

Hydrogen has an abundance of 1400 ppm on Earth including oceans and atmosphere.[12] Based on these numbers alone, there is theoretically plenty of hydrogen to provide energy on a global scale. Hydrogen is highly reactive, however, and consequently is not found naturally in its elemental state.[13] Instead, it is largely present on Earth in the form of water, as well as bound to carbon in hydrocarbons such as coal and petroleum, biological materials such as carbohydrates and proteins, and in minerals. As a result, hydrogen is not a primary energy source and its production from water or hydrocarbons must first be achieved before it can act as an energy carrier.

The predominant method of hydrogen extraction is through the steam reformation of natural gas (48% of global hydrogen production as of 2007).[8] This process would have to become less energy-intensive than petroleum refinement in order for the conversion to hydrogen to be economically viable. From an environmental perspective, dependency on a nonrenewable hydrogen source whose processing produces carbon dioxide is less than ideal. Likewise, manufacturing hydrogen from oil and coal (the most popular sources of hydrogen after natural gas)[8] poses similar issues. In contrast,

electrolysis of water produces very pure hydrogen with only oxygen as a byproduct. In addition, this method of production would make use of the most abundant source of hydrogen available. Currently, however, the electricity required to enable electrolysis is typically generated from fossil fuels which offsets the goal of reducing dependency on hydrocarbon energy sources. Efforts are now underway to increase the efficiency and lower the cost of electrolysis by way of solar photovoltaics.

The development of a low-cost and environmentally friendly method of hydrogen production is merely one item on a list of criteria to be met. Another major issue is the storage of hydrogen onboard vehicles in an analogous manner to conventional gasoline. In recent years, the endeavors to make a hydrogen-fueled future a reality have been further motivated by the U.S. Department of Energy's (DOE) hydrogen storage system targets (Table 1.1).[14] Technical targets for 2010 included a gravimetric capacity of 1.5 kWh/kg and a volumetric capacity of 0.9 kWh/L. Unfortunately, these goals could not be met and the new targets for 2015 are even more demanding.

1.3 *Hydrogen Storage*

Storing hydrogen onboard a vehicle as a gas is great technical challenge. The amount of hydrogen required to power a fuel cell-equipped car for a distance of 400 km would occupy a volume of 45 m^3 at STP.[11] Compression reduces the volume but introduces additional problems such as suitable hydrogen-inert materials for the tank and additional pressure control in order to maintain a tank overpressure. Safety concerns with regards to high pressure hydrogen tanks onboard passenger vehicles makes compression an unattractive storage method.

Table 1.1 *U.S. DOE Onboard Hydrogen Storage Targets*[14]

Storage Parameter	Units	2010	2015	Ultimate
System Gravimetric Capacity: Usable, specific-energy from H_2 (net useful energy/max system mass)	kWh/kg (kg H_2/kg system)	1.5 (0.045)	1.8 (0.055)	2.5 (0.075)
System Volumetric Capacity: Usable energy density from H_2 (net useful energy/max system volume)	kWh/L (kg H_2/L system)	0.9 (0.028)	1.3 (0.040)	2.3 (0.070)
Fuel Cost	$/gge at pump	3 – 7	2 – 6	2 – 3
Durability/Operability:				
Operating ambient temperature	° C	–30/50 (sun)	–40/60 (sun)	–40/60 (sun)
Min/max delivery temperature	° C	–40/85	–40/85	–40/85
Operational cycle life (1/4 tank to full)	Cycles	1000	1500	1500
Min delivery pressure from storage system; FC= fuel cell, ICE= internal combustion engine	bar	5 FC 35 ICE	5 FC 35 ICE	5 FC 35 ICE
Max delivery pressure from storage system	bar	12	12	12
Charging/discharging Rates:				
System fill time (for 5 kg H_2)	min (kg H_2/min)	4.2 (1.2)	3.3 (1.5)	2.5 (2.0)
Environmental Health & Safety	–			
Permeation & leakage	Scc/h	Meets or exceeds applicable standards		
Toxicity	–			
Safety	–			
Loss of useable H_2	(g/h)/kg H_2 stored	0.1	0.05	0.05

A better way to store hydrogen is by condensation into a liquid. This requires cryogenic techniques to minimize both loss of hydrogen and overpressure from the continually evaporating hydrogen which has a critical temperature of 32 K.[11] Since heat transfer through the tank results in hydrogen loss, larger tanks minimize boil-off but tank sizes are limited by the dimensions and carrying capacities of automobiles. There have already been examples of aircraft successfully fueled by liquid hydrogen and BMW has developed several hydrogen-powered cars with tanks that exhibit minimal loss of hydrogen[11] but these models have yet to become economically viable.

Table 1.2[1] summarizes the six main methods of storing hydrogen. As discussed, the use of compressed gas and liquid hydrogen are less than ideal. While metals and complexes in water possess the highest gravimetric densities, the lack of reversibility poses a major barrier. The remaining methods each have their own benefits and flaws but have the most potential to become viable hydrogen storage materials.

Reversible storage on solid materials capable of adsorbing or chemically bonding with hydrogen is an appealing alternative to storage by compressed gas or liquid. The ideal material would be stable at ambient temperature and pressure but would release hydrogen readily when exposed to the operating temperature of the onboard system. This material must also be easily rehydrogenated in order to be a reusable and sustainable storage device.

Table 1.2 Basic hydrogen storage methods. The gravimetric density ρ_m, the volumetric density ρ_v, the working temperature T and pressure p are given.[1]

Storage Method	ρ_m (mass%)	ρ_v (kg H_2 m^{-3})	T (ºC)	P (bar)	Phenomena and remarks
High-pressure gas cylinder	13	40	RT	800	Compressed gas (molecular H_2) in lightweight composite cylinder
Liquid hydrogen in cryogenic tanks	Size dependent	70.8	-252	1	Liquid hydrogen (molecular H_2), continuous loss of a few % per day of hydrogen at RT
Adsorbed hydrogen	~2	20	-80	100	Physisorption (molecular H_2) on materials, e.g. carbon with a very large specific surface area, fully reversible
Absorbed in interstitial sites in a host metal	~2	150	RT	1	Hydrogen (atomic H) intercalation in host metals, metallic hydrides working at RT are fully reversible
Complex compounds	<18	150	>100	1	Complex compounds ($[AlH_4]^-$ or $[BH_4]^-$), desorption at elevated temperature, adsorption at high pressures
Metals and complexes together with water	<40	>150	RT	1	Chemical oxidation of metals with water and liberation of hydrogen, not directly reversible?

Adsorption of hydrogen onto materials or intercalated within interstitial sites of metal hosts such as zeolites or metal-organic frameworks (MOFs) has been studied intensely in recent years. Only very low gravimetric densities have been achieved so far, with the only reported storage of 14 to 20 mass% on K and Li-doped multi-walled carbon

nanotubes[15] being later attributed to oxidation of the metals rather than hydrogen uptake.[16] As well, physisorption usually requires temperatures of about 77 K,[17] well below the typical operating temperatures of PEM fuel cells (~353-373 K).

Hydrogen storage on complex compounds relies on chemical bonding between hydrogen anions and an electron deficient atom. This category includes binary metal hydrides, ternary hydrides, AB_5 (ie. $LaNi_5$) type hydrides, and complex hydrides (ie. $LiBH_4$). The strength of hydrogen binding depends on the thermodynamic properties of the complex and the release of hydrogen, typically requires high temperatures of >500 K, in contrast to physisorption. Ideally, a compound with a ΔH^o of 27-50 kJ/mol,[17] based on the ΔS^o of gas phase hydrogen, would have the appropriate enthalpy to release hydrogen between ambient temperature and 403 K. Although a species with an inherent combination of thermodynamic properties and fast kinetics to allow for reversible dehydrogenation under mild conditions has not been found, the complex hydrides show great potential.

1.4 *Complex Hydrides for Hydrogen Storage*

Many metals form hydrides and the light metal hydrides in particular have attracted attention due to their high gravimetric storage capacities and reversible hydrogen uptake. The use of these materials, however, are hindered by issues such as thermodynamic and kinetic barriers. For example, magnesium hydride, MgH_2, has a gravimetic density of 7.6 mass % hydrogen and 90 % of this hydrogen content has been recovered upon desorption.[18] Along with the natural abundance and relatively low cost of magnesium, MgH_2 was thought to be a promising candidate for hydrogen storage. A

major drawback has been its thermodynamic requirement for temperatures well above 573 K for dehydrogenation[19] resulting from its high stability (ΔH_f = -74.5 kJ/mol).[20] While attempts to improve the kinetics of dehydrogenation by structure refinement through ball-milling[21] and alloying with transition metal catalysts[22–24] have been successful, the intrinsic high enthalpic barrier of MgH_2 prevents it application towards reversible storage.

Owing to their high hydrogen capacities, research has turned to the complex metal hydrides in recent years. The three major classes of these compounds include the alanates, the amides, and the borohydrides. Reversibility in the alanates ($[AlH_4^-]$) has been demonstrated upon doping with titanium based compounds,[25] a finding that has drastically changed the prospects of complex hydrides for hydrogen storage. These complex hydrides contain 5-11 wt % hydrogen[26–31] and dehydrogenate in the range of 473-573 K.[32] Doping with titanium lowers the kinetic barrier dramatically; in the case of $NaAlH_4$, dehydrogenation was found to occur at 423 K and rehydrogenation at 443 K.[25] In spite of its ability to cycle hydrogen, the practical application of this material is seriously hindered by its low cycling capacity of 3-4 wt % hydrogen.[32]

The amides ($[NH_2^-]$) also show a significant decrease in hydrogen storage capacity upon cycling.[33,34] Partial cation substitution of lithium amide with magnesium has been found to lower the desorption temperature from 550 K to 373 K[35] and hydrogen weight capacities for these complexes range from 2 to 9 %.[32] A major problem during the decomposition of the amides, however, is the formation of ammonia which leads to contamination of fuel cells. This issue, as well as the optimization of composition ratios

and particle size must be resolved before the amides can be considered likely candidates for hydrogen storage.

The final class of complex hydrides is comprised of the borohydrides ($[BH_4^-]$). The first published synthesis of a pure alkali metal borohydride complex was lithium borohydride in 1940.[36] Since then, many alkali, alkaline, and transition metal borohydrides have been synthesized, either by a metathesis with $LiBH_4$ or $NaBH_4$, or through a direct route. The research outlined in this dissertation has focused exclusively on the borohydride complexes and specifically on $Mg(BH_4)_2$ and several bimetallic borohydrides.

1.5 *Borohydrides*

In order to achieve maximum hydrogen capacity, research on the borohydrides has been directed primarily towards the light members of the Group I and II metal complexes. While the bonding within the tetrahedral BH_4^- is covalent, the bonding between the metal and the complex is ionic, resulting in thermodynamically stable compounds. Detailed studies on hydrogen release in borohydrides commenced with $LiBH_4$, a result of its high gravimetric hydrogen density (18.5 wt %) and its well-established synthesis decades ago.[36] Early dehydrogenation trials found that 80 % of the hydrogen content in $LiBH_4$ was released at a minimum temperature of 653 K.[37] A few years later, the decomposition pathway of the alkali metal borohydrides was proposed to follow two possible paths:[38]

$$MBH_4 \rightarrow M+B+2H_2 \quad \text{or} \quad MBH_4 \rightarrow MH+B+3/2H_2 \qquad (1.1)$$

More recently, $LiBH_4$ was observed to release hydrogen over multiple steps with 4.5 wt % of the hydrogen bound as LiH in the final desorbed product.[39]

Partial reversibility has been achieved through exposure of the decomposition products of $LiBH_4$ to high temperature (873 K) and pressure (35 MPa H_2).[40] The harsh conditions required to facilitate both dehydrogenation and subsequent rehydrogenation exemplifies some of the challenges associated with the complex hydrides that are due to intrinsic physical barriers. Over the last decade, several of the borohydride complexes incorporating other members of the Group I as well as Group II metals have been synthesized and studied in an effort to find a species with more appropriate thermodynamic properties.

Sodium borohydride and potassium borohydride, with hydrogen weight capacities of 10.6 and 7.4 % respectively, have both been found to require temperatures higher than 700 K[41] in order to facilitate full dehydrogenation. Of the Group II metal borohydride complexes, beryllium poses a major health hazard due to its toxicity. Magnesium, calcium, as well as aluminum borohydride (though not a member of the Group II metals) all possess attractively high hydrogen gravimetric densities of 14.8, 11.5, and 16.78 % respectively. In the case of $Ca(BH_4)_2$, temperatures above 623 K are needed to initiate hydrogen release.[42] Theoretically 9.6 wt % H_2 is reversible under 700 bar H_2 pressure and 713 K[42] but experimentally, only 9.0 wt % H_2 has been liberated after dehydrogenation at 823 K.[43]

Aluminum borohydride, $Al(BH_4)_3$, is notably different from its magnesium and calcium analogues in that it is a liquid and releases hydrogen spontaneously at room temperature.[32] Little work has been done on this complex hydride as a hydrogen storage

material in spite of its high gravimetric hydrogen density due to its instability and highly pyrophoric nature. In contrast, magnesium borohydride, $Mg(BH_4)_2$, has been the subject of intense research efforts spanning several nations, largely due to its combination of high hydrogen content and favorable thermodynamic stability.[41]

Initially, the dehydrogenation of $Mg(BH_4)_2$ was thought to exhibit a small enthalpy value of 41 kJ/mol H_2 based on the assumption that dehydrogenation led to the formation of elemental Mg.[44] Comparison with the calculated enthalpy of decomposition for $LiBH_4$ of -177.4 kJ/mol[32] led to the proposition that $Mg(BH_4)_2$ should theoretically dehydrogenate at a much lower temperature than $LiBH_4$. Experimental evidence has confirmed that the desorption temperature for $Mg(BH_4)_2$ is about 100 K lower than that for $LiBH_4$ but is still impractically high for commercial use. Consequently, investigations have been launched to explore the mechanism of the dehydrogenation pathway to better understand the thermodynamics involved as well as possible manipulation of the kinetic barriers that may impede the release of hydrogen.

1.6 *Thermal Decomposition of $Mg(BH_4)_2$*

From a thermodynamic perspective, dehydrogenation requires the release of gaseous H_2 and is driven by a positive change in entropy according to $\Delta G = \Delta H - T\Delta S$. Thus, the reaction must overcome the enthalpy term in order to achieve spontaneity. In addition, in order to facilitate a reversible reaction (i.e. ΔG slightly positive), a balance between ΔH and T is necessary where the enthalpy value must remain small in order to maintain a low T.

There have been conflicting reports for the desorption enthalpies for various borohydrides,[38,45–47] probably due to a limited understanding of the decomposition pathways of these complexes. The ΔH will vary depending on the stability of the dehydrogenated product but there is still a lack of consensus regarding the products of dehydrogenation. Studies have found that the decomposition pathway is complex and the desorption temperature ultimately dictates what species are formed.

Initially it was thought that the decomposition of $Mg(BH_4)_2$ was a two-step process that ultimately led to the formation of elemental Mg:[48]

$$Mg(BH_4)_2 \rightarrow MgH_2 + 2B + 3H_2 \quad (1.2a)$$

$$MgH_2 \rightarrow Mg + H_2 \quad (1.2b)$$

The first step occurred at 563 K and the second at greater than 590 K. It was assumed that amorphous boron was one of the products in the first step due to the inability of powder X-ray diffraction to resolve species that do not have well-defined crystal structures. Nuclear magnetic resonance spectroscopy revealed that the boron, after full dehydrogenation, was in fact in the form of MgB_2.[49] Analysis by temperature-programmed desorption (TPD) showed that the dehydrogenation of $Mg(BH_4)_2$ up to 823 K involved 4 steps, with the majority of the hydrogen released during the first two steps.

The evidence that dehydrogenation occurs through a multi-step process implies that at least one intermediate boron species must be formed before reaching the final MgB_2 product. Comparison of the weight % of H_2 released from dehydrogenated $Mg(BH_4)_2$ after rehydrogenation (543 K at 40 MPa for 48 hours) to the theoretical H_2 weight percents of possible borane candidates brought forth $MgB_{12}H_{12}$ as a possible intermediate.[46]

The condensation pathway of boron hydrides in solution ultimately terminates with the formation of dodecaborane ($B_{12}H_{12}^{2-}$).[50] The stability of this borane is exceptionally high, exhibiting unusual resistance to heat and oxidizing agents in comparison to most other boron hydrides.[51] Its resilience can be attributed to its structure; the twelve boron atoms are arranged in an icosahedral cage with the hydridic hydrogens bound to the exterior of the cage. This closed-cage, highly symmetrical configuration (I_h) allows for the delocalization of B-B bonding and consequent high stability analogous to that of benzene.[50]

The dodecaborane anion was investigated as a possible intermediate in the thermal decomposition of $LiBH_4$. Of the borane species investigated ($Li_2B_xH_x$, x =5-12) first-principles calculations predicted $Li_2B_{12}H_{12}$ to be the most stable intermediate.[52] Subsequently, $MgB_{12}H_{12}$ was also calculated to be the lowest energy intermediate in the $Mg(BH_4)_2$ system[53,54] and its formation during the dehydrogenation of $Mg(BH_4)_2$ was confirmed initially by Raman spectroscopy.[53] Its presence has also been verified by both solution state and MAS nuclear magnetic resonance spectroscopy.[55]

1.7 *Reversibility in $Mg(BH_4)_2$*

The potential of a material to be rehydrogenated back to the original borohydride will be largely dependent on what species are formed upon dehydrogenation. For example, if the borohydride simply loses H_2 and disproportionates into less stable boron species, the reformation of the borohydride may be possible under sufficient H_2 pressure and heat. It has been found, however, that certain borohydride complexes, such as the transition metal borohydrides,[56] tend to release diborane (B_2H_6) upon decomposition. In

such cases, reversibility in such cases is essentially impossible under H_2 pressure alone due to the loss of boron.

A recent study aimed at characterizing the gaseous decomposition products of $Mg(BH_4)_2$ found that the complex, after annealing to remove residual solvent, did not release B_2H_6 at a decomposition temperature of 573 K.[57] Although rehydrogenation of decomposed $Mg(BH_4)_2$ under moderate conditions has yet to be achieved, the lack of diborane emission is promising. In addition, the multi-step decomposition route raises questions about whether the potential for reversibility differs amongst the various intermediates formed.

Attempts to cycle hydrogen on $Mg(BH_4)_2$ have demonstrated how the high stability of the $B_{12}H_{12}^{2-}$ anion prevents reversibility. Magnesium borohydride was dehydrogenated at 573 K to a mixture of MgH_2 and possibly amorphous boron and then rehydrogenated at 543 K under 40 MPa H_2 for 48 hours.[46] The powder, after rehydrogenation, was found to exhibit Raman vibration modes consistent with those calculated for $B_{12}H_{12}^{2-}$, exemplifying how this species can act as a terminal borane within both the dehydrogenation and rehydrogenation mechanisms. A subsequent study demonstrated that $B_{12}H_{12}^{2-}$ is produced during the desorption of several different borohydride complexes, confirming that it has a major role in the decomposition pathway.[55] The results of these studies present convincing evidence that dodecaborane is not simply an intermediate but rather a thermodynamic sink which, once formed, prevents recombination with hydrogen to produce the borohydride unit.

These findings were initially disappointing with regards to the use of borohydrides for hydrogen storage but also had the effect of directing research towards

examining whether the formation of $B_{12}H_{12}^{2-}$ could be avoided by manipulating reaction conditions. Varying the dehydrogenation or rehydrogenation temperatures and pressure could perhaps enable the process to occur via a different reaction pathway. As well, it seemed likely that other, less stable, borane intermediates were produced during the observed multi-step dehydrogenation pathway, possibly with more favorable properties for reversibility.

Severa *et al*.[58] were able to successfully hydrogenate MgB_2 to $Mg(BH_4)_2$ under 75-90 MPa H_2 and 673 K. The $B_{12}H_{12}^{2-}$ signal observed in the ^{11}B MAS NMR spectrum of the hydrogenated material comprised less than 5% of the sample, suggesting that its formation was either avoided or the exceedingly high pressure was able to force the hydrogenation to completion. Although the pressure needed for hydrogenation is impractically high, the results of this study demonstrated that there is potential for reversibility in $Mg(BH_4)_2$ and that its dehydrogenation and rehydrogenation mechanisms deserve further elucidation.

1.8 *Thermodynamic Tuning of Borohydrides*

Attempts to lower the kinetic barriers preventing fast hydrogen cycling in the borohydrides have been partially successful in reducing the amount of time needed for dehydrogenation and subsequent rehydrogenation. The group I borohydrides, however, are not only limited by kinetics but also face thermodynamic barriers that do not allow for dehydrogenation under mild conditions. The use of additives presents a potential solution to the thermodynamic barriers that prevent low temperature decomposition. By mixing $LiBH_4$ with MgH_2, Vajo *et al*.[59] were able to reduce the enthalpy of

hydrogenation/dehydrogenation of $LiBH_4$ by 25 kJ/mol. The driving force behind the lowered stability was the formation of MgB_2, effectively stabilizing the dehydrogenated state while destabilizing $LiBH_4$, as illustrated in Fig. 1.3.[60]

This concept of thermodynamic tuning of complex borohydrides evolved after DFT calculations were applied to a large number of mixtures, helping to identify combinations that would result in species with more favorable thermodynamic properties.[61–63] Another study examining the calculated enthalpy of formation, ΔH_f, of several borohydride complexes[41] found that transition metal borohydrides decomposed at much lower temperatures than the Group I or II borohydrides.[41] This led to the proposal by Li *et al*.[64] that the high-speed mechanical milling of a transition metal chloride with $LiBH_4$

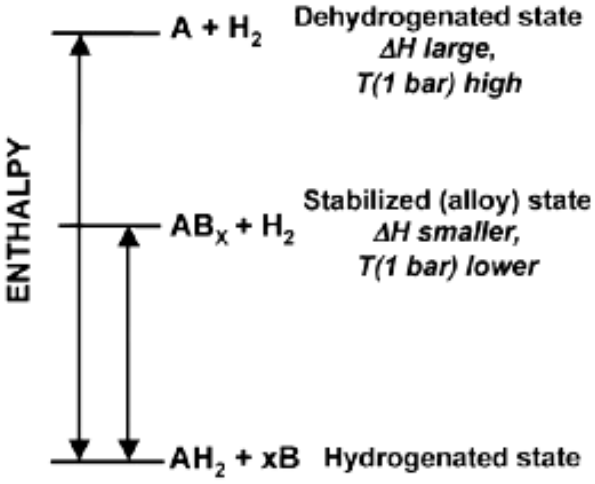

Fig. 1.3 Generalized enthalpy diagram illustrating destabilization through alloy formation upon dehydrogenation. Including the alloying additive, B, reduces the enthalpy for dehydrogenation AH_2 through the formation of AB_x and effectively destabilizes the hydride.[60]

would facilitate the synthesis of a new complex with a stability that fell between that of $LiBH_4$ and of the volatile transition metal borohydrides.

Lithium borohydride was mixed with chlorides of either Zn, Al, or Zr and X-ray diffraction analysis of all mixtures confirmed no starting material was present after ballmilling.[64] The resulting bimetallic Zn/Li and Al/Li complexes disproportionated into the corresponding transition metal borohydride and $LiBH_4$ upon thermal dehydrogenation but the Zr/Li complex was found to dehydrogenate at temperatures in between the temperatures calculated for $Zr(BH_4)_2$ and $LiBH_4$. The difference between the Zr/Li mixture and the other two transition metal mixtures was not understood but the results demonstrated that by combining certain metals with Li, the resulting complex could be dehydrogenated at a lower temperature than $LiBH_4$.

Ravnsbaek *et al*.[65] investigated a series of alkali metal/Zn borohydrides and found that all complexes decomposed at much lower temperatures than the corresponding alkali borohydride. In some cases, the complexes were too unstable for practical use: both $LiZn_2(BH_4)_5$ and $NaZn(BH_4)_5$ decomposed slowly over time at room temperature to eventually form metallic zinc. In addition, significant quantities of diborane were evolved during decomposition, suggesting that these mixtures with zinc were inappropriate for hydrogen storage. Nonetheless, the successful lowering of desorption temperatures helped to support the proposal that the thermodynamic stabilities of the borohydrides could be manipulated.

The interest in mixing alkali metal borohydrides with transition metals gained momentum with the realization that certain transition metals form anionic borohydrides.[66] These complexes were more stable than the neutral transition metal borohydrides, raising

the possibility that diborane release could be avoided. Scandium and manganese were both found to form anionic borohydrides and the potential to release H_2 under mild conditions without evolving diborane made these metals particularly interesting. These complexes are easily formed by ballmilling scandium chloride or manganese chloride with appropriate ratios of alkali metal borohydrides to produce the corresponding bimetallic borohydride.[67–70]

The scandium based complexes were all found to begin decomposing below 473 K, resulting in the formation of the analogous alkali metal borohydride as well as scandium boride and ternary bimetallic chlorides in the cases of Na and K.[67,69,71] Currently, little is known about the decomposition mechanism of these borohydride complexes. Dehydrogenation was observed to occur over multiple steps but it has not been determined whether any of those steps involve the release of diborane.

The manganese complexes were found to begin releasing hydrogen below 423 K[70] but the desorption products could not be identified due to the amorphous nature of he material and paramagnetic property of manganese. The question of diborane formation in these borohydrides is also unanswered and needs to be clarified.

1.9 *Motivation for this Dissertation*

In this body of work, the primary focus was to elucidate the dehydrogenation mechanism of magnesium borohydride, as well as bimetallic borohydride complexes, and how the desorption path affects reversibility. Chapter 2 of this dissertation presents the initial dehydrogenation trials and the boron species produced upon decomposition as characterized by NMR. Gradual lowering of the desorption temperature eventually

revealed the predominance of the $Mg(B_3H_8)_2$ intermediate species. Experiments investigating the gas phase decomposition products were performed, with a primary objective of detecting diborane. Variations in dehydrogenation kinetics due to structural phase changes in $Mg(BH_4)_2$ were also explored. In addition, the role of another decomposition intermediate, $B_{10}H_{10}^{2-}$, was examined and attempts to synthesize this polyhedral borane were undertaken.

In Chapter 3, evidence that $Mg(B_3H_8)_2$ readily regenerates $Mg(BH_4)_2$ under heat and hydrogen pressure is provided and a possible rehydrogenation mechanism is offered. In order to fully understand the mechanism and energetics involved in the rehydrogenation route, a method for the synthesis of $Mg(B_3H_8)_2$ was found and used to prepare a THF adduct of the complex. This material was hydrogenated in the presence of a metal hydride whose presence has been determined to play a key role in enabling formation of the borohydride unit. Characterization of the products was accomplished through NMR and differential scanning calorimetry (DSC). These trials provided valuable insight into the stepwise decomposition route of $Mg(BH_4)_2$ and demonstrated that reversibility was possible under moderate conditions.

The decomposition pathways of bimetallic scandium and manganese borohydrides were studied and identification of the resulting species, as determined by NMR and powder X-ray diffraction (XRD), are given in Chapter 4. Gas phase products were analyzed by an *in situ* infrared spectroscopic (IR) method and the effect of lowering desorption temperatures on the borane species produced was investigated.

CHAPTER 2 DEHYDROGENATION STUDIES OF MAGNESIUM BOROHYDRIDE

2.1 *Introduction*

Of the different complex hydrides considered to be potential hydrogen storage materials, the Group I and II borohydrides possess some of the highest hydrogen content. The requirements for an ideal hydrogen storage candidate include dehydrogenation at temperatures similar to the operating temperature of polymer electrolyte membrane (PEM) fuel cells as well as the ability to regenerate the original borohydride. Theoretically, magnesium borohydride, $Mg(BH_4)_2$, has the appropriate thermodynamics[41] and hydrogen weight capacity to meet these criteria.

Magnesium borohydride has a hydrogen weight content of 14.9%, high enough that even if it were only partially reversible under moderate conditions, ie. mild temperatures and pressure, there would be great potential for this material.[72] Early studies on the dehydrogenation properties of $Mg(BH_4)_2$ found that temperatures up to 800 K were required to release 14.4% of its mass as hydrogen.[44] By monitoring the isothermal desorption at 623 K of the complex and analyzing the products by powder X-ray diffraction, two distinct steps were identified and assigned to:

First step: $Mg(BH_4)_2 \rightarrow MgH_2 + 2B + 3H_2$ (2.1)

Second step: $MgH_2 \rightarrow Mg + H_2$ (2.2)

The final product after full dehydrogenation was later found to be MgB_2 by NMR rather than decomposition to the elements.[49] Examination of the dehydrogenation by thermogravimetry (TGA) revealed that the initial decomposition to MgH_2 (Eq. 2.1)

actually consisted of three steps,[46] suggesting that the mechanism was much more complicated than previously anticipated. NMR spectra taken at varying desorption temperatures indicated that intermediate polyborane species were formed in addition to those originally identified by X-ray diffraction (XRD).[49]

The formation of an array of boranes is known to occur during the decomposition of BH_4^- in solution.[50] In this process, diborane is formed upon dissolution. A BH_4^- unit inserts itself into diborane (B_2H_6), forming a new structure with three B atoms and releasing H_2. This process continues, with the diborane condensing into increasingly larger boranes, until dodecaborane ($B_{12}H_{12}^{2-}$), is ultimately formed.

Dodecaborane is a highly stable icosahedron with an unusual resistance to oxidation and hydrolysis relative to other polyhedral boranes. The recognition of its role in decomposition in the solution phase has led to the proposal that it is also one of the intermediates formed during dehydrogenation of $Mg(BH_4)_2$ in the solid state.[46,49,53,55] Its presence in dehydrogenated $Mg(BH_4)_2$ was confirmed conclusively by NMR in materials decomposed at temperatures $\geq$573 K.[55] Rehydrogenation trials have discovered that hydrogenation of decomposed $Mg(BH_4)_2$ is halted after the formation of $MgB_{12}H_{12}$,[46] demonstrating that its thermal stability poses a major barrier to reversibility.

An important question arising from these studies is whether the formation of $MgB_{12}H_{12}$ can be avoided and furthermore, by doing so, is reversibility within the $Mg(BH_4)_2$ system possible? MgB_2 has been directly hydrogenated to form $Mg(BH_4)_2$ under exceedingly high pressure with only trace levels of $MgB_{12}H_{12}$ detected.[58] Although it is not clear whether $MgB_{12}H_{12}$ is an intermediate in this reaction, these results confirm that full reversibility is possible and also highlights the very limited

understanding of the mechanisms involved in the dehydrogenation and rehydrogenation pathways.

Interestingly, the release of diborane has not been detected by *in situ* infrared spectroscopy (IR) beyond impurity levels during the solid phase dehydrogenation of $Mg(BH_4)_2$,[57] implying that either it immediately reacts upon formation or the mechanism of decomposition in the solid state is very different from that which occurs in solution. In light of this, the dehydrogenation of $Mg(BH_4)_2$ was investigated with an emphasis on low temperature decomposition and identification of the intermediates generated during this process.

Additionally, magnesium borohydride is understood to undergo a phase transition ($\alpha \rightarrow \beta$) when exposed to temperatures $\geq$508 K[73] and more recently, a low density cubic polymorph (γ-phase) has been synthesized.[74] The authors found that the pore volume in γ-$Mg(BH_4)_2$ accounts for 33% of its structure versus 6.4% for the α-phase. This material is capable of absorbing N_2 and dichloromethane molecules and may have potential as a nanoporous scaffold for hydrogen storage.[74] We attempted to lower dehydrogenation kinetics by examining the relationship between phase structure and decomposition temperature. The dehydrogenation of the γ polymorph was compared to that of the α-phase and its propensity towards diborane evolution was also evaluated. Finally, nanoconfinement of metal hydride additives within the porous structure of γ-$Mg(BH_4)_2$ was attempted followed by isothermal dehydrogenation experiments to determine whether nanostructuring could lower kinetic barriers.

2.2 *Experimental*

All sample preparation and handling was conducted either in an argon glovebox or manipulated on a Schlenk line under inert gas with minimal exposure to atmosphere. Glassware was routinely oven-dried and flushed with argon or nitrogen before addition of reagents. Solvents were purified by a Solvent Purification System (SPS) and dispensed directly into an argon glovebox.

2.2.1 *Synthesis of starting materials*

Preparation of α-$Mg(BH_4)_2$:

Magnesium borohydride was prepared by a modified procedure originally developed by Chlopek *et al*.[72] Magnesium hydride (Geleste, Inc., 1.48 g) was activated by mechanical milling with stainless steel ball bearings for two hours at 350 rpm and then added to borane-triethylamine complex ($BH_3 \cdot N(CH_2CH_3)_3$, Sigma Aldrich, 13.0 g). The mixture was refluxed at 373 K for one hour after which the heat was increased to 418 K and maintained for 8 hours. A dark gray slurry formed to which 40 mL of diethyl ether was added and stirred for several hours. The solution was filtered through a sintered glass crucible and the ether was removed *in vacuo*, resulting in a viscous liquid. The product was heated at 463 K *in vacuo* for two hours, yielding a fine white powder.

Preparation of γ-$Mg(BH_4)_2$:

The γ polymorph of magnesium borohydride was prepared according to a synthesis proposed by Filinchuk *et al*.[74] Dibutylmagnesium (10 mL, Sigma Aldrich, 1M solution in heptane) was slowly added dropwise to a solution of borane-dimethylsulfide

(18 mL, Acrōs Organics, 2 M in toluene) in an argon glovebox. The solution was allowed to stir for a minimum of two hours after which the mixture was filtered through a sintered glass crucible and washed with toluene. The resulting white powder, a dimethylsulfide magnesium borohydride adduct ($Mg(BH_4)_2 \cdot 1/2S(CH_3)_2$) was dried *in vacuo* at room temperature for 12-16 hours after which afforded solvent-free γ-magnesium borohydride.

Preparation of $Mg(B_3H_8)_2 \cdot x$THF:

A THF adduct of $Mg(B_3H_8)_2$ was prepared by reaction of a Mg/Hg amalgam with $BH_3 \cdot$THF complex. The synthesis of this species was essential to the rehydrogenation studies discussed in Chapter 3 and the detailed protocol will be given there.

2.2.2 *Isothermal decomposition*

Dehydrogenation experiments were carried out on a Suzuki Shokan PCT-2SDWIN Sievert type apparatus. Precise temperature control was achieved using customized heating mantle sleeves. Reactors with fixed volumes were initially evacuated prior to dehydrogenation trials.

2.2.3 *NMR characterization*

^{11}B NMR spectroscopic experiments were performed on a Varian Unity Innova 500 MHz spectrometer with ^{11}B chemical shifts referenced to $BF_3 \cdot OEt_2$ (δ =0 ppm) at 293 K. Spectra were recorded both with and without decoupling. A comparison of different solvents indicated that deuterium oxide allowed for the highest dissolution rate

and resolution of closed-cage structure boranes with species such as *nido* and *arachno*-boranes appearing as boric acid due to hydrolysis.

2.2.4 *In situ thermogravimetric (TG)/infrared (IR) analysis*

Samples were loaded into a magnetic suspension balance (Rubotherm, Bochum) and modified to allow the measurements to take place under controlled gas flow. The system was connected to an IR gas analyser (Bruker Alpha spectrometer equipped with a 8 cm gas cell at a resolution of 0.9 cm^{-1}). Dehydrogenation reactions were conducted under 150 mL/min hydrogen flow at 0.1 MPa. A detailed description of the experimental set-up can be found in a previous study.[57]

2.2.5 *Analysis of gas phase decomposition products by NMR*

The gas phase products released from dehydrogenation of mixtures of as-prepared $Mg(B_3H_8)_2$ and MgH_2 as well as $Mg(B_3H_8)_2$ and LiH were analyzed following a method described by Huang *et al*.[75] The powder was decomposed in a Schlenk flask *in vacuo* for a designated period of time, then connected to another flask containing THF with a hollow needle and cooled in dry ice/acetone. Nitrogen flow was used to push the gas in the reaction flask into the cooled THF to condense gas phase products. The THF containing dissolved gases was then analyzed by ^{11}B NMR.

2.2.6 *Diffraction experiments*

Powder X-ray diffraction data was collected on a Rigaku MiniFlex II diffractometer with Cu-Kα radiation. Hermetic beryllium sample holders were used.

2.3 *Results and Discussion*

2.3.1 *Effect of dehydrogenation temperature on polyborane speciation*

Analysis by both XRD (Fig. 2.1) and ^{11}B NMR (Fig. 2.2) confirmed the successful synthesis of α-$Mg(BH_4)$ via reaction of MgH_2 and $BH_3{\cdot}N(CH_2CH_3)_3$.

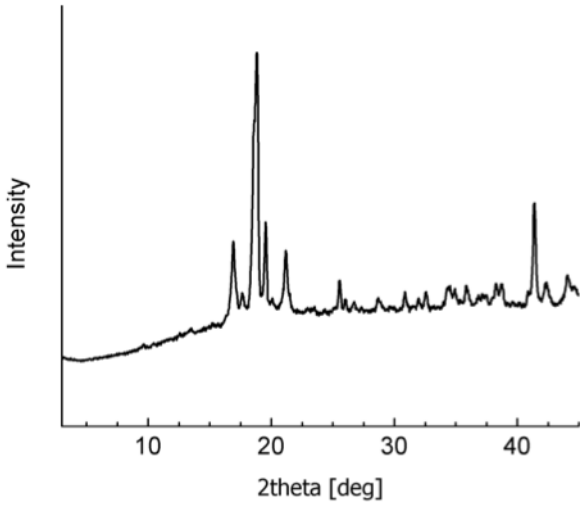

Fig. 2.1 XRD profile of α-$Mg(BH_4)_2$

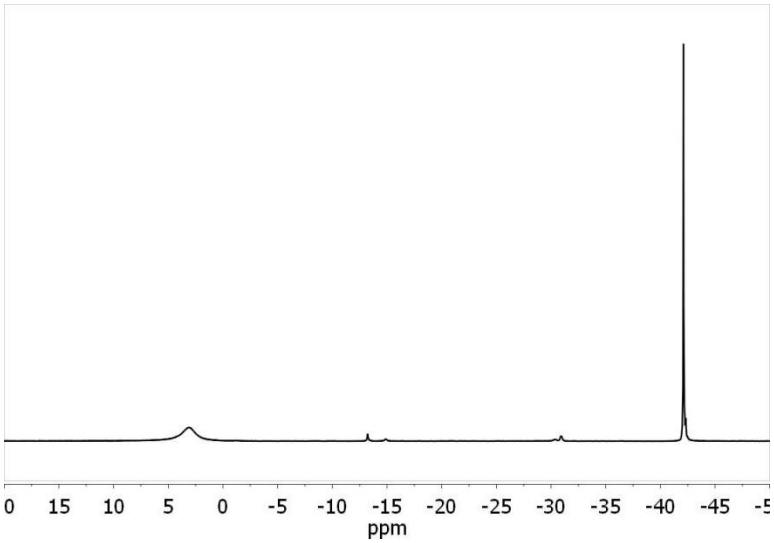

Fig. 2.2 $^{11}B\{^1H\}$ NMR of α-$Mg(BH_4)_2$.

Reflections for α- $Mg(BH_4)$ were observed between 16-50°,[72] with prominent reflections at 17.5, 18.8, 19.5, and 21.6°. Only peaks for the Be sample holder were present at greater than 50°. The profile shown in Fig. 2.1 confirmed the preparation of well-ordered crystals and agreed well with published spectra.[72]

Initial attempts to characterize $Mg(BH_4)_2$ decomposition products by ^{11}B Magic Angle Spin (MAS) NMR revealed the inability of this method to resolve species within a specific chemical shift range (between –15 to –50 ppm). ^{11}B MAS NMR tends to produce broad features which is characteristic of quadrupolar nuclei (^{11}B = spin 3/2) and prevents identification of the individual boranes in this range. As a result, solution NMR was the primary analytical tool for these studies.

Solution phase ^{11}B NMR is a more suitable characterization method not only due to the ability to resolve boron species that cannot be detected by MAS NMR or by XRD but also by providing additional structural information through proton coupling. This allows for much easier identification of specific borane species. Deuterium oxide was found to be the most appropriate solvent in which stable *closo*-boranes remain intact upon dissolution. Less stable boranes, however, such as *arachno*- and *nido*-boranes were consequently hydrolyzed and formed boric acid. Thus, resonances between 0 to 5 ppm in the ^{11}B NMR spectra can be attributed to either the formation of open-cage boranes during preparation or partial decomposition of borohydride complexes upon dissolution in deuterium oxide.

Boric acid was present in the ^{11}B NMR profile for α- $Mg(BH_4)_2$ (Fig. 2.2) at 3 ppm. The other major resonance at –42 ppm in the spectrum was consistent with the

chemical shift of tetrahydroborates. The identity of the resonance was further confirmed by the splitting of the signal into a quintet when coupled to the proton signal.

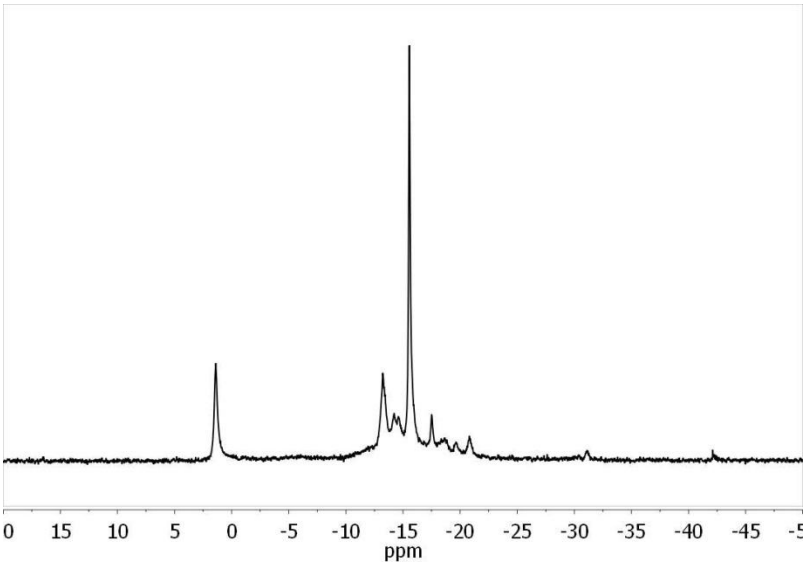

Fig. 2.3 $^{11}B\{^{1}H\}$ NMR of $Mg(BH_4)_2$ dehydrogenated 653 K, 24 h.

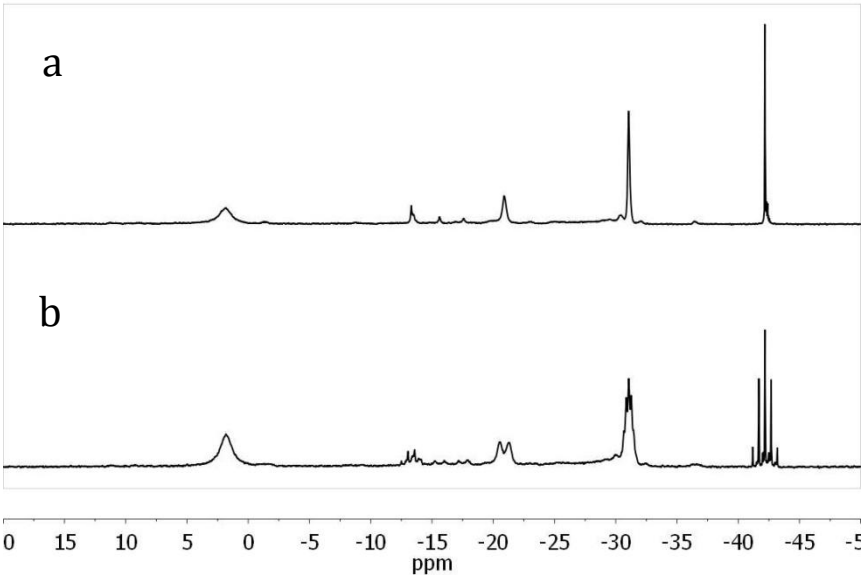

Fig. 2.4 $^{11}B\{^{1}H\}$ NMR (a) and ^{11}B NMR (b) of $Mg(BH_4)_2$ dehydrogenated at 573 K, ~ 1 h

The prepared α-$Mg(BH_4)_2$ was then dehydrogenated in the PCT at 653 K for 24 hours at 0 MPa. This temperature was chosen as a starting point for investigating potential intermediate species because full dehydrogenation of $Mg(BH_4)_2$ requires a temperature of at least 873 K. The ^{11}B NMR spectra of the decomposed product (Fig. 2.3) confirmed that $MgB_{12}H_{12}$ (–15.5 ppm) was the predominant species along with a scattering of various polyboranes between –13 to –21 ppm. Hydrolyzed species appeared again as boric acid at 1.4 ppm.

At a lower temperature of 573 K, one hour of dehydrogenation yielded distinct changes in the resulting ^{11}B NMR spectrum (Fig. 2.4) of the products in deuterium oxide. While some $Mg(BH_4)_2$ remained, the array of polyboranes observed upon decomposition at 653 K disappeared, displaying only a peak due to $Mg(B_3H_8)_2$ at –31 ppm with a shoulder at –30.5 ppm due to $MgB_{10}H_{10}$. The identity of the $Mg(B_3H_8)_2$ peak was confirmed by the proton coupled ^{11}B NMR which depicted the splitting of this signal into a nonet (Fig. 2.4 b). Minor resonances representing residual BH_3·THF at –13 ppm and an unidentified species at –22 ppm were also present. Prolonged decomposition for 4 weeks at 573 K resulted in a ^{11}B NMR spectrum (Fig. 2.5) with a major resonance for $MgB_{12}H_{12}$ (–15 ppm) and a substantial increase in the resonance at –22 ppm, resembling the results of desorption at 653 K.

The increase in $B_{12}H_{12}^{2-}$ upon prolonged heating at 573 K suggests a mechanism similar to the condensation pathway of borohydride decomposition in solution.[50] Initially dehydrogenation at this temperature appeared to strongly favor $Mg(B_3H_8)_2$, suggesting that the energy available at 573 K was insufficient to overcome the activation energy required to facilitate boron aggregation to form a large boron cage. A longer

dehydrogenation period resulted in the formation of additional $MgB_{12}H_{12}$ as well as several other polyborane species. If a condensation process does indeed occur in the solid state the kinetics are, not surprisingly, much slower in the solid state compared to reaction rates in solution.

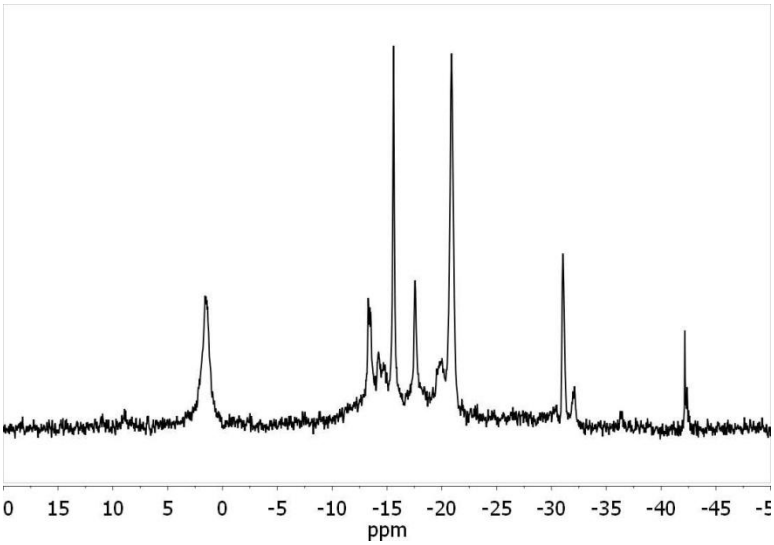

Fig. 2.5 $^{11}B\{^1H\}$ NMR of $Mg(BH_4)_2$ dehydrogenated 573 K, 4 weeks.

The results of these dehydrogenation trials at 573 K piqued our interest in $Mg(B_3H_8)_2$ as a dehydrogenation product that forms at a lower temperature than $MgB_{12}H_{12}$. Condensation of polyboranes in solution proceeds through the formation of $Mg(B_3H_8)_2$ early in the reaction pathway, hence this species must be less thermodynamically stable than $MgB_{12}H_{12}$. During solid state decomposition, $Mg(B_3H_8)_2$ tends to persist but only at temperatures ≤573 K again indicating that it is less stable than $MgB_{12}H_{12}$. The discovery of more volatile decomposition intermediates consequently drew attention to their formation as potential routes through which reversibility could be attained. In order to explore this possibility, $Mg(BH_4)_2$ was dehydrogenated at 473 K in an attempt to isolate the specific conversion of $Mg(BH_4)_2$ to $Mg(B_3H_8)_2$.

Magnesium borohydride was dehydrogenated at 473 K and sampled periodically to monitor the reaction progress by NMR. Boric acid was always observed in the ^{11}B NMR spectra of the decomposed products. The increase in the proportion of $B_3H_8^-$ relative to boric acid and $Mg(BH_4)_2$ with time is illustrated in Fig. 2.6 and the percent compositions, as determined by peak area integration normalized to a 87 mM aminoborane (NH_2BH_2) internal standard, of the boron species formed upon dehydrogenation, are given in Table 2.1. Magnesium triborane is clearly the preferred product at 473 K, increasing to 40 % of the total boron content by six weeks of dehydrogenation. Extending the decomposition time to eight weeks did not effect much change in the composition, suggesting that the formation of $Mg(B_3H_8)_2$ plateaus after six weeks.

The amount of boric acid also varied greatly, starting at 62 % in the original sample prior to dehydrogenation. Although the change in boric acid did not follow a linear trend, in general its composition decreased with time. Within a week of dehydrogenation, the boric acid only increased slightly while the $Mg(BH_4)_2$ decreased from 33 % to 9 %. The increase in $Mg(B_3H_8)_2$ was the most dramatic during this initial period, indicating that the decrease in $Mg(BH_4)_2$ must be directly correlated to the formation of $Mg(B_3H_8)_2$. Interestingly, the proportion of the boron bound as $Mg(BH_4)_2$ increased with longer dehydrogenation periods, corresponding to a decrease in boric acid. The open cage higher boranes (*nido* and *arachno*) must decompose over time, possibly reacting with the H_2 released during the decomposition of $Mg(BH_4)_2$ to $Mg(B_3H_8)_2$ to form more BH_4^-.

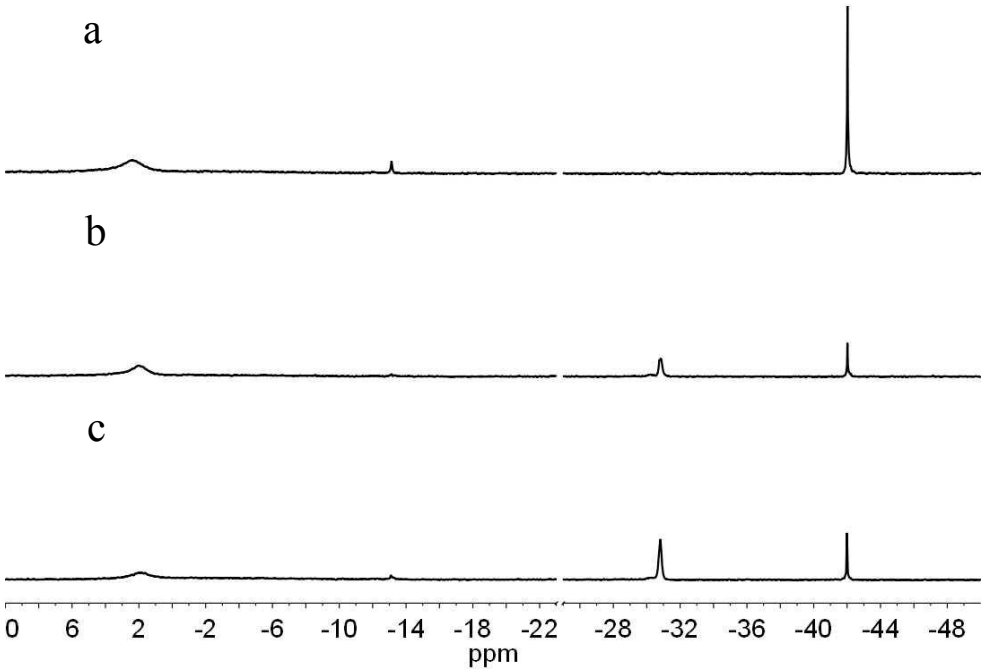

Fig. 2.6 $^{11}B\{^{1}H\}$ NMR of (a) $Mg(BH_4)_2$; (b) dehydrogenated at 473 K for 1 week; (c) after dehydrogeantion for 5 weeks. Peaks have been normalized to an aminoborane standard which has been removed (-24 ppm) for clarity.

Table 2.1 Percent composition of dehydrogenated $Mg(BH_4)_2$ at 473 K

Dehydrogenation time	**Boric acid**	**$B_3H_8^-$**	**BH_4^-**
0 week	62		33
1 week	69	17	9
3 weeks	60	26	8
5 weeks	48	33	11
6 weeks	34	40	17

The dehydrogenation trials discussed above were performed under static vacuum (0 MPa) which assisted in driving the reaction forward (ie. H_2 loss). The sample mass relative to reservoir volume was always small enough to prevent significant back pressure due to the H_2 evolved during dehydrogenation. Nonetheless, any potential effect of back pressure was tested by repeating the dehydrogenation at 573 K under 0.1 MPa H_2 for approximately one hour and the resulting ^{11}B NMR spectrum is given in Fig. 2.7. A comparison of the products suggests that the H_2 back pressure does not have any significant effect on the dehydrogenation route at this temperature. Again, trace amounts of boron species at -13 and -22 ppm were present in Fig. 2.7 indicating that the main product was $Mg(B_3H_8)_2$.

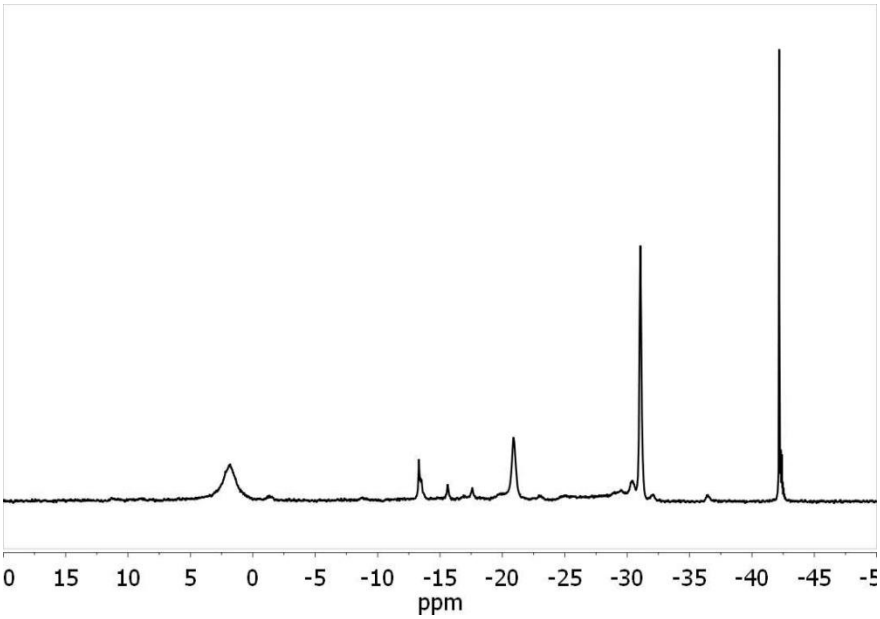

Fig. 2.7 $^{11}B\{^1H\}$ NMR of $Mg(BH_4)_2$ dehydrogenated at 573 K, ~ 1h, with 0.1 MPa H_2 back pressure.

The $B_3H_8^-$ ion possesses a cyclic structure (Fig. 2.8) that is analogous to cyclopropane but with two bridging hydrides incorporated into the ring. This is the only

stable borane consisting of three B atoms and its formation during BH_4^- decomposition in solution has been experimentally confirmed.[50] Similar to the condensation mechanism in aqueous solution, our results indicate that $B_3H_8^-$ is an early intermediate and hence must be less stable than $B_{12}H_{12}^{2-}$.

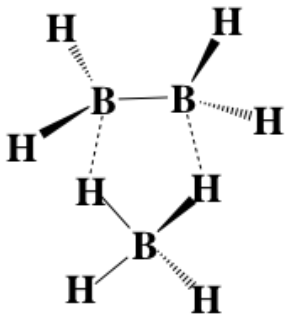

Fig. 2.8 Structure of $B_3H_8^-$ ion

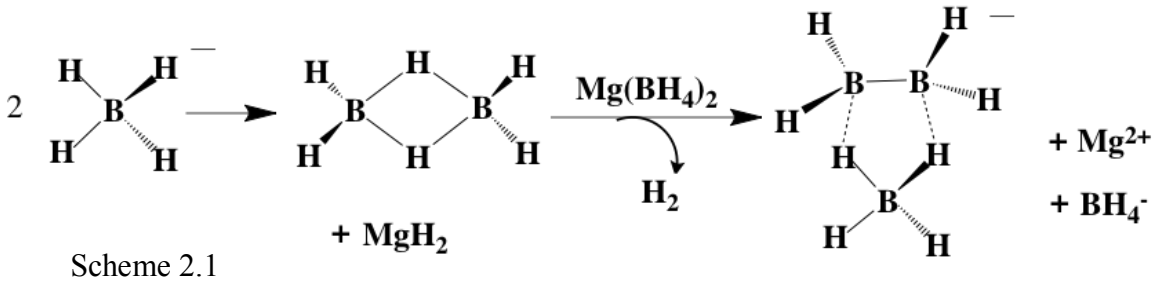

Scheme 2.1

Equation 2.3 describes the decomposition pathway of $Mg(BH_4)_2$ to $Mg(B_3H_8)_2$:

$$3Mg(BH_4)_2 \rightarrow Mg(B_3H_8)_2 + 2MgH_2 + 2H_2 \qquad (2.3)$$

A possible mechanism is given in Scheme 2.1. Two BH_4^- units condense to give diborane, accompanied by formation of MgH_2. A BH_4^- inserts between the B-H-B bonds to yield the B-H ring and release of H_2.

The decomposition of $Mg(BH_4)_2$ to $Mg(B_3H_8)_2$ should theoretically release 2.5 wt % H_2. Although this gravimetric capacity is low, the ability to cycle hydrogen would present significant progress in understanding the criteria affecting reversibility**.** The rehydrogenation of decomposed $Mg(BH_4)_2$ was subsequently explored to determine the conditions needed to facilitate reversible storage through $Mg(B_3H_8)_2$.

2.3.2 *Rehydrogenation of decomposed $Mg(BH_4)_2$*

Hydrogenation of decomposed $Mg(BH_4)_2$ was conducted at 523 K for 48 hours under 12 MPa H_2. Analysis by solution NMR revealed a significant reduction in the $Mg(B_3H_8)_2$ resonance relative to $Mg(BH_4)_2$ (Fig. 2.9 a,b). A trace amount of $MgB_{12}H_{12}$ at –15 ppm appeared after hydrogenation but the quantity present, as determined by integration of peak area, was not enough to account for the decrease in $Mg(B_3H_8)_2$ and thus can be attributed to the formation of $Mg(BH_4)_2$. Cycling between $Mg(B_3H_8)_2$ and $Mg(BH_4)_2$ was evident in the second dehydrogenation/rehydrogenation cycle (Fig. 2.9 c,d), establishing that decomposition to the $Mg(B_3H_8)_2$ intermediate is fully reversible.

The hydrogenation of $Mg(B_3H_8)_2$ to $Mg(BH_4)_2$ requires the addition of hydridic anions to the cyclic $B_3H_8^-$ in order to facilitate B-B bond breakage. This process is dependent on the availability of hydridic anions which can only be supplied by either heterolytic splitting of H_2 (which typically requires catalytic activation) or by donation from MgH_2. Furthermore, the bond dissociation energy of H_2 is 436 kJ/mol at 298 K[76] versus 197 kJ/mol[77] for MgH_2. Thus the most probable hydride source is MgH_2 and experiments examining its role in rehydrogenation will be presented in Chapter 3.

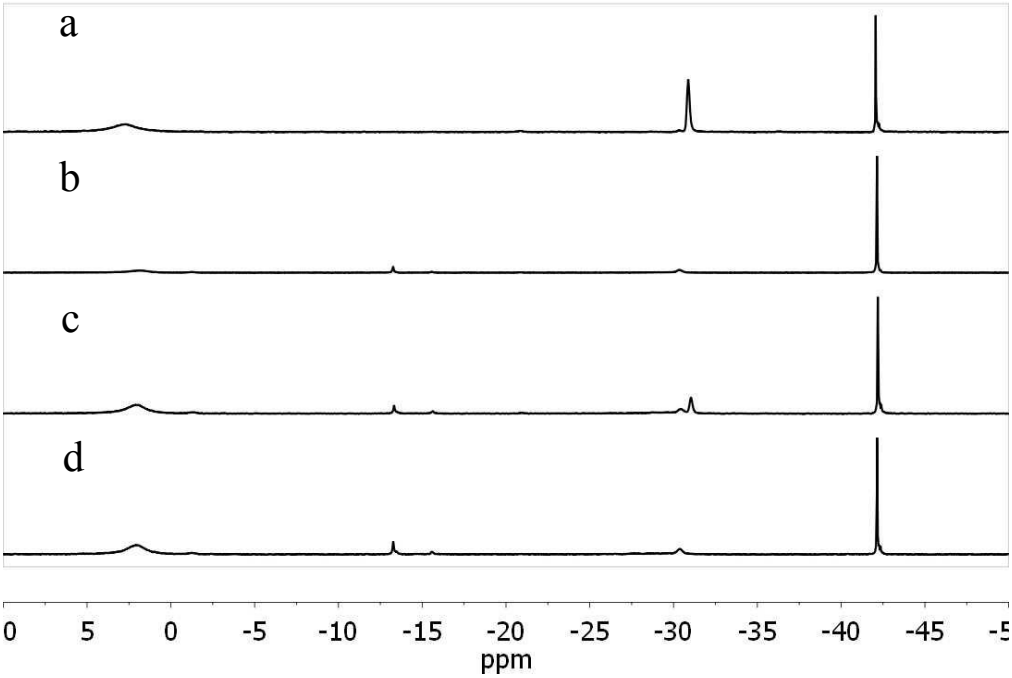

Fig. 2.9 $^{11}B\{^{1}H\}$ NMR of (a) $Mg(BH_4)_2$ dehydrogenated at 573 K, 5 weeks; (b) rehydrogenated at 523 K, 48 h, 120 atm H_2 ; (c) 2nd dehydrogenation at 573 K, 1 week and (d) 2nd rehydrogenated at 523 K, 48 h, 1.2 MPa H_2 .

2.3.3 *Effect of $Mg(BH_4)_2$ morphology on decomposition and analysis of gas-phase decomposition products*

Magnesium borohydride is understood to undergo a phase transition ($\alpha \rightarrow \beta$) when exposed to temperatures ≥508 K[73] and more recently, a low density cubic polymorph (γ-phase) has been synthesized and its structure solved by synchrotron powder diffraction.[74] The authors found that the pore volume in γ-$Mg(BH_4)_2$ accounts for 33% of its structure versus 6.4% for the α-phase. This material is capable of absorbing N_2 and dichloromethane molecules and may have potential as a nanoporous scaffold for hydrogen storage.[74] The dependency of decomposition temperature on the morphology

of $Mg(BH_4)_2$ was examined to evaluate possible effects of phase structure on rates of dehydrogenation. This was accomplished by comparing dehydrogenation of the γ-polymorph to that of the α-phase. In addition, the gas-phase decomposition products of γ-$Mg(BH_4)_2$ were analysed by *in situ* IR spectroscopy to determine whether diborane was released. Finally, nanoconfinement of metal hydride additives within the porous structure of γ-$Mg(BH_4)_2$ was attempted followed by isothermal dehydrogenation experiments to determine whether nanostructuring could lower kinetic barriers.

The XRD spectra for $Mg(BH_4)_2$ (prepared as according to the synthesis for γ-phase) is given in Fig. 2.10. The attempt to prepare the γ-phase resulted in a somewhat amorphous material as depicted by the broad feature in the baseline at ~10°. The profile has fewer well-defined signals than XRD data for α-$Mg(BH_4)_2$ and the major reflection at 13° does not coincide with α-$Mg(BH_4)_2$.[72] The profile also does not display the low angle reflections detected in other previous work.[74] Attempts to prepare pure γ-$Mg(BH_4)_2$ has led to the realization that the synthesis tends to yield mixtures of both α- and γ-phases which cannot be separated.[78] In spite of the failure to isolate pure γ-$Mg(BH_4)_2$, a dehydrogenation trial was conducted on the mixture to determine if the presence of a more porous phase of $Mg(BH_4)_2$ could affect the rate of decomposition.

A comparison of the results of dehydrogenating both mixed γ/α-$Mg(BH_4)_2$ and α-$Mg(BH_4)_2$ for 1 day at 473 K (Fig. 2.11) suggests that the porous structure of the γ-phase may be more susceptible to thermal decomposition. Approximately 9 % more $Mg(B_3H_8)_2$ was formed in the γ/α mixture than from the pure α-$Mg(BH_4)_2$. The porous

framework of γ-$Mg(BH_4)_2$ must consist of fewer interconnecting bonding interactions between $Mg(BH_4)_2$ units and consequently requires less thermal input to decompose the

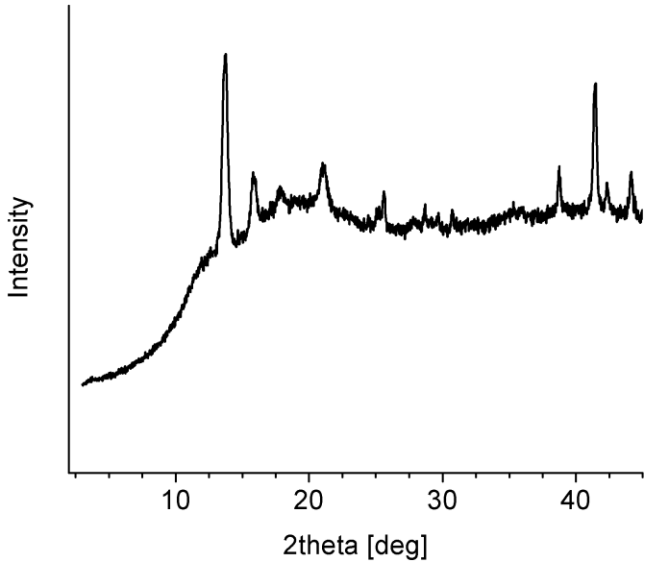

Fig. 2.10 XRD spectra as-prepared γ-$Mg(BH_4)_2$

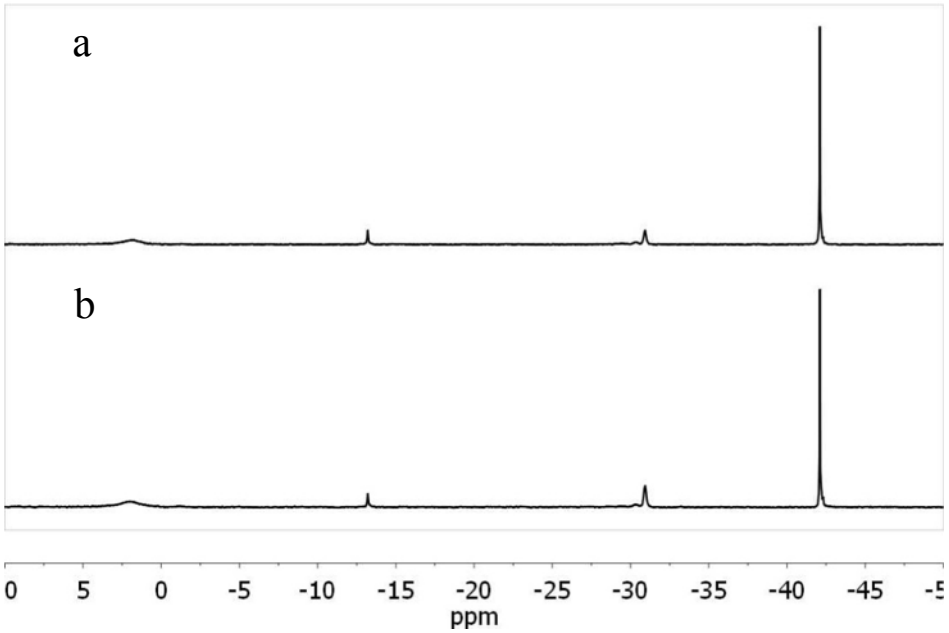

Fig. 2.11 $^{11}B\{^1H\}$ NMR of (a) α-$Mg(BH)_2$; (b) γ/α-$Mg(BH)_2$after dehydrogenation at 473 K, 1 day.

lattice. A pure sample of γ-$Mg(BH_4)_2$ could then potentially yield significantly more $Mg(B_3H_8)_2$ than α-$Mg(BH_4)_2$.

When monitored by *in situ* IR, thermal desorption of the α/γ mixture of $Mg(BH_4)_2$ was not found to emit diborane in the gas phase, confirming that the observed mass loss was fully attributable to H_2 release. Only trace levels of atmospheric impurities such as water, CO_2 and THF were detected and decomposition began at about 393 K. Correlation of the mass loss rate with temperature (Fig. 2.12) for γ/α-$Mg(BH_4)_2$ versus results for α-$Mg(BH_4)_2$[57] confirmed that both phases began dehydrogenating at similar temperatures and experienced increased mass loss rates starting at about 443 K. These results indicate that either diborane plays a minor role in the dehydrogenation or that it is immediately consumed as an intermediate, regardless of the morphology of $Mg(BH_4)_2$.

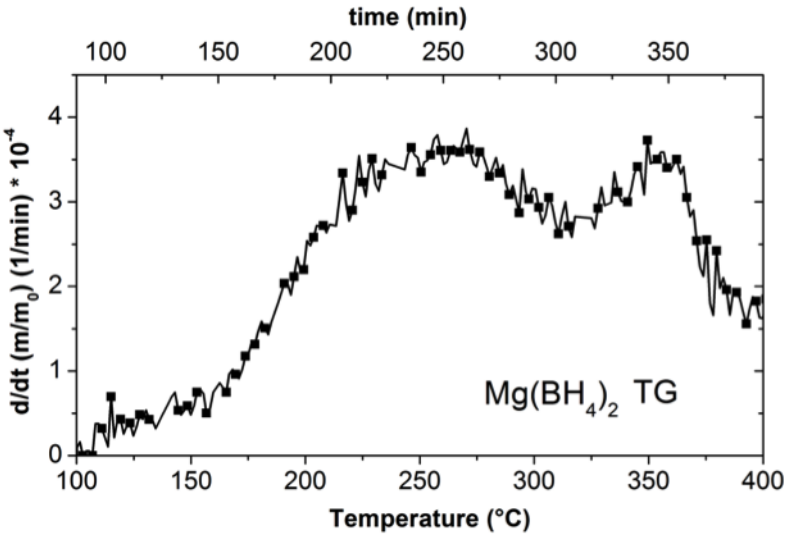

Fig. 2.12 Plot of mass loss rate of γ/α-$Mg(BH_4)_2$ vs. temperature as determined by TGA

Filinchuk *et al*. have demonstrated the ability of the porous γ-$Mg(BH_4)_2$ to reversibly adsorb N_2 and suggest the possibility of hydrogen storage in the same manner.[74] We attempted to nanoconfine the light metal hydrides AlH_3 and MgH_2 within the pores of γ-$Mg(BH_4)_2$. These experiments did not yield any difference in decomposition rates thus the details regarding these trials are given in Appendix A.

2.3.4 *Dehydrogenation of $Mg(B_3H_8)_2/MgH_2$ mixture*

In hopes of gaining additional insight into the dehydrogenation pathway of $Mg(BH_4)_2$ via the $B_3H_8^-$ intermediate, as-prepared $Mg(B_3H_8)_2$ was decomposed neat and in combination with different mole ratios of MgH_2. As described in the decomposition trials of $Mg(BH_4)_2$ at 473 K, prolonged dehydrogenation was found to favor the formation of $Mg(B_3H_8)_2$. Continuing the experiment beyond eight weeks would presumably continue converting BH_4^- to $B_3H_8^-$ until a thermodynamic equilibrium was attained. Thus the results of dehydrogenation trials with mixtures of $Mg(B_3H_8)_2$ and MgH_2 were somewhat surprising.

Dehydrogenation of $Mg(B_3H_8)_2$ without MgH_2 at 473 K for one day favored the formation of $B_{10}H_{10}^{2-}$ (appearing at –30 and –1 ppm in a 4:1 ratio) in addition to $B_{12}H_{12}^{2-}$ and BH_4^- (Fig. 2.13). This suggests both disproportionation of $B_3H_8^-$ to give BH_4^- followed by condensation into stable polyboranes. Repeating the experiment with one equivalent of MgH_2 further promoted $MgB_{10}H_{10}$ formation (Fig. 2.14) but subsequent dehydrogenation with a mixture of 2:1 MgH_2 to $Mg(B_3H_8)_2$ produced a very different NMR spectrum (Fig. 2.15) with only $Mg(BH_4)_2$ formed upon desorption. Similar results emerged upon dehydrogenation of a 4:1 ratio of MgH_2 to $Mg(B_3H_8)_2$.

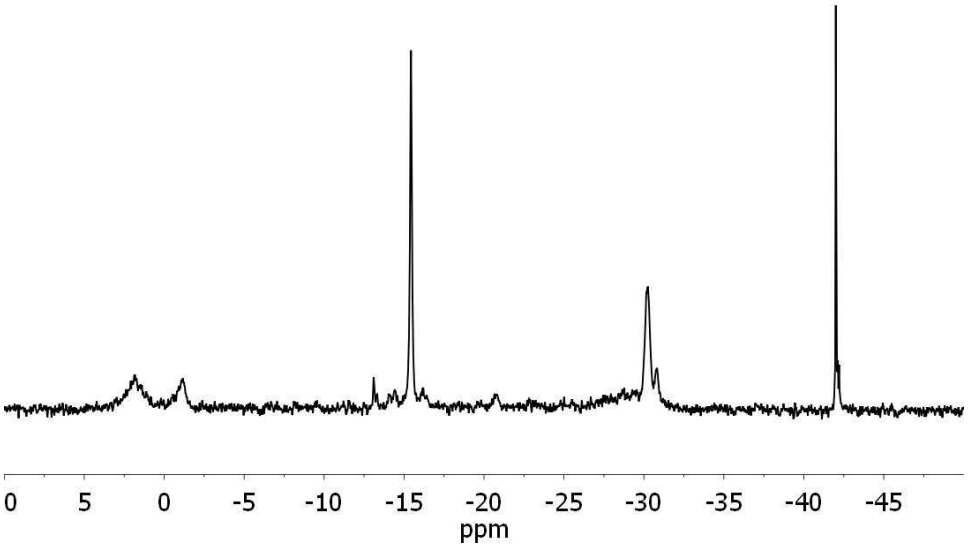

Fig. 2.13 $^{11}B\{^{1}H\}$ NMR of $Mg(B_3H_8)_2$ dehydrogenated at 473 K, 1 day.

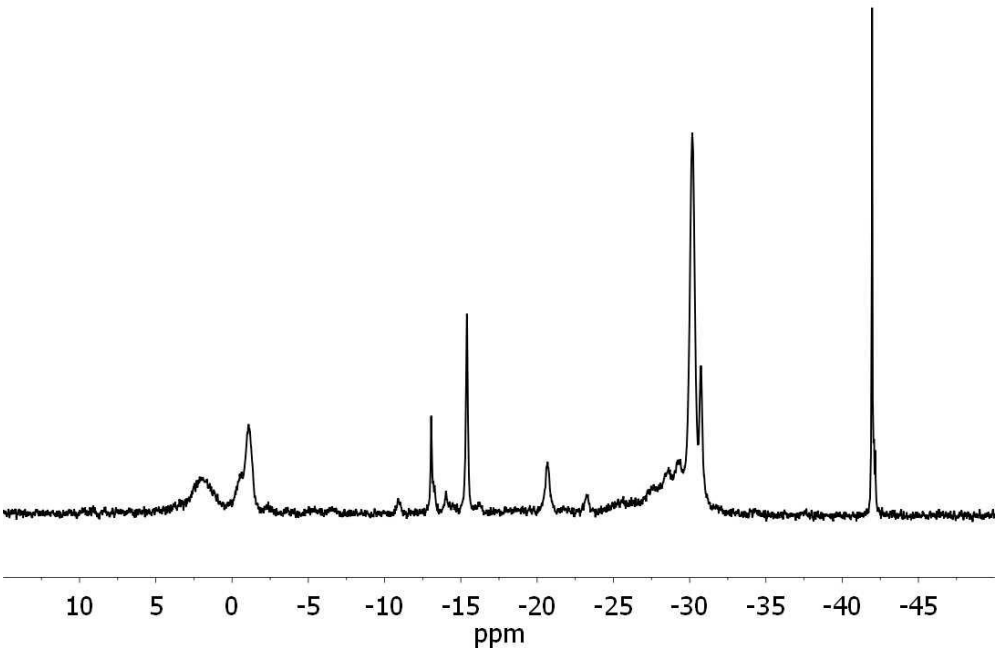

Fig. 2.14 $^{11}B\{^{1}H\}$ NMR of $Mg(B_3H_8)_2/MgH_2$, dehydrogenated at 473 K, 1 day.

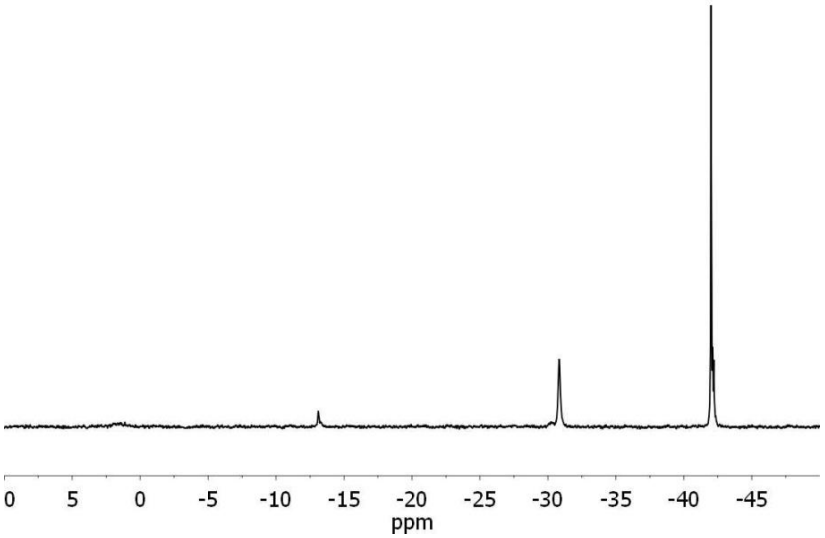

Fig. 2.15 $^{11}B\{^{1}H\}$ NMR of $Mg(B_3H_8)_2/2MgH_2$, dehydrogenated at 473 K, 1 day.

The preferential formation of $Mg(BH_4)_2$ upon addition of 2:1 MgH_2 to $Mg(B_3H_8)_2$ reveals the highly reversible nature of the equilibrium between the BH_4^- and $B_3H_8^-$ species at 473 K. Heating under vacuum at this temperature provides sufficient energy to decompose the $B_3H_8^-$ ring into single B units. Although MgH_2 typically does not decompose at 473 K, it must provide the necessary hydridic anions as there are no other hydride sources present in the system. Thus, under these reaction conditions and in proximity to these materials, it must readily decompose in order to transfer hydridic anions to the B units.

Upon characterization in solution, $Mg(BH_4)_2$ appeared to be the predominant product detected by ^{11}B NMR after dehydrogenation. It is possible, however, that

gaseous boranes such as diborane may have formed. Thus, vapors emitted during decomposition were collected by condensation in THF followed by NMR analysis.

The $^{11}B\{^{1}H\}$ NMR spectrum for a gas phase products derived from a dehydrogenated (5 hours at 473 K) mixture of 2:1 MgH_2 to $Mg(B_3H_8)_2$ revealed the presence of diborane at 0 ppm[75] as well as trace quantities of unidentified species at -7 and 21 ppm and a pronounced signal at 27 ppm (Fig. 2.16). At this downfield chemical shift of 27 ppm, a highly oxidized boron species would be expected but interestingly this signal is seen as a doublet in the proton coupled spectrum, representative of a species such as $BH(THF)_x$.

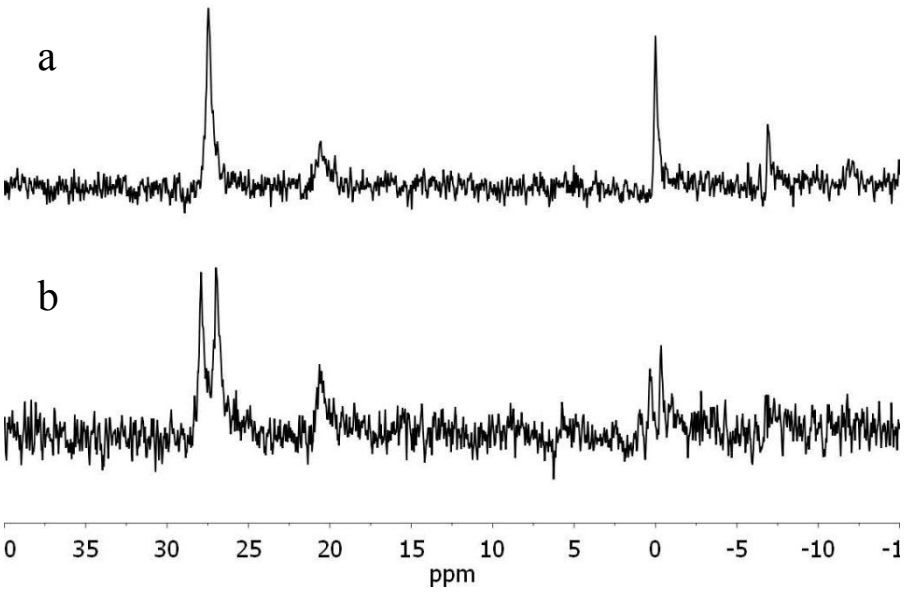

Fig. 2.16 (a) $^{11}B\{^{1}H\}$ NMR; (b) ^{11}B NMR of gas phase decomposition products of $Mg(B_3H_8)_2 + 2MgH_2$ condensed in THF after dehydrogenation at 473 K, 5 h.

Although the amount of diborane released during dehydrogenation of $Mg(B_3H_8)_2$ and MgH_2 cannot be determined, the evidence for its production suggests a decomposition route such as:

$$Mg(B_3H_8)_2 + 2MgH_2 \rightarrow Mg(BH_4)_2 + 2B_2H_6 + 2Mg \quad (2.4)$$

Varying the amount of MgH_2 available to $Mg(B_3H_8)_2$ as a hydride source evidently controls the species formed after dehydrogenation. In contrast to our results, the *in situ* IR analysis of the dehydrogenation of annealed $Mg(BH_4)_2$ from a previous study did not detect any diborane upon heating up to 753 K.[57] The dimethyl sulfide adduct of $Mg(BH_4)_2$, however, was found to emit significant levels of diborane at 363 K which was thought to result from either partial decomposition of the borohydride upon solvent release or from the synthesis of $Mg(BH_4)_2$ via $BH_3{\cdot}S(CH_3)_2$.[57] In our experiment the solvation of $Mg(B_3H_8)_2$ by THF or its preparation from $BH_3{\cdot}$THF may lead to the the same effects.

The gas phase condensate in THF derived from dehydrogenation of $Mg(BH_4)_2$ for five hours at 473 K was not found to contain diborane. Although the formation of diborane as a result of solvent effects on $Mg(B_3H_8)_2$ cannot be ruled out, the reaction given in Eq. 2.4 suggests it is a necessary side product for $Mg(B_3H_8)_2$ to decompose to $Mg(BH_4)_2$. The prolonged decomposition of $Mg(BH_4)_2$, however, continues to produce $Mg(B_3H_8)_2$ (and MgH_2) until a thermal equilibrium is attained at which the formation of $Mg(B_3H_8)_2$ appears to plateau. This equilibrium is supported by the results of dehydrogenation of the mixture of $Mg(B_3H_8)_2$ and MgH_2, suggesting there must be a small enthalpy difference between the $Mg(BH_4)_2$ and $Mg(B_3H_8)_2$.

2.3.5 *Dehydrogenation of $Mg(BH_4)_2$ with LiH*

Recently, Yang *et al*. were able to recharge 3.6 wt % H_2 on a $Mg(BH_4)_2$/LiH composite for 20 cycles at 453 K.[79] The authors determined that a polyborane

intermediate species was formed during cycling but its identity could not be resolved through solid state NMR. The mechanically milled mixture of $Mg(BH_4)_2$ and 0.5 LiH released 3.6 wt % of H_2 after 12 hours of dehydrogenation at 453 K and could be recharged over 20 cycles. The LiH was thought to aid in promoting the formation of intermediate species such as $Mg(B_3H_8)_2$ or MgB_2H_6 and was found, based on DSC data, to lower the activation energy of dehydrogenation of $Mg(BH_4)_2$ from 25.3 to 12.5 kJ/mol.

In order to better understand the molecular basis of these findings, collaborative studies were carried out with a visiting scholar, J. Yang of Peking University in which solution NMR was utilized to characterize the dehydrogenation products of this composite. In these experiments the as-synthesized $Mg(B_3H_8)_2$ was first hydrogenated with two equivalents of MgH_2 and three equivalents of LiH to yield $Mg(BH_4)_2$ and LiH:

$$Mg(B_3H_8)_2 + 2\ MgH_2 + 3LiH + 2H_2 \rightarrow 3Mg(BH_4)_2 + 3LiH \qquad (2.5)$$

This resulted in a 1:1 mixture of $Mg(BH_4)_2$ and LiH which was then dehydrogenated at 423 K for 3 days. ^{11}B NMR analysis of the product revealed the prevalence of the $B_{10}H_{10}^{2-}$ peak at –30 ppm (Fig. 2.17) along with a large amount of boric acid centered at ~3 ppm, and BH_4^-. The same dehydrogenation trial was repeated on a mixture of 1:1 $Mg(BH_4)_2$ to LiH which yielded a similar results according to characterization by ^{11}B NMR. From this, it was concluded that the hydrogenation of $Mg(B_3H_8)_2/MgH_2/LiH$ formed $Mg(BH_4)_2$ and not $LiBH_4$ although this could not be confirmed by the available characterization tools.

Subsequent rehydrogenation of the powder at 453 K for 12 hours under 8 MPa H_2 resulted in a dramatic reduction in the $B_{10}H_{10}^{2-}$ peak (Fig. 2.18), leaving boric acid and BH_4^- as the final species, indicating highly reversible cycling between $B_{10}H_{10}^{2-}$ and BH_4^-.

Unfortunately, the metal cation coordinated to $B_{10}H_{10}^{2-}$ could not be identified by NMR. The deshielding effect of Mg^{2+} vs. Li^{+} did not change enough to detect a difference in the chemical shift in ^{11}B NMR. Since lithium tends to form salts that dissociate

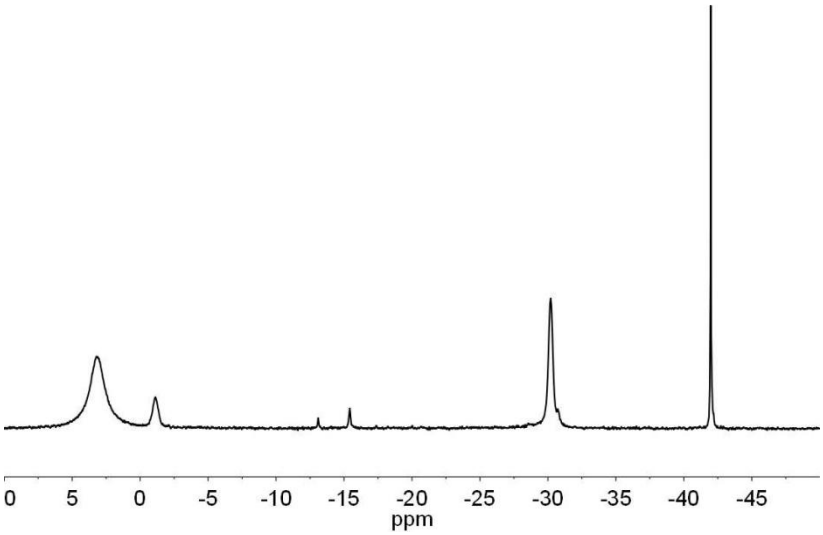

Fig. 2.17 $^{11}B\{^{1}H\}$ NMR of hydrogenated $Mg(B_3H_8)_2$ +2MgH_2+3LiH, dehydrogenated at 453 K, 3 days.

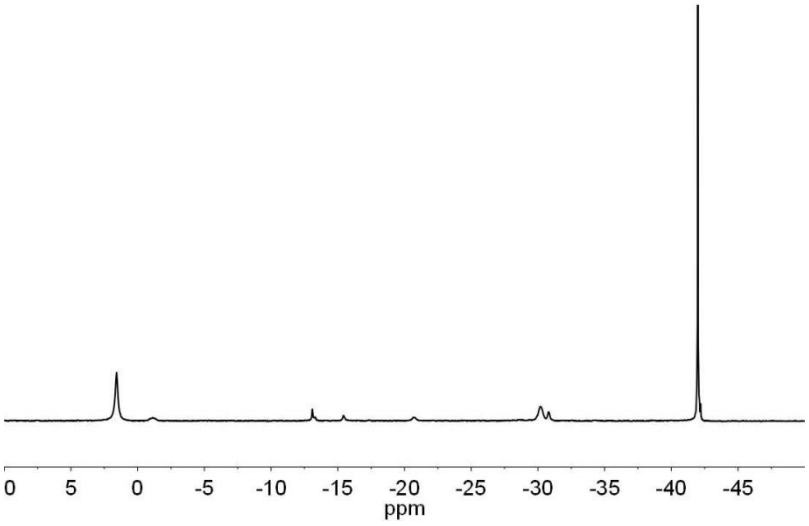

Fig. 2.18 $^{11}B\{^{1}H\}$ NMR $Mg(B_3H_8)_2$/2MgH_2/3LiH of hydrogenated, then dehydrogenated at 453 K, 3 days and finally rehydrogenated at 453 K, 8 MPa H_2, 12 h.

completely in aqueous media, analysis by solid state ^{7}Li MAS NMR was also examined but no variation in the chemical shift of the Li species before and after dehydrogenation was observed. The XRD analysis did not exhibit reflections characteristic of LiH but this may have been a consequence of the amorphous nature of the powder.

Whether $Li_2B_{10}H_{10}$ or $MgB_{10}H_{10}$ is the decomposition product of the $Mg(BH_4)_2$/LiH mixture, the dehydrogenation mechanism of $Mg(BH_4)_2$ is clearly altered by the presence of LiH. Dehydrogenation of only $Mg(BH_4)_2$ at 423 K for three days yields a small amount of $Mg(B_3H_8)_2$ but the addition of LiH not only lowers the kinetic barrier to dehydrogenation but also promotes condensation to $MgB_{10}H_{10}$ rather than $Mg(B_3H_8)_2$.

Although the details of the reaction taking place upon dehydrogenation of the $Mg(BH_4)_2$/LiH composite are not fully elucidated, it is clear that $B_{10}H_{10}^{2-}$ is the key species involved in cycling hydrogen for this material. The results of these trials along with those of Yang *et al*.[79] are convincing evidence for the role of $B_{10}H_{10}^{2-}$ in providing an alternative pathway for the dehydrogenation of $Mg(BH_4)_2$. It should be noted that the $B_{10}H_{10}^{2-}$ species can potentially cycle 7.4 wt % H_2, (almost three times more than $Mg(B_3H_8)_2$).

2.4 Conclusions

The dehydrogenation of $Mg(BH_4)_2$ requires impractically high temperatures and pressures in order to discharge its full hydrogen content. By exploring decomposition at low temperatures, we have identified the intermediate species, $Mg(B_3H_8)_2$ whereby

rehydrogenation readily yields the original borohydride. At 473 K there exists an equilibrium between the two species that appears to prevent full conversion of $Mg(BH_4)_2$ to $Mg(B_3H_8)_2$. As well, continued dehydrogenation of $Mg(B_3H_8)_2$ and MgH_2 proceeds to form $Mg(BH_4)_2$ confirming the highly reversible nature of the interconversion between these two species.

Although only 2.5 wt % can be cycled through this species, its observed reversibility at temperatures <573 K opens up the possibility that there are other reversible B intermediates with greater hydrogen capacity. The stable $B_{10}H_{10}^{2-}$ has emerged as another dehydrogenation product capable of regenerating $Mg(BH_4)_2$ under mild conditions. Only small quantities of $B_{10}H_{10}^{2-}$ are formed when $Mg(BH_4)_2$ is decomposed at 573 K but its yield is dramatically enhanced in the presence of LiH.

The potential for $B_{10}H_{10}^{2-}$ to reversibly store up to 7.4 wt % H_2 is especially appealing. It may be the first B species to exhibit low temperature cycling at a gravimetric capacity approaching that required by the U.S. Department of Energy (DOE). Neither the role of LiH nor the mechanism behind this reaction is clear but the promising results of the cycling trials of the $Mg(BH_4)_2$/LiH composite will hopefully motivate further investigation.

The decomposition route from $Mg(BH_4)_2$ to $Mg(B_3H_8)_2$ must also form MgH_2 in addition to H_2 release in order to satisfy the mass balance of the reaction. *In situ* IR analysis has confirmed that diborane gas is not emitted during this process and so dehydrogenation must proceed as described in Eq. 2.3 following the mechanism outlined in Scheme 2.1. Consequently, for rehydrogenation to occur, the MgH_2 must interact with the $B_3H_8^-$, readily donating hydridic anions that must facilitate the breaking of B-B

bonds. This implies that the MgH_2 must have a low enough stability to decompose at less than 573 K and rehydrogenation must therefore be dependent upon the thermodynamic stability of the metal hydride donor.

To test this hypothesis, the isolation of $Mg(B_3H_8)_2$ was necessary in order to conduct hydrogenation studies with hydride sources of varying stability. The independent preparation of $Mg(B_3H_8)_2$ was therefore the next research objective and its synthesis and subsequent hydrogenation experiments will be presented in the following chapter.

CHAPTER 3 HYDROGENATION STUDIES ON THE INTERMEDIATE SPECIES, $Mg(B_3H_8)_2$

3.1 *Introduction*

A variety of materials have been investigated in the search for a viable candidate with the potential to reversibly store hydrogen. The stringent guidelines set by the DOE, however, has narrowed the possibilities to only a handful of solid state compounds with the capacity to cycle a useful amount of hydrogen. The lightweight Group I and II borohydrides in particular have appealing hydrogen gravimetric and volumetric densities but the alkali metal borohydrides tend to be too stable to conform to practical operating conditions for dehydrogenation. Within the Group II borohydrides, magnesium borohydride is thought to possess favorable thermodynamic properties[41] and gravimetric hydrogen content (14.9 wt%) to perform as an ideal hydrogen storage material.

Early studies by Orimo's laboratory at Tohoku University investigated the stabilities of various borohydride complexes.[41] This led to the identification of $Mg(BH_4)_2$ as a complex with a theoretical enthalpy of desorption, ΔH_{des}, that fell between that of the highly stable $LiBH_4$ and the volatile transition metal borohydrides. A subsequent study found that $Mg(BH_4)_2$ began releasing hydrogen at 100K lower than $LiBH_4$ and the decomposition occurred in two distinct steps.[48] The first step resulted in the formation of MgH_2 at 563 K and the second step involved the dehydrogenation of MgH_2 to Mg at >590 K with the assumption that amorphous boron was also formed as product. A separate study, however, identified the final decomposition product to be MgB_2 by a combination of X-ray diffraction (XRD) and nuclear magnetic resonance (NMR).[49]

Continued exploration of the desorption properties of the borohydrides eventually revealed that dodecaborane, $B_{12}H_{12}^{2-}$, plays an important role in the solid state decomposition pathway. It has both been calculated and experimentally proven to form at temperatures >573 K[49,52–55] upon dehydrogenation. Rehydrogenation at 543 K and 40 MPa H_2 of fully decomposed $Mg(BH_4)_2$ has also been found to terminate upon formation of $MgB_{12}H_{12}$,[46] providing convincing evidence that the stability of $B_{12}H_{12}^{2-}$ renders it a thermodynamically favorable species that prevents full reversibility.

In spite of the preferential formation of $MgB_{12}H_{12}$, a high pressure study performed by Severa *et al*. at Sandia National Laboratories has successfully hydrogenated MgB_2 to $Mg(BH_4)_2$.[58] Although it was not verified whether $MgB_{12}H_{12}$ was an intermediate in this reaction or if formation was suppressed, this achievement was a major breakthrough in evaluating the potential for reversibility within the $Mg(BH_4)_2$ system. It must be noted that this hydrogenation required exceedingly high pressures of 76-91 MPa H_2 and considering that commercial applicability is the ultimate goal, reaction conditions should progress towards more moderate and practical conditions. Thus reversibility under mild temperatures and conditions is currently being pursued.

In the previous chapter we found that the decomposition of $Mg(BH_4)_2$ in the solid state proceeds via a pathway that includes the early formation of $Mg(B_3H_8)_2$ as well as MgH_2. This led to the suggestion that, similar to decomposition of BH_4^- in solution,[50] thermal dehydrogenation of solid state $Mg(BH_4)_2$ occurs via a mechanism involving consecutive condensation steps which results in the formation of increasingly large and stable polyhedral boranes. At temperatures <573 K, the most thermally stable decomposition product was $Mg(B_3H_8)_2$.

Hydrogenation of the decomposed material which consisted of $Mg(B_3H_8)_2$, MgH_2, residual $Mg(BH_4)_2$, and some hydrolysable boron species as observed by ^{11}B NMR, resulted in only $Mg(BH_4)_2$,[80] demonstrating that some degree of reversibility can be achieved under much milder conditions than those used in previous studies. The decomposition to $Mg(B_3H_8)_2$ was proposed to follow the reaction:

$$3\ Mg(BH_4)_2 \Leftrightarrow Mg(B_3H_8)_2 + 2MgH_2 + 2H_2 \qquad (3.1)$$

From this it can be seen that the presence of the metal hydride plays a key role in the reverse reaction to re-form magnesium borohydride.

This development prompted us to find a method to synthesize $Mg(B_3H_8)_2$ independently. By doing so, studies on the isolated $Mg(B_3H_8)_2$ could be conducted in order to elucidate the mechanism behind its hydrogenation, in combination with MgH_2, to yield $Mg(BH_4)_2$. Substitution of MgH_2 with either LiH or NaH should also provide insight as to the role of the stability of the metal hydride with regards to how readily $Mg(BH_4)_2$ is produced.

Subsequent hydrogenation trials by pressure-composition-temperature (PCT) measurements as well as analysis by differential scanning calorimetry (DSC) then would yield products to be characterized by ^{11}B and ^{11}B MAS NMR spectroscopy. NMR spectroscopy was chosen as the primary method of characterization because of its ability, as discussed in the previous chapter, to resolve signals for different boron species in spite of the amorphous nature of the products.

3.2 *Experimental*

All sample preparation and handling was conducted either in an argon or nitrogen glovebox or using standard Schlenk techniques. Glassware was routinely oven-dried before addition of reagents. Solvents were purified by an SPS system or distilled over a drying agent as needed.

3.2.1 *Characterization of $Mg(B_3H_8)_2$*

Infrared (IR) spectra were obtained from a Shimadzu IRAfinity-1 FTIR. Samples were pressed into a KBR pellet in the glovebox and kept in an airtight sampling unit during measurements.

Solution state NMR analyses were carried out on a Varian Unity Innova 500 MHz spectrometer with ^{11}B chemical shifts referenced to $BF_3 \cdot OEt_2$ (δ=0 ppm) at 20°C. Deuterium oxide was chosen as the solvent for NMR studies because it allowed for the most complete dissolution of the sample powders. As a consequence, however, any boranes possessing open cage, such as *nido* or *arachno*boranes tended to hydrolyze,[80] usually appearing somewhat downfield of 0 ppm. Magic angle spin (MAS) NMR was also used to provide a comparison of NMR characterization without the effects of hydrolysis.

Solid state MAS NMR was measured on a Varian Unity Innova 400 MHz with a 3.2 mm HX CPMAS probe. Sample powders were packed into zirconium oxide rotors and spun at 12 kHz. A spectral frequency of 128.32 MHz was used for ^{11}B MAS NMR measurements with a 1M boric acid solution (δ=0 ppm) as a reference. One-dimensional spectra were obtained after a 1 μs single pulse with ^{1}H decoupling. In contrast to solution

phase ^{11}B NMR, $Mg(B_3H_8)_2$ was observed as a singlet at –22 ppm and $Mg(BH_4)_2$ at –31 ppm.

3.2.2 *Preparation of $Mg(B_3H_8)_2$*

Magnesium ribbon (0.2 g) was cut into small pieces and added to ~7 mL of mercury. The mixture was heated to 180°C for 1 hour with vigorous stirring, during which the magnesium melted, and was then allowed to cool to room temperature. A 1 M solution of borane-tetrahydrofuran (BH_3·THF) complex was added (50 mL) with a syringe and the solution was allowed to stir for 2-5 days. The solution gradually turned white and opaque after which the precipitated magnesium octahydrotriborate was isolated by filtration and washed several times with THF to remove any residual $Mg(BH_4)_2$. The resulting white powder was dried overnight on a vacuum line at 50°C. Drying the product at a higher temperature (>80°C) caused the solid to melt and crystallize upon cooling into a gray and sometimes waxy material.

3.2.3 *Preparation of NaB_3H_8*

In a similar procedure to that for the synthesis of $Mg(B_3H_8)_2$, 0.41-0.44 g of Na metal was cut into small pieces and added to mercury under inert gas flow, allowing time for the heat from this reaction to dissipate in between additions. The Na/Hg amalgam was stirred for a minimum of 2 hours after which 54 mL of BH_3·THF complex was added by syringe. The mixture was allowed to stir for 24 hours during which the solution changed from a cloudy gray suspension to a clear, colourless liquid. The solution was then filtered and the collected filtrate was heated to 75°C until most of the THF had

evaporated. The precipitate was recrystallized in diethyl ether, which removed most of the $NaBH_4$, and finally dried *in vacuo* at 60°C overnight. The final product was a yellowish-white powder, the purity of which was highly dependent on the purity of the mercury.

3.2.4 *Preparation of mixtures of $Mg(B_3H_8)_2$ or NaB_3H_8 with metal hydrides*

$Mg(B_3H_8)_2$ or NaB_3H_8 was either ballmilled or ground by hand with MgH_2 (activated before use by ballmilling) to ensure a homogeneous mixture. NMR analysis of the ballmilled vs. hand ground mixtures of $Mg(B_3H_8)_2$ and MgH_2 showed no difference before hydrogenation. Results of both NMR and DSC showed no differences between mixing methods during and after hydrogenation. Mixtures of $Mg(B_3H_8)_2$ with LiH or NaH and NaB_3H_8 with NaH were ground by hand.

3.2.5 *Isothermal hydrogenation studies*

Hydrogenation studies were carried out isothermally on a Suzuki Shokan PCT-2SDWIN Sievert type apparatus. Precise temperature control was achieved using customized heating mantle sleeves. Reactors with fixed volumes were initially evacuated prior to dehydrogenation experiments. Differential scanning calorimetry was performed on a Mettler Toledo Inc. DSC827e instrument in a helium glovebox using aluminum sample cells. The sample compartment was pressurized to 5 MPa H_2 and heated at a rate of 5 $K \cdot min^{-1}$ with a H_2 flow of 200 $mL \cdot min^{-1}$.

3.3 *Results and Discussion*

3.3.1 *Characterization of $Mg(B_3H_8)_2$ and NaB_3H_8*

NaB_3H_8 was initially prepared to be used as a precursor to $Mg(B_3H_8)_2$ since its solvent-free synthesis has been experimentally confirmed.[81] The authors reported that mechanical agitation of NaB_3H_8 and $MgBr_2$ yielded solvent-free $Mg(B_3H_8)_2$ that could be isolated by sublimation. Attempts to reproduce this procedure were unsuccessful and led to the adaptation of the synthesis of NaB_3H_8 utilizing Mg ribbon as a precursor instead of Na metal. Although the formation of NaB_3H_8 has not been observed experimentally during the dehydrogenation of $NaBH_4$, we chose to conduct hydrogenation trials on this species that were analogous to those performed on $Mg(B_3H_8)_2$. This may be useful by providing a comparison of the hydrogenation pathway of a $B_3H_8^-$ complex with a different metal cation and thus a different stability.

The preparation of NaB_3H_8 followed a procedure first outlined by Hill *et al.*[82] and later modified by Hoy.[81] This method has also yielded $B_3H_8^-$ complexes with several alkali and transition metals.[82] Our subsequent modification of the method to yield the magnesium complex followed the reaction:

$$2Mg/Hg + 8BH_3{\cdot}THF \rightarrow Mg(B_3H_8)_2 + Mg(BH_4)_2 + 8THF + Hg \qquad (3.2)$$

The successful formation of the metal-$B_3H_8^-$ species is dependent on how readily the mercury amalgam forms. Alkali metals form amalgams exothermically but heating was necessary to drive the amalgamation of Mg. As well, once the Mg amalgam cooled, the Mg tended to sink to the bottom of the reaction flask, preventing interaction with the overlying $BH_3{\cdot}THF$ layer. Contact between the magnesium and $BH_3{\cdot}THF$ solution had to

be maintained while stirring by frequently changing the angle at which the round bottom flask was tilted over the duration of the reaction.

The IR spectrum for the as-synthesized $Mg(B_3H_8)_2$ displayed terminal B-H stretches at 2450 and 2446 cm^{-1} and confirmed the formation of Mg-H-B bonds by the presence of a band around 2300 cm^{-1}.[83] The Mg-H-B bridge suggested by the IR data indicated that the product had a different structure than the complex obtained by Kim *et al*.[83] whose IR spectrum did not exhibit a Mg-H-B band. The authors proposed a $[Mg(THF)_6][B_3H_8]_2$ adduct but our data pointed to direct coordination of Mg to the triborane and therefore the Mg cation must be surrounded by less than six THF molecules. The ^1H NMR was then used to determine the ratio of protons assigned to $B_3H_8^-$ versus THF .

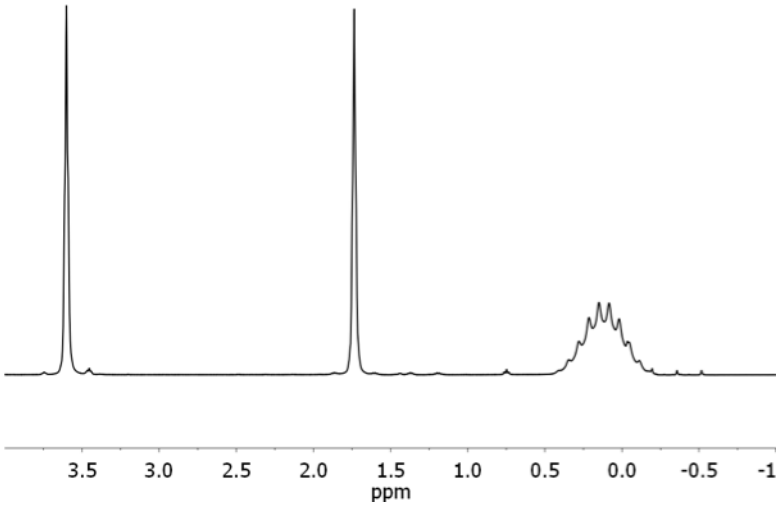

Fig. 3.1 ^1H NMR of as-synthesized $Mg(B_3H_8)_2$. A trace signal can be seen for $Mg(BH_4)_2$ centered around 0.25 ppm which partially overlaps with the 10-line signal for $Mg(B_3H_8)_2$.

The ^{1}H NMR spectrum for $Mg(B_3H_8)_2$ (Fig. 3.1) clearly displayed THF resonances at 1.85 and 3.75 ppm as well as an 10-line signal centered around 0.6 ppm, representing $B_3H_8^-$. Integration of the peaks revealed a 1:1 ratio of THF hydrogen atoms to $B_3H_8^-$, suggesting that the structure of the adduct was $Mg(B_3H_8)_2 \cdot 2THF$. Attempts to remove the THF by heating close to its boiling point only resulted in deterioration of the magnesium triborane which decomposes at 90°C.[81]

In the ^{11}B NMR spectra for the as-prepared $Mg(B_3H_8)_2$ (Fig. 3.2), the three B atoms in the $B_3H_8^-$ ring appeared as a singlet at –31 ppm in Fig. 3.2 that split into a nonet when coupled to ^{1}H (Fig. 3.2 b). Although the structure of $B_3H_8^-$ (see Fig. 2.8) suggests that the B atoms are not chemically equivalent, *ab initio* computations found that the anion is highly fluxional in nature and the bridging hydrides migrate freely around the B_3 ring.[84] The B core was calculated to possess a 3 center-2 electron bonding scheme with σ-aromaticity[84] which likely contributes to its role as a stable dehydrogenation intermediate.

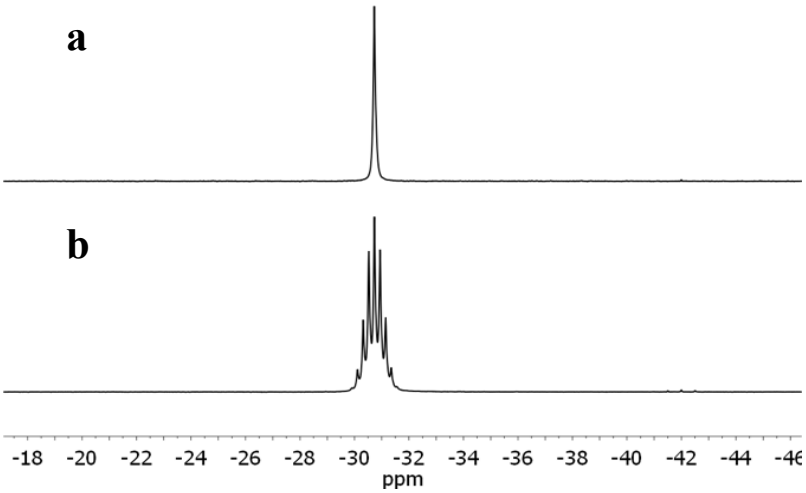

Fig. 3.2 (a) $^{11}B\{^{1}H\}$ NMR of as-synthesized $Mg(B_3H_8)_2$; (b) ^{11}B NMR for the same material.

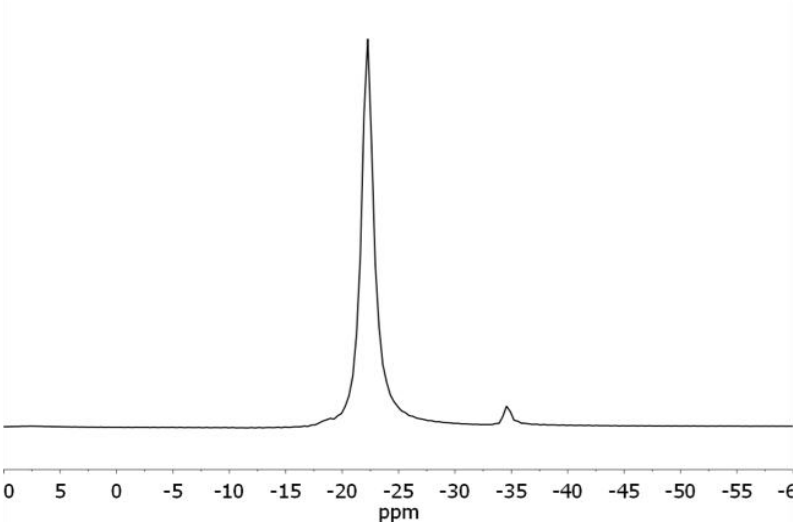

Fig. 3.3 ^{11}B MAS NMR of as-synthesized $Mg(B_3H_8)_2$.

Only minimal contamination from residual $Mg(BH_4)_2$ could be detected at –42 ppm. As well, only trace levels of boric acid representing hydrolyzed open cage boranes was observed. For comparison, ^{11}B MAS NMR for the same powder revealed a prominent resonance at –22 ppm for the $B_3H_8^-$ (Fig. 3.3) with a much smaller signal at –35 ppm representing $Mg(BH_4)_2$. The results of the NMR analyses, both ^{1}H and ^{11}B, confirm that our preparation of $Mg(B_3H_8)_2$ yielded a pure product, albeit solvated by THF.

3.3.2 *Hydrogenation of $Mg(B_3H_8)_2$*

Hydrogenation trials were carried out on $Mg(B_3H_8)_2$ at relatively low temperatures and pressures relative to conditions typically used to facilitate rehydrogenation of decomposed $Mg(BH_4)_2$ (i.e. ≥270ºC, 40 MPa).[46,58,85] The products, after heating to 200°C under 5 MPa H_2 pressure and immediate cooling, were characterized by ^{11}B NMR and found to consist primarily of about 10:2:1 $B_{12}H_{12}^{2-}$ (–15

ppm) to $B_{10}H_{10}^{2-}$(–0.9 and –30 ppm) to BH_4^- (–41 ppm) (Fig. 3.4) with no $Mg(B_3H_8)_2$ remaining. Heating for a prolonged period of time (2 days) at 250°C and 7 MPa H_2 resulted in the formation of additional polyborane species with chemical shifts falling within –15 to –25 ppm and a large amount of hydrolyzed material around 3 ppm. The resonance for $B_{12}H_{12}^{2-}$ became even more prominent under these more severe conditions while the BH_4^- completely decomposed.

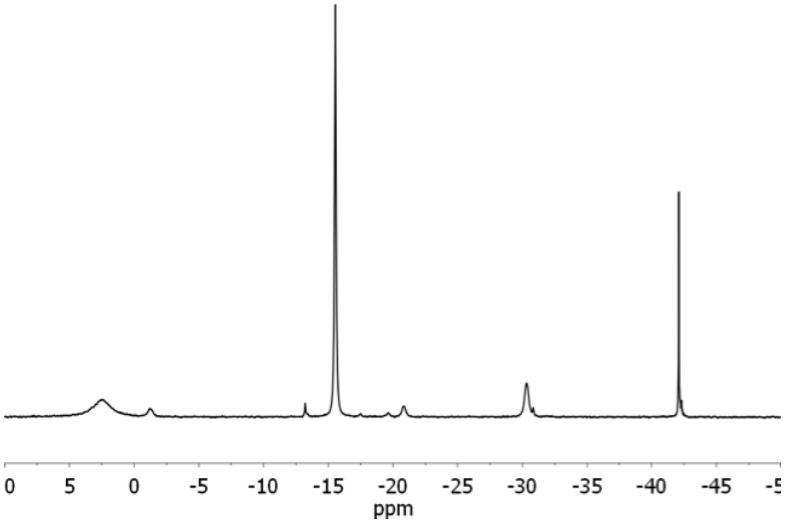

Fig. 3.4 $^{11}B\{^1H\}$ NMR of $Mg(B_3H_8)_2$ hydrogenated at 200°C under 5 MPa H_2 pressure followed by immediately cooling.

These results imply that a complex disproportionation reaction occurs in the solid state, even under H_2 pressure, that appears to be analogous to the condensation process that occurs in aqueous solution.[50] Decomposition and subsequent condensation of borane units form increasingly large and stable cages until the B cluster reaches $B_{12}H_{12}^{2-}$, marking the termination point of the condensation process . In the solid state, $Mg(B_3H_8)_2$

decomposes once the temperature rises above 90ºC. The B ring must break to form BH_4^- which then proceeds via condensation to form $B_{12}H_{12}^{2-}$. The kinetic barrier to forming BH_4^- from $B_3H_8^-$ must be relatively low, allowing this reaction to occur readily at 200ºC. Increasing the temperature for a longer period of time, however, provides the energy to overcome kinetic barriers, thus forming additional and more thermodynamically favored species, with $B_{12}H_{12}^{2-}$ as the irreversible endpoint.

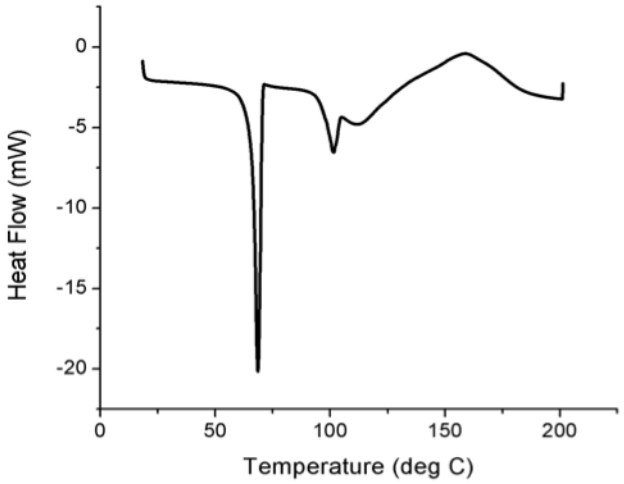

Fig. 3.5 DSC profile of $Mg(B_3H_8)_2$, ramped to 200°C under 5 MPa H_2.

The DSC profile (Fig. 3.5) for $Mg(B_3H_8)_2$ revealed a sharp endothermic step beginning at about 65°C which corresponded to the observed melting of the complex. Beginning at about 90°C, the profile became somewhat convoluted, probably a result of overlapping reaction steps. A small endothermic signal was present at about 100°C, probably due to the decomposition of the $B_3H_8^-$ ring. The subsequent broad exothermic

feature spanning the temperature range of 120-200°C can then be attributed to the aforementioned clustering/condensation process to form larger polyboranes including $B_{12}H_{12}^{2-}$.

3.3.3 *Hydrogenation of dehydrogenated $Mg(BH_4)_2$*

Magnesium borohydride was dehydrogenated for 4 weeks at 200°C, 0 MPa in the PCT. The ^{11}B NMR for the product is given in Fig. 3.6 a, representing a 36% conversion to $Mg(B_3H_8)_2$. Heating of the dehydrogenated material by DSC to 200°C under 5 MPa H_2 resulted in a broad exothermic step with a maximum at approximately 120°C (Fig. 3.7). Comparison with the ^{11}B NMR of the hydrogenated product (Fig. 3.6 b) confirmed that the exothermic reaction could be assigned to the hydrogenation of a portion of the $Mg(B_3H_8)_2$ to $Mg(BH_4)_2$. The disappearance of the $Mg(B_3H_8)_2$ resonance in Fig. 3.6 c after hydrogenation at higher temperature and pressure further corroborated the direct conversion of $B_3H_8^-$ to BH_4^-.

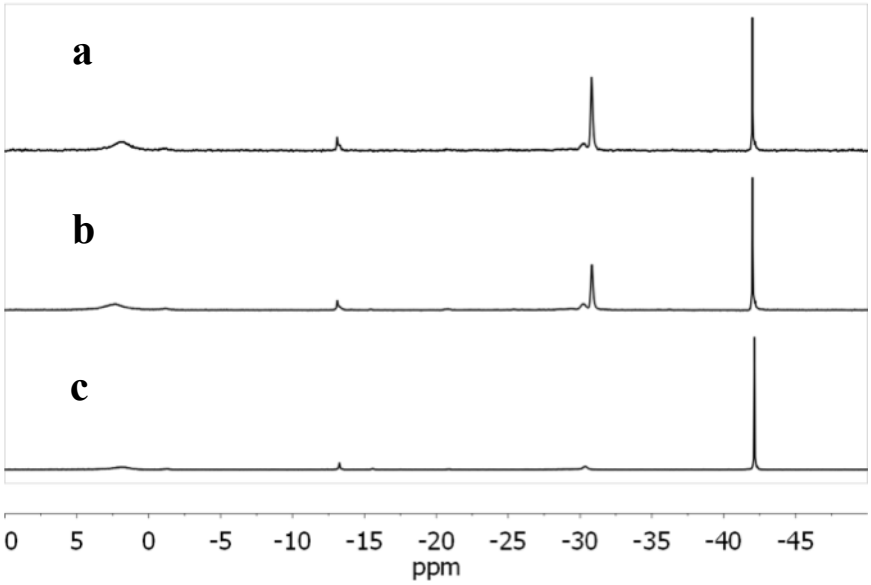

Fig. 3.6 $^{11}B\{^1H\}$ NMR of a) $Mg(BH_4)_2$ dehydrogenated 4 weeks, 200°C; b) rehydrogenation at 200°C, 5 MPa H_2, cooled immediately; c) rehydrogenation at 250°C, 12 MPa H_2, 48 h.

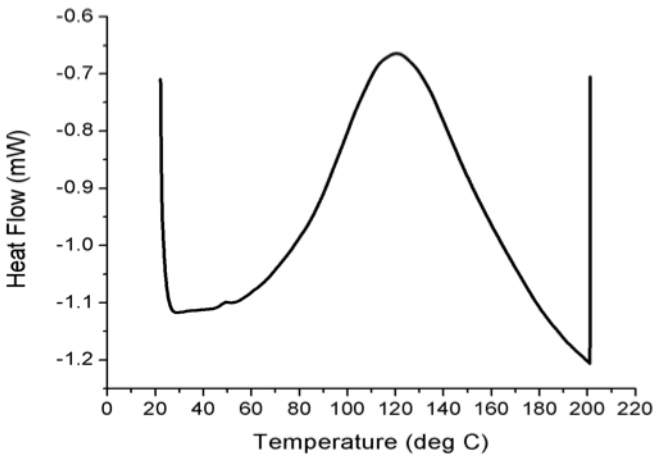

Fig. 3.7 DSC profile of $Mg(BH_4)_2$ (dehydrogenated 5 weeks, 200°C, 0 MPa), ramped to 200°C under 5 MPa H_2.

3.3.4 *Hydrogenation of $Mg(B_3H_8)_2$ and MgH_2*

3.3.4.1 1:2 $Mg(B_3H_8)_2$ to MgH_2

In the decomposition of $Mg(BH_4)_2$ (Eq. 3.1), $Mg(B_3H_8)_2$ and MgH_2 were proposed to form in a 1:2 molar ratio. In order to best simulate the rehydrogenation of the products after dehydrogenation to the $Mg(B_3H_8)_2$ intermediate, as-prepared $Mg(B_3H_8)_2$ and MgH_2 were mixed and then hydrogenated at 200°C for 2 hours under 5 MPa of H_2. The resulting ^{11}B NMR spectrum is given in Fig. 3.8 along with the spectrum for the starting material. $Mg(B_3H_8)_2$, as well as the hydrolyzed open cage boranes at 3 ppm, appeared to convert entirely to $Mg(BH_4)_2$. This verifies that the reaction,

$$Mg(B_3H_8)_2 + 2MgH_2 + 2H_2 \rightarrow 3Mg(BH_4)_2 \qquad (3.3)$$

did indeed take place. The notable absence of $MgB_{12}H_{12}$ suggests that the presence of a metal hydride may alter the hydrogenation mechanism so that $B_{12}H_{12}^{2-}$ does not form.

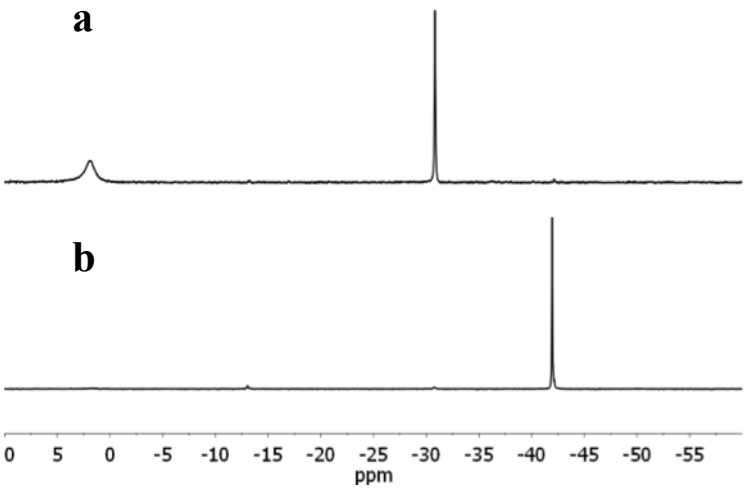

Fig. 3.8 $^{11}B\{^{1}H\}$ NMR of (a) $Mg(B_3H_8)_2$ and MgH_2 before hydrogenation; (b) after hydrogenation at 200°C, 2 h, 5 MPa H_2.

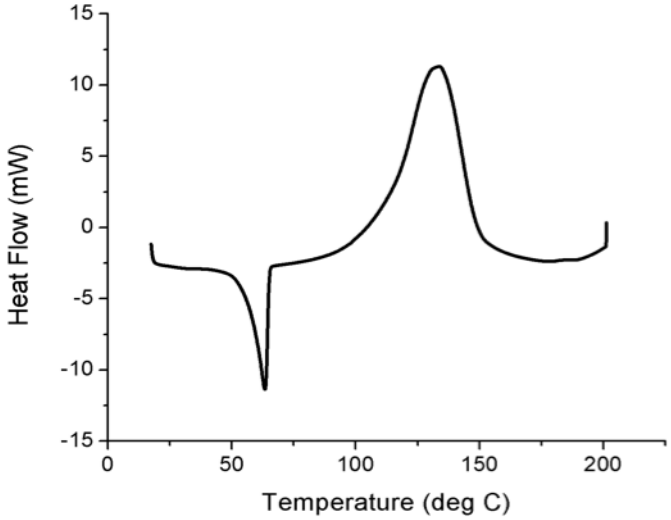

Fig. 3.9 DSC profile of $Mg(B_3H_8)_2$ and MgH_2 (1:2) under 5 MPa H_2.

The DSC for the $Mg(B_3H_8)_2/MgH_2$ mixture (Fig. 3.9) demonstrated that, after melting at 65°C, hydrogenation occurred as a large single exothermic step beginning at 100°C and ending at 160°C. This must correspond to the energetically favorable conversion from $B_3H_8^-$ to BH_4^-. The ^{11}B NMR characterization of the reaction mixture following the DSC experiment gave a 1:2 ratio of $Mg(B_3H_8)_2$ and $Mg(BH_4)_2$. There was also a small shoulder on the $B_3H_8^-$ resonance at –30 ppm that was respresentative of $B_{10}H_{10}^{2-}$ and a small signal at –13 ppm that was mostly likely residual $BH_3{\cdot}THF$. The presence of a significant amount of $Mg(B_3H_8)_2$ remaining after heating to 200°C suggests that more time is needed for the complete conversion to $Mg(BH_4)_2$ than was allowed during the period of immediate cooling after ramping to 200°C in the DSC scan.

^{11}B NMR was also used to characterize hydrogenated samples (5 MPa H_2) at temperatures associated with the start and end of the endo/exothermic steps observed up to 200°C in the DSC profile. At 80°C the mixture was still predominantly $Mg(B_3H_8)_2$, verifying that the endothermic step at about 65°C represents the melting point of the solvated complex. At 105°C and then 130°C increasing levels of $Mg(BH_4)_2$ relative to $Mg(B_3H_8)_2$ were seen. Since no other boron species were observed in the NMR spectra, the large exothermic process was solely attributable to the hydrogenation of $Mg(B_3H_8)_2$ to $Mg(BH_4)_2$.

In order to determine whether dissolution in deuterium oxide affects the speciation of the hydrogenated material in solution, ^{11}B MAS NMR was also used to analyze the final products. The spectra for both the initial mixture and the hydrogenated material are given in Fig. 3.10. The mixture before hydrogenation displayed a single resonance at –22 ppm ($B_3H_8^-$) but after hydrogenation, this signal was replaced by a

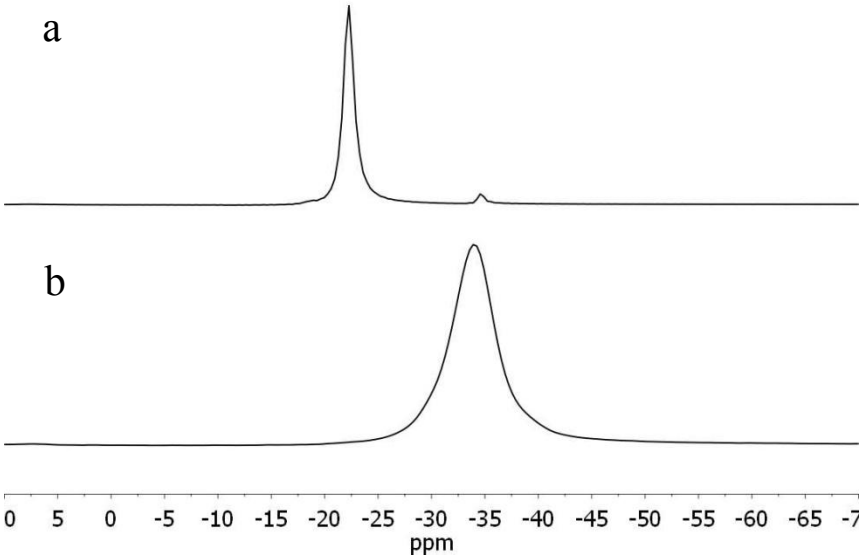

Fig. 3.10 ^{11}B MAS NMR of (a) $Mg(B_3H_8)_2$ and MgH_2 before hydrogenation; (b) $Mg(B_3H_8)_2$ and MgH_2 after hydrogenation at 200°C, 2 h, 5 MPa H_2.

resonance at –31 ppm (BH_4^-). These results confirm that the major species observed in solution state NMR were also the predominant species before dissolution in D_2O.

Although a melting step was not observed in the hydrogenation of decomposed $Mg(BH_4)_2$ (Fig. 3.7) both the authentic sample (dehydrogenated $Mg(BH_4)_2$) and the prepared $Mg(B_3H_8)_2/MgH_2$ mixture displayed a single large exothermic step resulting in a $Mg(BH_4)_2$ product. The energy involved in hydrogenation of the two materials differ: 10 kJ/mol for the dehydrogenated $Mg(BH_4)_2$ and 21 kJ/mol for the $Mg(B_3H_8)_2{\cdot}x$THF/MgH_2 mixture. as The temperature ranges over which decomposition took place also differed, with lower temperatures and a broader range observed for the dehydrogenated sample. The differences in the DSC profiles suggests that the THF adduct has a lower kinetic barrier to hydrogenation, probably arising from its low melting

point which allowed it to be in the liquid state during the reaction. Hydrogenation occurs in both cases, however, without forming other polyborane intermediates.

3.3.4.2 1:1 and 1:4 $Mg(B_3H_8)_2$ to MgH_2

The effect of varying the ratio of $Mg(B_3H_8)_2$ to MgH_2 was investigated. When equimolar amounts of the $Mg(B_3H_8)_2$ and MgH_2 were mixed, DSC analysis and subsequent ^{11}B NMR of the hydrogenated material (ramped to 200°C and immediately cooled) revealed very similar results to that of 1:2 $Mg(B_3H_8)_2$: MgH_2 except for an additional resonance in the ^{11}B NMR representing $B_{10}H_{10}^{2-}$. This suggests that the 1:1 ratio resulted in hydrogenation of a fraction of $Mg(B_3H_8)_2$ without MgH_2, leading to condensation to form $B_{10}H_{10}^{2-}$. The DSC scan for 1:4 $Mg(B_3H_8)_2$ to MgH_2 also exhibited a similar profile to the 1:2 sample but with an additional exothermic step commencing at 190°C which corresponds to the decomposition of the excess MgH_2.[86]

3.3.5 *Hydrogenation of $Mg(B_3H_8)_2$ and LiH*

Based on the stoichiometry determined for the hydrogenation of $Mg(B_3H_8)_2$ and MgH_2 to form $Mg(BH_4)_2$, a molar ratio of 1:4 $Mg(B_3H_8)_2$ to LiH was assumed and used for all trials involving this mixture. ^{11}B NMR analysis of the powder after hydrogenation at 200°C for one hour (Fig. 3.11) yielded major resonances for $B_{12}H_{12}^{2-}$ (–15 ppm), $B_{10}H_{10}^{2-}$ (–30 ppm), and BH_4^- (–42 ppm) in a 2:1:1 ratio of the integrated signal areas. Additional resonances at –13 (residual $BH_3 \cdot THF$) and –22 ppm (unidentified) were also detected. The spectrum for this hydrogenation closely resembled that of $Mg(B_3H_8)_2$ (Fig. 3.4) where the complex was hydrogenated without any metal hydride present. In

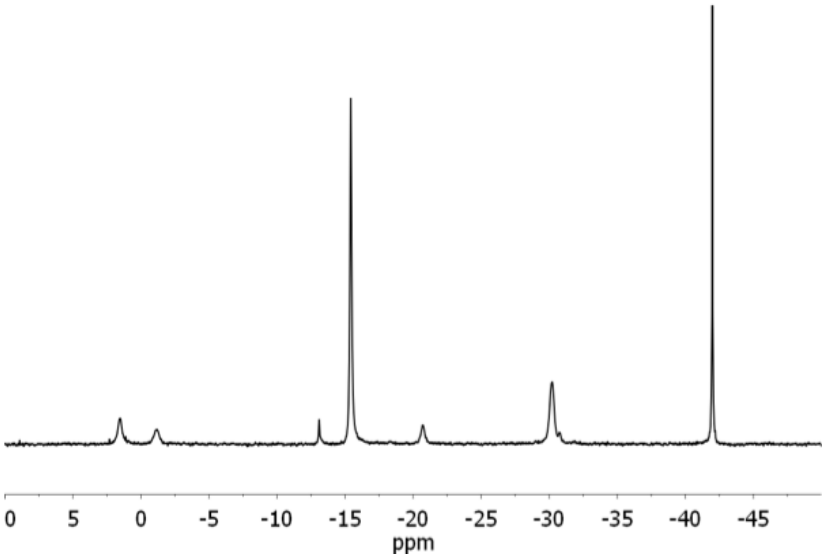

Fig. 3.11 $^{11}B\{^{1}H\}$ NMR of $Mg(B_3H_8)_2$ and LiH (1:4) after hydrogenation at 200°C, 1 h, 5 MPa H_2.

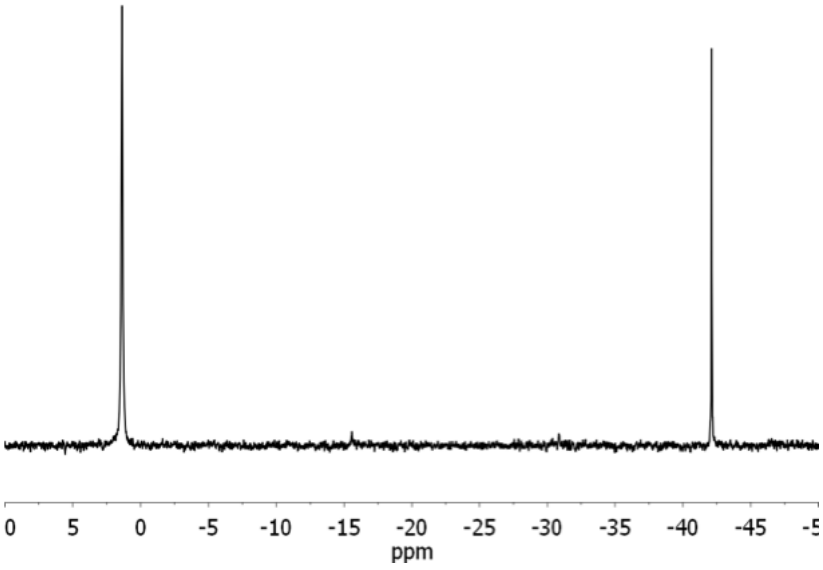

Fig. 3.12 $^{11}B\{^{1}H\}$ NMR of $Mg(B_3H_8)_2$ and LiH (1:4) after hydrogenation to 225°C, 5 MPa H_2, immediately cooled.

contrast, when the mixture was hydrogenated under 5 MPa of H_2 with a temperature ramp up to 225°C followed by immediate cooling, the ^{11}B NMR (Fig. 3.12) featured only two species: BH_4^- and boric acid (indicative of unstable, hydrolysable polyboranes). Finally, when the mixture was hydrogenated for 2.5 days at 7 MPa and 250°C, the ^{11}B NMR of the products indicated that the $B_3H_8^-$ mostly formed BH_4^-, with a small amount of boric acid and trace quantities of $B_{12}H_{12}^{2-}$ and $B_{10}H_{10}^{2-}$.

The DSC measurement under 5 MPa H_2 (Fig. 3.13), corresponding to the reaction represented by Fig. 3.11, displayed the expected endothermic melting process around 60°C followed by a major exothermic step between 120-160° that was both preceded and followed by much smaller signals representing additional exothermic steps. The large peak corresponded to the formation of either $B_{12}H_{12}^{2-}$ or BH_4^- and the smaller signals must then represent conversions to the other B species that were present in the ^{11}B NMR.

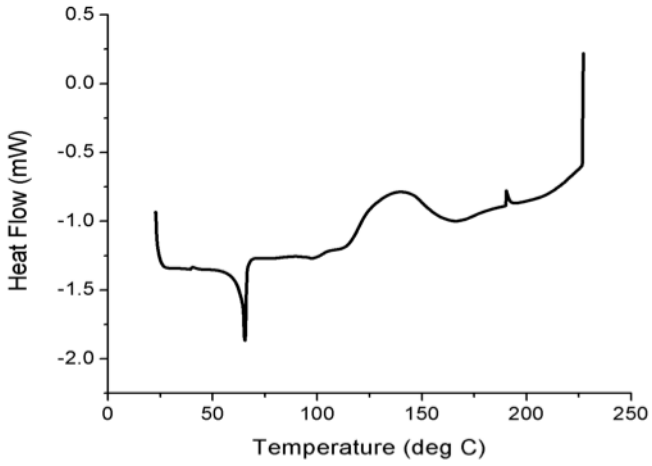

Fig. 3.13 DSC profile of $Mg(B_3H_8)_2$ and LiH (1:4) under 5 MPa H_2.

It appears that temperature is a key factor in dictating which species are formed upon hydrogenation of the $Mg(B_3H_8)_2$/LiH mixture. The available energy at 200°C is evidently insufficient to activate the LiH, thus hydrogenation of the material proceeded as though it consisted of $Mg(B_3H_8)_2$ only. Condensation of the decomposition products of $Mg(B_3H_8)_2$ ultimately resulted in the formation of a series of thermally stable species. An increase in hydrogenation temperature to 225°C was able to facilitate the conversion of all the $Mg(B_3H_8)_2$ to either BH_4^- or higher polyboranes. A further increase in temperature to 250°C as well as a longer heating time led to BH_4^- as the predominant product but also led to the formation of highly stable species ($B_{12}H_{12}^{2-}$, $B_{10}H_{10}^{2-}$) which are either thermodynamically favorable products or formed as intermediates during hydrogenation.

3.3.6 *Hydrogenation of $Mg(B_3H_8)_2$ and NaH*

The same molar ratio from the $Mg(B_3H_8)_2$/LiH mixture was used for $Mg(B_3H_8)_2$ and NaH. Hydrogenation of this mixture to 225°C under 5 MPa H_2 resulted in two main boron species: boric acid, again signifying open-cage boranes, and BH_4^- (Fig. 3.14). Small quantities of $B_{12}H_{12}^{2-}$ and residual $B_3H_8^-$ were also present. The corresponding DSC profile (Fig. 3.15) exhibited two large distinct exothermic steps between 80 and 150°C. The mixture was then hydrogenated at a temperature of 130°C, which is approximately in the middle of the two peaks, in an attempt to assign a specific reaction to each of the exothermic steps. The resulting ^{11}B NMR spectrum is given in Fig. 3.16.

The ^{11}B NMR characterization of the results from the hydrogenation to 130°C (Fig. 3.16) shows a noticeably larger boric acid signal than that of $Mg(BH_4)_2$. Thus, the first heat-evolving step displayed in the DSC profile can be assigned to the formation of

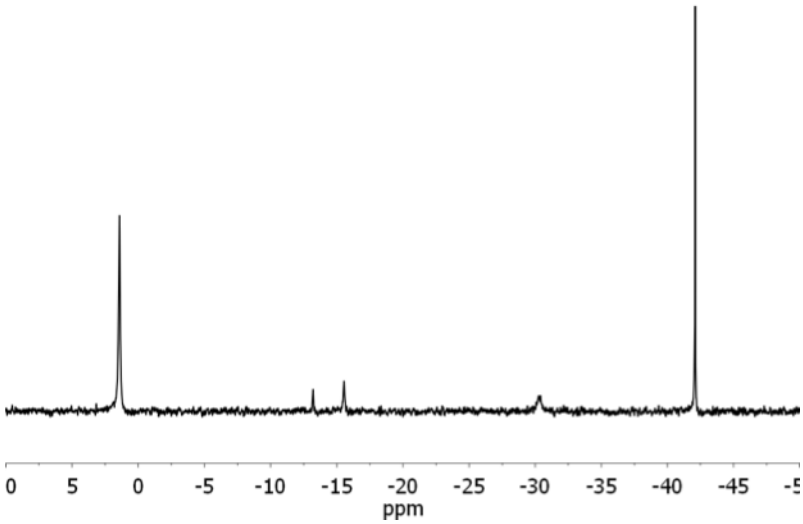

Fig. 3.14 $^{11}B\{^1H\}$ NMR of $Mg(B_3H_8)_2$ and NaH (1:4) after hydrogenation to 225°C, 5 MPa H_2, immediately cooled.

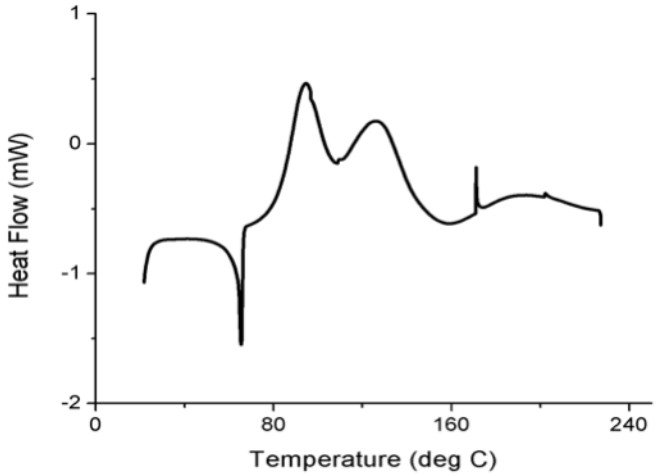

Fig. 3.15 DSC profile of $Mg(B_3H_8)_2$ and NaH (1:4) under 5 MPa H_2.

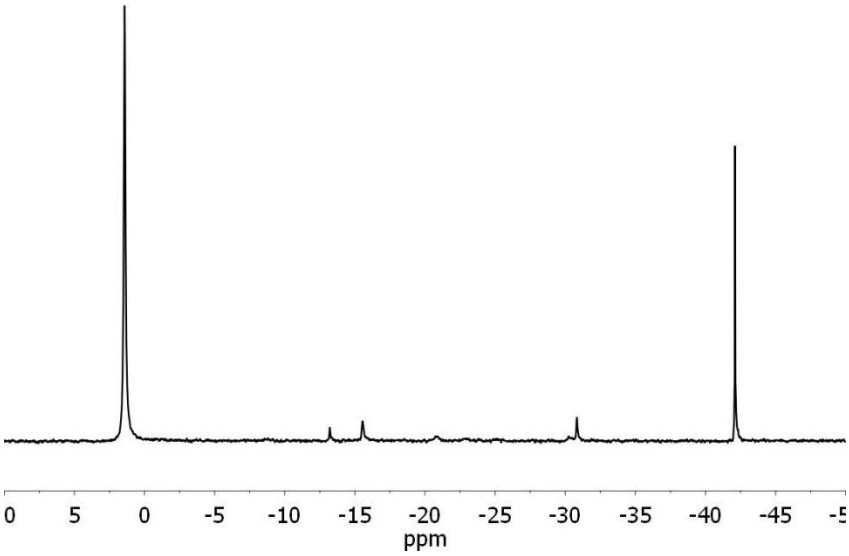

Fig. 3.16 $^{11}B\{^{1}H\}$ spectra of $Mg(B_3H_8)_2$ and NaH (1:4) after hydrogenation to 130°C, 5MPa H_2, immediately cooled.

higher and hydrolysable polyboranes and the subsequent step at higher temperature represents the formation of BH_4^-.

These findings indicate that hydrogenation of $Mg(B_3H_8)_2$ with NaH follows a different route than that of MgH_2 or LiH. Two mechanisms were invoked upon applying hydrogenating conditions: a clustering process in which the initial borane decomposed and proceeded to successively condense and form increasingly large and stable structures, and an alternative route in which the presence of a metal hydride facilitated decomposition to BH_4^-. In the case of MgH_2, the formation of $Mg(BH_4)_2$ was the predominant course and for LiH, the condensation pathway leading to $B_{12}H_{12}^{2-}$ prevailed at insufficient temperatures to activate the metal hydride. At a temperature high enough

to overcome the minimum energy barrier, the formation of BH_4^- and other hydrolysable polyboranes then dominated. For NaH, however, the metal hydride appeared to interact even at low temperature, resulting in the formation of higher, open cage boranes but not the thermally stable $B_{12}H_{12}^{2-}$ and at temperatures >130°C, the BH_4^- pathway dominated the condensation process.

3.3.7 *Hydrogenation trials with NaB_3H_8*

The preparation of NaB_3H_8 according to Hoy[81] has been highlighted as a simple method that avoids the use of diborane as a precursor and results in a solvent-free product. ^1H NMR analysis of our product as prepared by this route confirmed that the complex was not an adduct and residual solvent signals representing diethyl ether were present only at trace levels. The $^{11}B\{^1H\}$ NMR spectrum for as-prepared NaB_3H_8 is given in Fig. 3.17 and again, the prominent peak at –31 ppm represented $B_3H_8^-$, indicating that the chemical shift of $B_3H_8^-$ does not change whether coordinated to Mg^{2+} or Na^+. A scattering of trace signals between –5 to –25 ppm was visible as well as a small resonance at –42 ppm ($NaBH_4$) indicating that this preparation method, while yielding a solvent-free complex, also resulted in formation of other polyboranes.

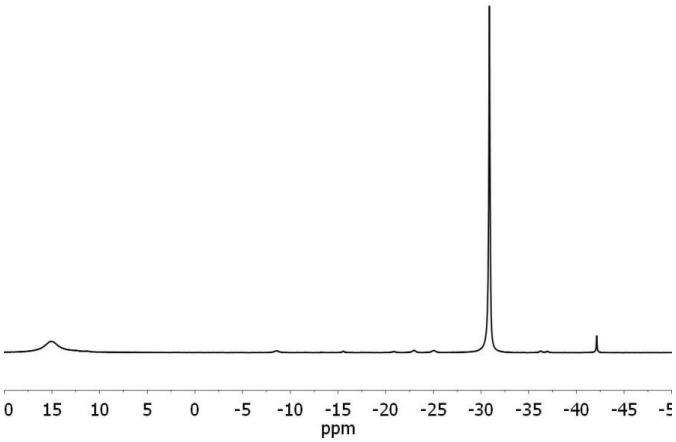

Fig. 3.17 $^{11}B\{^1H\}$ spectra of as-synthesized NaB_3H_8

Using a 2:1 molar ratio of NaH to NaB_3H_8, the mixture was hydrogenated during DSC to 200°C under 5 MPa H_2. The profile exhibited an initial dip at about 55°C, representing the melting of NaB_3H_8, that overlapped with an exothermic step, followed by two large exothermic steps, with maxima at 130 and 170°C. A much a sharper peak was present at 185°C (Fig. 3.18). The ^{11}B NMR spectrum of the hydrogenated powder (Fig. 3.19) suggested that these exothermic reactions represented the formation of unstable polyboranes (appearing as boric acid), BH_4^- and $B_{12}H_{12}^{2-}$. However, it was not clear whether the sharp peak at 185°C in the DSC profile could be attributed to a hydrogenation process or to signal noise. The NMR analysis also revealed small quantities of $B_{10}H_{10}^{2-}$ and the unidentified species at –22 ppm.

The DSC measurement was repeated but with a mixture of NaB_3H_8 and MgH_2 in a 1:1 mole ratio. The DSC profile (Fig. 3.20) revealed three overlapping exothermic steps between 100-200°C, two of which corresponded to the formation of BH_4^- and $B_{12}H_{12}^{2-}$ in equal amounts as confirmed by ^{11}B NMR analysis (not shown). The NMR spectrum again displayed small resonances at –22 ppm and –30 ppm ($B_{10}H_{10}^{2-}$) either of which could account for the third exothermic peak. Less boric acid was observed in this hydrogenated product than the NaB_3H_8/NaH mixture. Hydrogenating the same mixture for 24 hours resulted in an increase in the quantity of $B_{12}H_{12}^{2-}$ relative to BH_4^- as well as an increase in the formation of open cage polyboranes.

The results for the hydrogenation of NaB_3H_8 with either NaH or MgH_2 show interesting similarities to that of $Mg(B_3H_8)_2$. In spite of being solvent-free, the NaB_3H_8 melted at a lower temperature than $Mg(B_3H_8)_2$. This may provide an explanation for why it has not been observed experimentally: if it does form upon dehydrogenation of $NaBH_4$,

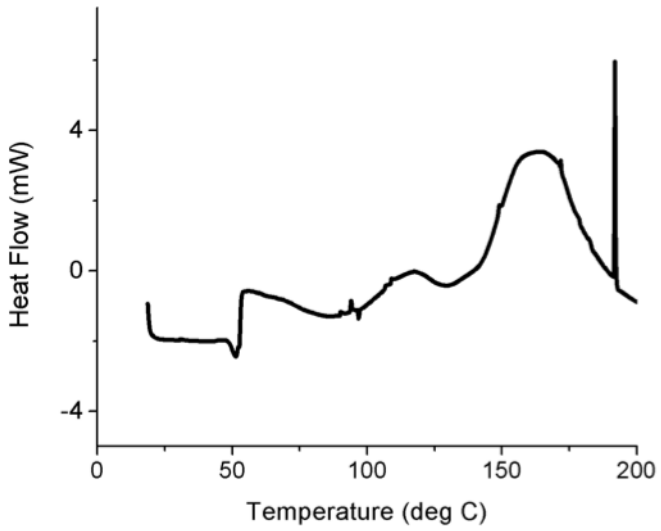

Fig. 3.18 DSC profile of NaB_3H_8 and NaH (1:2) under 5 MPa H_2.

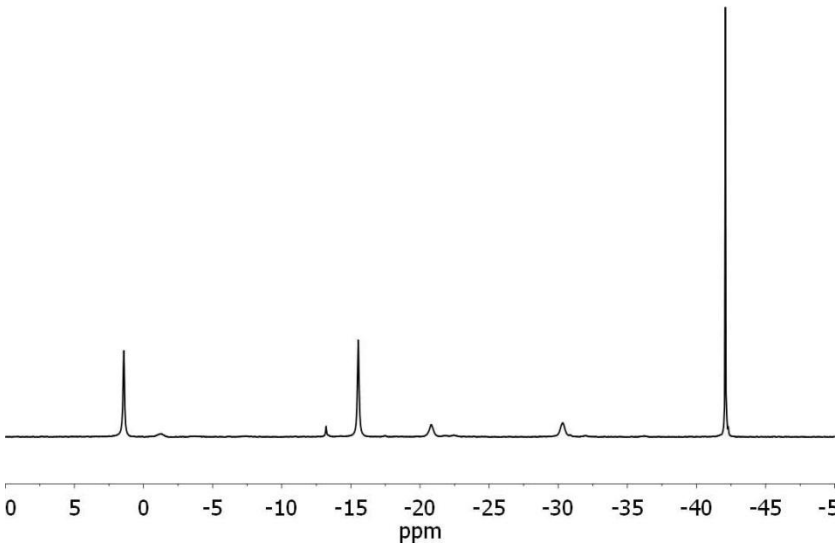

Fig. 3.19 $^{11}B\{^1H\}$ NMR of NaB_3H_8 and NaH (1:2) after hydrogenation to 200°C, 5 MPa H_2, immediately cooled.

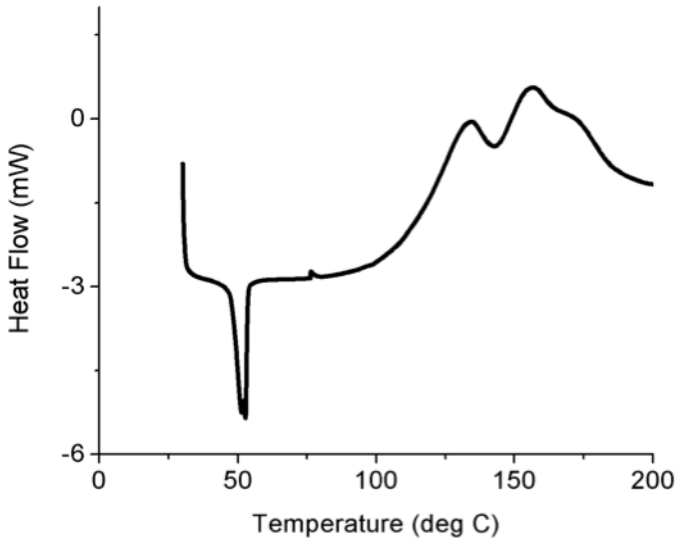

Fig. 3.20 DSC profile of NaB_3H_8 and MgH_2 (1:1) under 5MPa H_2.

its low melting point does not allow it to persist long in the solid state. Any NaB_3H_8 formed would immediately melt and condense to higher boranes. Our findings suggest that the presence of sodium tends to promote the formation of other polyboranes, most notably $B_{12}H_{12}^{2-}$ (in the case of NaB_3H_8) and unstable, open cage species (in the case of NaH). This was supported by the DSC profiles for both the $Mg(B_3H_8)_2$/NaH and NaB_3H_8/metal hydride mixtures, clearly showing at least two exothermic steps in the 100-200°C temperature range.

3.4 *Conclusions*

From these trials it is clear that the hydrogenation of $Mg(B_3H_8)_2$ back to $Mg(BH_4)_2$ occurs readily, indicating that it is a thermodynamically favorable pathway with much faster kinetics than the reverse reaction. The formation of $Mg(BH_4)_2$ from the

initial $Mg(B_3H_8)_2$/metal hydride mixture is consistently exothermic, indicating that the reverse reaction (i.e. dehydrogenation to $Mg(B_3H_8)_2$) requires greater thermal input to overcome both thermodynamic and kinetic barriers. One of the goals of these studies was to elucidate the role of the metal hydride in the formation of BH_4^-. From the NMR results, it can be seen that in the absence of MgH_2, hydrogenation of $Mg(B_3H_8)_2$ without a hydride source results in disproportionation to a mixture of $MgB_{12}H_{12}$, $MgB_{10}H_{10}$, $Mg(BH_4)_2$ and open cage polyboranes.

Upon addition of at least 2:1 MgH_2 to $Mg(B_3H_8)_2$, $Mg(BH_4)_2$ becomes the primary product after hydrogenation. The MgH_2 evidently has an active role in directing the hydrogenation path to yield only $Mg(BH_4)_2$. According to the mechanism proposed in Chapter 2, initial formation of diborane releases two hydridic anions to an available Mg^{2+}. Thus, during hydrogenation, the transfer of hydridic anions from the metal hydride to the $B_3H_8^-$ structure must be critical towards breaking B-B bonds.

The stabilities of LiH, NaH, and MgH_2 are respectively –181.6, –113, and –74.5 kJ/mol H_2.[20] The experiment substituting LiH for MgH_2 revealed that temperatures >200ºC are necessary to allow the transfer of H^- from LiH to the $B_3H_8^-$ ring. With NaH, hydrogenation follows a different path and occurs over two distinct exothermic steps. The intial reaction can be assigned to the formation of *arachno*- or *nido*-boranes and the subsequent step at higher temperature results in the formation of BH_4^-. A summary of the hydrogenation trials with $Mg(B_3H_8)_2$ is given in Fig. 3.21.

Our results confirm that the hydrogenation to BH_4^- becomes increasingly favorable and direct, the more readily the metal hydride can decompose. Cycling

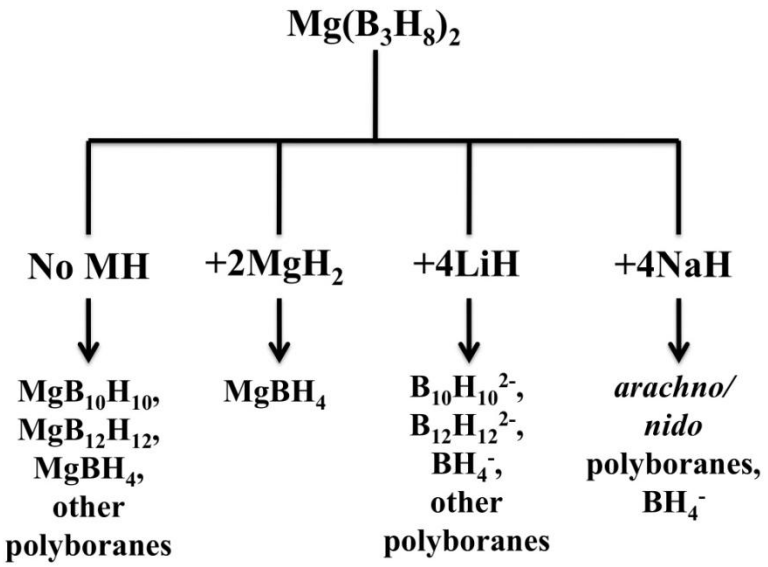

Fig. 3.21 Schematic of hydrogenation pathways of $Mg(B_3H_8)_2$ at 200°C, 5 MPa H_2 with no metal hydride (MH) and with the different metal hydrides studied.

between $Mg(B_3H_8)_2$ and $Mg(BH_4)_2$ is a single step reaction and avoids the formation of $MgB_{12}H_{12}$ as long as a metal hydride is present that can act as a hydride donor at the hydrogenation temperature used. This hydrogenation path seems to be unique to the Mg system; hydrogenation of NaB_3H_8, in contrast, consistently yields $B_{12}H_{12}^{2-}$ as a major product with both NaH and MgH_2.

An interesting experiment to conduct as a continuation of these studies is the hydrogenation of $Mg(B_3H_8)_2$ with a metal hydride of lower stability than MgH_2, such as a transition metal hydride. In mixtures involving different metals, ie. $Mg(B_3H_8)_2$/LiH or $Mg(B_3H_8)_2$/NaH, the products could only be characterized according to ^{11}B NMR and the metal cation to which the borane was coordinated could be not identified. Therefore hydrogenation with a less stable metal hydride may generate either a borohydride complex that undergoes dehydrogenation more readily than $Mg(BH_4)_2$, or perhaps a

unique bimetallic complex with new thermodynamic properties. The concept of bimetallic complexes for thermodynamic modification is appropriately the focus of the next chapter.

CHAPTER 4 DEHYDROGENATION STUDIES OF THE BIMETALLIC BOROHYDRIDES

4.1 *Introduction*

The lightweight group I borohydrides (ie. Li, Na, K) have some of the highest hydrogen weight capacities amongst the various complex hydrides that have been investigated for hydrogen storage. These complexes, however, have thermodynamic and kinetic barriers that prevent fast dehydrogenation under mild conditions. For example, lithium borohydride, $LiBH_4$, liberates 80% of its hydrogen at a minimum temperature of 653 K,[39] significantly higher than the typical operating temperatures of PEM fuel cells. Attempts to enhance the kinetics of dehydrogenation, including the incorporation of additives[39,40,87] and nanostructuring,[88–90] have proven to be effective ways to lower dehydrogenation temperatures as well as increase dehydrogenation rates. The stabilities of these borohydrides, however, are intrinsic properties that cannot be altered using the same techniques that have demonstrated success towards improving dehydrogenation kinetics.

Destabilization of the Group I borohydrides has been achieved by adding a metal known to form a comparatively less stable borohydride complex. This was demonstrated by Vajo *et al*. where $LiBH_4$ and MgH_2 were mechanically milled with 2-3 mol % $TiCl_3$ as a catalyst.[59] Dehydrogenation proceeded according to

$$LiBH_4 + 1/2MgH_2 \Leftrightarrow LiH + 1/2MgB_2 + 2H_2 \quad (4.1)$$

The formation of MgB_2 was found to stabilize the dehydrogenated state, consequently destabilizing the initial hydrogenated state, and effectively lowering the enthalpy of

dehydrogenation by 25 kJ/mol. These results initiated a new direction in the search for a hydrogen storage material: thermodynamic tuning through the use of additives.

The next step in the investigation of thermodynamic modification was to develop a rational strategy for choosing appropriate metal mixtures. One study utilized DFT calculations to predict which combinations of lightweight complexes with different metal hydrides had potential for reversibility.[63] These mixtures consisted primarily of Group I and II metals but also included several transition metals. Of the transition metals tested, scandium was found to show the greatest promise towards lowering the dehydrogenation temperature of Group I borohydrides due to the formation of highly stable scandium boride. Concomitantly, high throughput screening of borohydrides of the first row transition metals provided valuable insight into which of these metals may have appropriate physical properties.[66]

The volatility of transition metal borohydrides under ambient temperatures and pressures has been known since the middle of the 20th century.[91] While alkali metals form highly stable ionic interactions with BH_4^- and require high energy input in order to facilitate dehydrogenation, the transition metals bond covalently with the borohydride anion.[92] As a result, the transition metal borohydrides are often highly reactive with much lower dehydrogenation temperatures than the Group I complexes.[91] This issue, along with the evolution of diborane during decomposition, has eliminated the majority of the transition metal borohydrides from the pool of complex hydrides with hydrogen storage potential.

The high throughput screening of the transition metal borohydrides, while confirming that most transition metals were indeed unsuitable for hydrogen storage,

revealed that the Sc and Mn borohydride complexes were stable at room temperature and appeared to evolve much less diborane upon thermolysis.[66] Resolution of the structures of these complexes, however, proved to be a challenge that motivated subsequent characterization studies.

Another concurrent study presented a basis for the apparent stabilities of the different borohydride complexes by calculating the enthalpies and temperatures of dehydrogenation. The relationship between the electronegativity of the borohydride cation and the stability of the complex has been known since 1955[93] but was more recently revived by Nakamori *et al*.[41] The enthalpy of formation, ΔH_f, of the borohydride complex and the Pauling electronegativity, χ_p, of the metal cation, were calculated to follow a linear correlation described as $\Delta H_f = 248.7\chi_p - 390.8$. This relationship was also linked to the dehydrogenation temperature of the metal borohydride.

The results of the trials on the $LiBH_4/MgH_2$ composite, supported by the noted subsequent studies, ultimately led to the proposition that the thermodynamic stability could be tuned by combining metal cations of different electronegativities and therefore stabilities.[60,64] This theory was confirmed in a study by Nickels *et al*. in which heating $LiBH_4$ and KBH_4 together under vacuum was found to form the new species $LiK(BH_4)_2$ with a lattice structure incorporating both metals as counterions to the borohydride units.[94] The dehydrogenation temperature of this complex fell mid-way between those of $LiBH_4$ and KBH_4. It was then speculated that a bimetallic complex incorporating two metals with greater differences in electronegativities, i.e. a highly stable metal, such as Li or Na, with an overly volatile one, such as a transition metal, might result in a species with a stability appropriate for reversible hydrogen storage.

Over recent years, several studies have been published on the synthesis and dehydrogenation of mixed metal borohydrides.[64,65,67–69,71,95] Of the many different combinations examined, vibrational spectroscopy revealed that scandium[68] and manganese[70] have a tendency to form anionic borohydride species, ie. $Sc(BH_4)_4^-$ and $Mn(BH_4)_3^-$, which are then charge-balanced by alkali metal cations to form the neutral bimetallic complex. The anionic transition metal borohydrides have been found to be less volatile than their neutral counterparts[68,69,65] and dehydrogenation of these more stable borohydrides may avoid the release of diborane.

Studies investigating the dehydrogenation behavior of the Group I scandium borohydrides have revealed that upon heating, these compounds decompose into ScB_2[67,71] and the corresponding alkali borohydride.[67,69] While the predicted decomposition pathway of $LiSc(BH_4)_4$ consisted of numerous steps, diborane was not found to be a thermodynamically favorable intermediate or product.[71] Multiple hydrogen releasing steps were also detected during the thermal dehydrogenation of $NaSc(BH_4)_4$ but the decomposed material was not characterized.[67] In the case of $KSc(BH_4)_4$, two steps involving mass loss were observed which released a lower weight percent in total than the calculated hydrogen content of the starting material.[69] This convinced the authors that the evolution of diborane was unlikely.

The available data for the complex manganese borohydrides is rather limited in comparison to that for the complex scandium borohydrides, largely due to the difficulty in analyzing manganese compounds.[70] Interestingly, the mechanical milling of $LiBH_4$ with $MnCl_2$ resulted in the formation of neutral $Mn(BH_4)_2$ in contrast to the bimetallic complex produced upon milling with $NaBH_4$. Dehydrogenation of $Na_2Mn(BH_4)_4$ under

mild conditions (120-150°C) evolved much less hydrogen gas than the hydrogen content of the complex. Unfortunately, the material could not be detected by XRD or characterized by NMR due to the amorphous nature of the powder and paramagnetic property of Mn, but was tentatively assigned a structure based on vibrational spectroscopy data and DFT calculations. The potassium analogue, $K_2Mn(BH_4)_4$ has been synthesized recently and its structure resolved by *in situ* synchrotron radiation powder X-ray diffraction data.[96] Decomposition was found to proceed via the formation of KBH_4 and $KMn(BH_4)_3$ although the authors state that the identification of the latter species was somewhat ambiguous.[96]

We present a detailed characterization of the dehydrogenation products of the complex alkali scandium borohyrides by nuclear magnetic resonance (NMR) spectroscopy and analysis of the gas-phase products of both the complex scandium and manganese borohydrides by *in situ* infrared (IR) spectroscopy. Recently, the gaseous decomposition products of borohydride complexes have been analyzed by a combination of Fourier-Transform infrared (FTIR) spectroscopy and thermogravimetry (TG) that was developed to circumvent the conventional issues preventing the quantitative measurement of gases by mass spectrometry.[57] By this method it was determined that while solvent-free $Mg(BH_4)_2$ and $LiBH_4$ do not emit significant amounts of diborane, for $LiZn_2(BH_4)_5$, diborane is a major product during decomposition. The release of diborane is a critically important factor in determining the viability of a potential hydrogen storage material and thus its detection is an invaluable tool in evaluating the usefulness of the bimetallic borohydrides.

4.2 *Experimental*

4.2.1 *NMR spectroscopy*

Solid state Magic angle spin (MAS) NMR spectra were obtained on a Varian Inova spectrometer equipped with a 3.2 mm HX cross-polarization magic-angle spinning probe (Varian Chemagnetics, Ft. Collins, CO) at 128.3 and 97.2 MHz for ^{11}B and ^{45}Sc. Samples were packed into 3.2 mm zirconium oxide rotors and spun at 12 kHz. Single-pulse excitation was used with pulse widths of 1.0 and 6.0 μs for ^{11}B and ^{45}Sc respectively. Frequencies are reported with respect to boric acid for ^{11}B and aqueous $ScCl_3$ for ^{45}Sc (set at 0 ppm).

4.2.2 *IR spectroscopy for characterization of complex borohydrides*

IR spectra were obtained for ballmilled powders on a Shimadzu IRAfinity-1 FTIR. Samples were pressed into KBr pellets in the glovebox and loaded into an airtight sample holder prior to measurement.

4.2.3 *In situ TG-IR*

Samples were loaded into a magnetic suspension balance (Rubotherm, Bochum) modified to allow for the measurements to take place under controlled gas flow. The system was connected to an infrared gas analyser (Bruker Alpha spectrometer equipped with a 8 cm gas cell at a resolution of 0.9 cm^{-1}). Dehydrogenation reactions were conducted under 150 mL/min hydrogen flow at 1 bar. A detailed description of the experimental set-up can be found in a previous study.[57]

4.2.4 *Synthesis of complex borohydrides*

All sample preparation and manipulation was performed in an argon glovebox. Anhydrous $ScCl_3$ (Alfa Aesar, 99.9%) and either lithium (Alfa Aesar, 95%), sodium (Sigma-Aldrich, 99%), or potassium (Alfa Aesar, 98%) borohydride were added to 80 mL stainless steel vessels and milled under an argon atmosphere in a Fritsch Pulverisette 7 planetary mill with a 10 mm ball to sample mass ratio of approximately 35:1. Similarly, anhydrous $MnCl_2$ (Alfa Aesar, 97%) was ballmilled with either Li, Na, or K borohydride. Conditions for ballmilling are given in Table 4.1. Samples were characterized after ballmilling by IR spectroscopy and ^{11}B and ^{45}Sc MAS NMR (for the complex scandium borohydrides).

Table 4.1 Mechanical milling conditions for preparation of complex borohydrides

Mixture	Molar ratio	Milling speed (rpm)	Milling time (h)
$LiBH_4$+$ScCl_3$	4:1	350	10
$NaBH_4$+$ScCl_3$	2:1	350	20
KBH_4+$ScCl_3$	1.5:1	350	10
$LiBH_4$+$MnCl_2$	2:1	350	1.5
$NaBH_4$+$MnCl_2$	4:1	350	10
KBH_4+$MnCl_2$	2:1	350	16

4.2.5 *Thermal Dehydrogenation Studies*

Alkali metal scandium borohydride complexes were dehydrogenated isothermally for NMR analysis on a Suzuki Shokan PCT-2SDWIN Sievert type apparatus. The samples were heated to 473 K with a customized heating sleeve in an initially evacuated fixed volume reactor for 24 hours.

4.3 *Results and Discussion*

4.3.1 *NMR characterization of starting complexes and dehydrogenated products*

The preparation of bimetallic complexes by mechanical milling followed literature methods[67–70] and crystal structures have been determined for the majority of the complexes with the exception of $Na_2Mn(BH_4)_4$. This technique has been found to be the most successful way to prepare solvent-free materials.

4.3.2 *$LiBH_4$/ $ScCl_3$*

The ^{11}B MAS NMR spectrum of the ballmilled sample is given in Fig. 4.1 along with the spectra for the dehydrogenated materials after trials conducted at 373, 473, and 573 K. Prior to dehydrogenation, the ballmilled powder consisted predominantly of $LiSc(BH_4)_4$, depicted as a large resonance at –17 ppm in the ^{11}B NMR analysis with a secondary species representing residual $LiBH_4$ at –34 ppm.[71] After dehydrogenation for 1 day at 373 K, very little change was observed in the ^{11}B MAS NMR of the products but dehydrogenation at 473 K found that the materials decomposed to $LiBH_4$. Dehydrogenation for 1 week at 573 K yielded the same result.

The presence of a single resonance at 105 ppm in the ^{45}Sc MAS NMR (Fig. 4.2 a) confirmed the complete reaction of $ScCl_3$ to form $LiSc(BH_4)_4$.[71] Dehydrogenation at 373 K also did not present any change in the ^{11}B or ^{45}Sc MAS NMR results (Figs. 4.1 b and 4.2 b) but the powder exhibited a distinct color change from white to orange. A change in color is indicative of an electronic transition in the Sc and although the Sc spectra appear identical before and after dehydrogenation at 373 K, a small quantity of a species such as ScB_x must have formed.

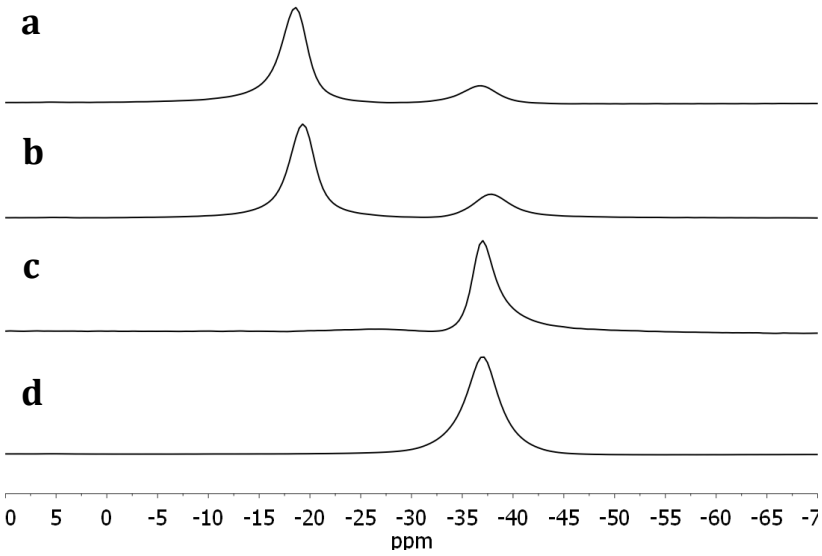

Fig. 4.1 ^{11}B MAS NMR of (a) $LiSc(BH_4)_4$ and then after dehydrogenation at (b) 373 K, 1 day; (c) 473 K, 1 day; d) 573 K, 1 week.

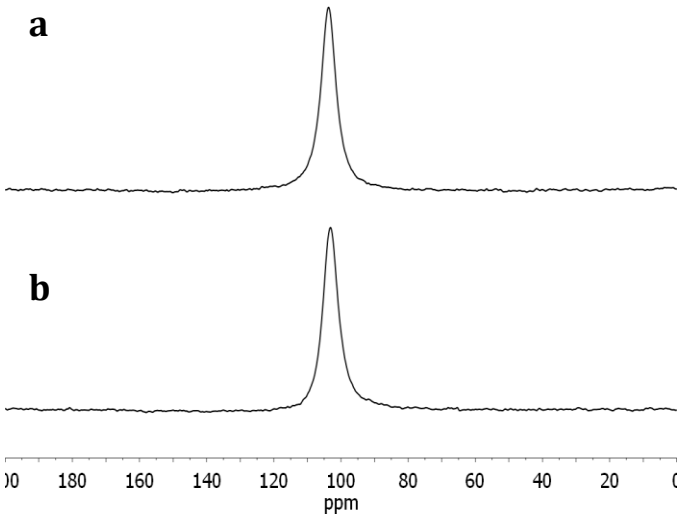

Fig. 4.2 ^{45}Sc MAS NMR of (a) $LiSc(BH_4)_4$; (b) after dehydrogenation at 373 K.

At a higher dehydrogenation temperature of 473 K, however, the B is completely converted to $LiBH_4$ (Fig. 4.1 c). Prolonged dehydrogenation at 573 K produced similar results, confirming that the complex simply decomposes to the thermally stable Group I borohydride upon heating. Attempts to observe a ^{45}Sc signal were unsuccessful for which there are two possible explanations. A paramagnetic phase of ScB_x may have formed or the Sc in the dehydrogenated material was contained within a highly asymmetric environment resulting in extreme broadening of the signal. Both scenarios would effectively prevent detection by NMR. It was unlikely, however, that the Sc was in a paramagnetic state as a precursory test with a bar magnet indicated that there were no magnetic species present. In addition, no secondary paramagnetic effect was observed in the ^{11}B MAS NMR results. Quadrupolar broadening appeared to be the most probable explanation, also accounting for the absence of a boride resonance in the ^{11}B MAS NMR since the B would also experience asymmetric bonding.

The results of characterization by NMR confirmed that the starting material consisted of a mix of lithium scandium borohydride and lithium chloride[68] (as well as unreacted $LiBH_4$) in the following reaction:

$$4LiBH_4 + ScCl_3 \rightarrow LiSc(BH_4)_4 + 3LiCl \qquad (4.1)$$

Low temperature dehydrogenation succeeded in initiating enough decomposition to effect a change in color, again suggestive of a new Sc species such as ScB_x. Once the dehydrogenation temperature reached 473 K, the ^{11}B MAS NMR spectrum indicated that $LiSc(BH_4)_4$ had decomposed to $LiBH_4$. The decomposition very likely follows a path similar to that of $LiZn_2(BH_4)_5$[57] which was found to disproportionate into the corresponding Group I and transition metal borohydrides,[57] or $LiBH_4$ and the unstable

$Sc(BH_4)_3$ in our case, followed by rapid decomposition of $Sc(BH_4)_3$. The process may or may not include the formation of diborane. The dehydrogenation reaction can be described as (assuming no diborane evolution):

$$LiSc(BH_4)_4 \rightarrow LiBH_4 + Sc(BH_4)_3 \rightarrow LiBH_4 + ScB_x + 6H_2 \quad (4.2)$$

As noted earlier, neither the ^{11}B or ^{45}Sc NMR demonstrated any evidence for the formation of ScB_x. Scandium boride has been found to exist in various nonstoichiometric combinations such as ScB_{12} and ScB_{19},[97] further supporting the likelihood of quadrupolar signal broadening.

Dehydrogenation at both 673 and 723 K of ballmilled $ScCl_3$ and $LiBH_4$ has previously been found to produce a mixture of ScB_2, $B_{12}H_{12}^{2-}$, and $LiBH_4$.[55,71] Our findings show that even the low temperature dehydrogenation promotes the decomposition of $LiSc(BH_4)_4$ to the more stable $LiBH_4$ along with the highly volatile $Sc(BH_4)_3$ species which immediately dehydrogenates to scandium boride. With higher temperatures, the mixture of $LiBH_4$ and scandium boride proceeds to decompose according to the well-studied lithium borohydride dehydrogenation pathway[39,52,98,99] which includes the formation of $LiB_{12}H_{12}$.

The powder that had been dehydrogenated for 1 day at 473 K was returned to the reaction vessel and hydrogenated for 2 days at 523 K under 12 MPa H_2 pressure. Surprisingly, the ^{11}B MAS NMR spectrum showed a small amount of $B_{12}H_{12}^{2-}$ (-15 ppm,[55] Fig. 4.3 b), a species known to be a thermally stable decomposition product. The metal cation could be either Sc^{2+} or Li^{+} as both these species as $B_{12}H_{12}^{2-}$ complexes have a similar chemical shift in ^{11}B MAS NMR.[55] The formation of $B_{12}H_{12}^{2-}$ may arise from the presence of a variety of boron compounds that are present in the ^{11}B MAS spectrum

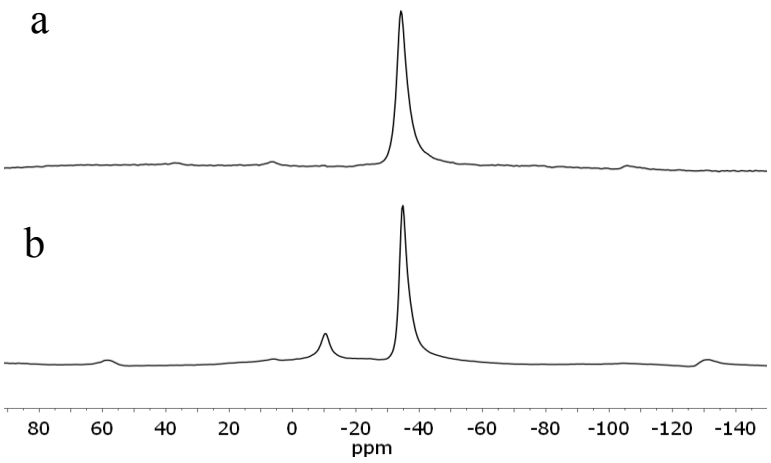

Fig. 4.3 ^{11}B MAS NMR of (a) $LiSc(BH_4)_4$ dehydrogenated 473 K, 1 day; (b) rehydrogenated at 523 K, 2 days, 12 MPa.

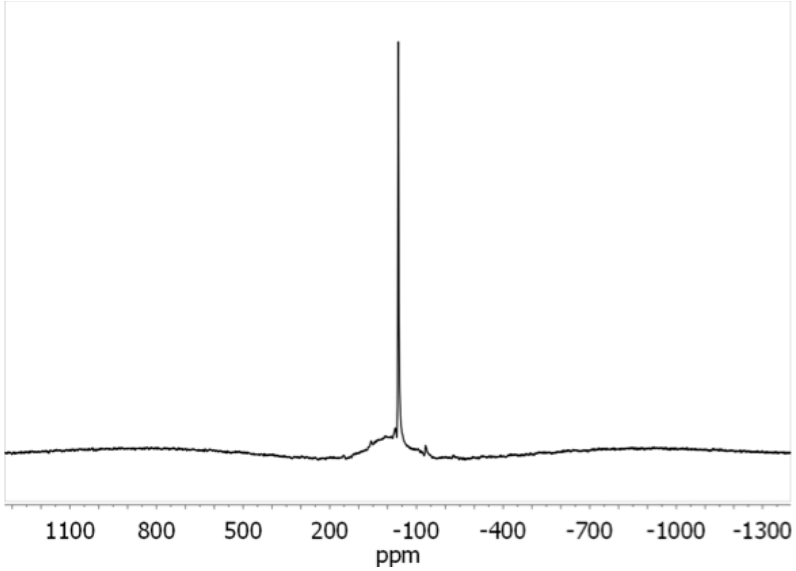

Fig. 4.4 ^{11}B MAS NMR of $LiSc(BH_4)_4$ dehydrogenated 473 K, 1 day with expanded scale.

of dehydrogenated $LiSc(BH_4)_4$, appearing as a large broad feature that overlaps with the $LiBH_4$ resonance (Fig. 4.4). These unresolved signals likely represent an array of boron hydrides with similar chemical shifts which, upon heating, condense to form $B_{12}H_{12}^{2-}$.

Reversible dehydrogenation of $LiSc(BH_4)_4$ does not appear possible under these thermal conditions. While the decomposition of the complex occurs readily, the resulting formation of $LiBH_4$ will then require much higher temperatures to continue decomposing. Hydrogenation to regenerate the original borohydride is extremely unlikely as this would first require the decomposition of $LiBH_4$ and scandium boride to allow $Sc(BH_4)_4^-$ to form. The presence of $Li_2B_{12}H_{12}$ after rehydrogenation at 523 K further emphasizes the preference for the system to convert to more thermodynamically stable species. Once $Li_2B_{12}H_{12}$ has formed, it is essentially impossible to hydrogenate this species to $LiBH_4$ and then to $LiSc(BH_4)_4$ under practical operating conditions.

4.3.3 *$NaBH_4$/ $ScCl_3$*

Two primary resonances are evident in the ^{11}B MAS NMR spectra (Fig. 5.5 a) for the ballmilled mixture, $NaBH_4/ScCl_3$, representing $NaBH_4$ at –37 ppm and a larger signal centered around –18 with a small shoulder that has been attributed to two different B environments in $NaSc(BH_4)_4$.[67] More complete conversion to $NaSc(BH_4)_4$ has been demonstrated by ballmilling under the same conditions[67] but in our case, even ballmilling an additional 20 hours did not increase the yield of $NaSc(BH_4)_4$. While the ^{11}B MAS NMR confirmed that more of the boron in the sample was found in $NaSc(BH_4)_4$ than in $NaBH_4$, the ^{45}Sc MAS NMR (Fig. 4.6 a) showed that the major portion of the Sc content

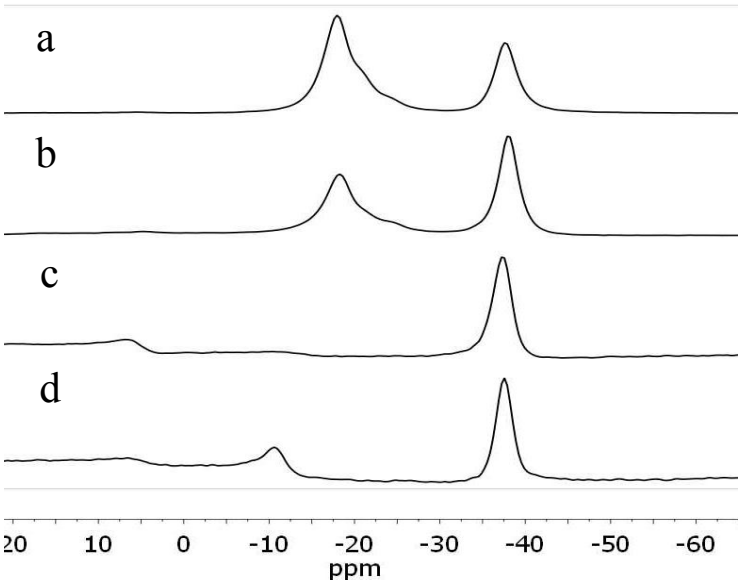

Fig. 4.5 ^{11}B MAS NMR of (a) $NaSc(BH_4)_4$; (b) after dehydrogenation at 373 K, 1day; (c) after dehydrogenation at 473 K, 1 day; (d) rehydrogenation of powder from (c) at 523 K, 5 days, 12 MPa.

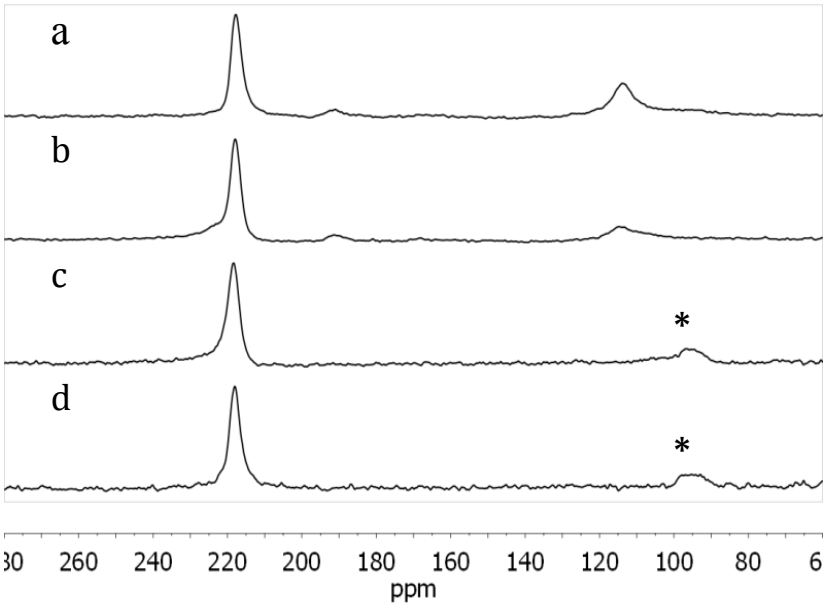

Fig. 4.6 ^{45}Sc MAS NMR of (a) $NaSc(BH_4)_4$; (b) after dehydrogenation at 373 K, 1day; (c) after dehydrogenation at 473 K, 1 day; (d) rehydrogenation of powder from (c) at 523 K, 5 days, 12 MPa. Asterisks denote spinning sidebands.

was bound in Na_3ScCl_6 (219 ppm) rather than $NaSc(BH_4)_4$ (115 ppm).[67] Trace levels of an unidentified Sc species at 190 ppm was present as well.

From the above results it appears that the ballmilling preparation produced:

$$4NaBH_4 + 2ScCl_3 \rightarrow NaSc(BH_4)_4 + Na_3ScCl_6 \quad (4.3)$$

although a significant amount of unreacted $NaBH_4$ remained. According to ^{11}B MAS NMR (Fig. 4.5 b), the dehydrogenation at 373 K resulted in an increase in $NaBH_4$ with a concomitant decrease in $NaSc(BH_4)_4$. The ^{45}Sc MAS NMR spectrum also depicted a noticeable decrease in the Sc associated with $NaSc(BH_4)_4$ which, without evidence for any new Sc species, either formed more Na_3ScCl_6 or decomposed to scandium boride. The same change in color from white to orange that occurred when $LiSc(BH_4)_4$ was decomposed at 373 K was observed for this sample as well.

At 473 K, dehydrogenation promoted the complete decomposition of $NaSc(BH_4)_4$ to $NaBH_4$ with a trace amount of an oxidized boron species at about 8 ppm (Fig. 4.5 c), indicating some exposure of the sample to atmosphere. The $NaSc(BH_4)_4$ resonance in the ^{45}Sc MAS NMR spectrum is no longer visible (Fig. 4.6 c) and only Na_3ScCl_6 was evident after dehydrogenation at 473 K. It is difficult to determine from the ^{45}Sc MAS NMR what the fate of the Sc released from $NaSc(BH_4)_4$ upon decomposition may have been. It is unlikely that it formed more Na_3ScCl_6 as this would require a Cl^- source and the ^{45}Sc MAS NMR of the starting material (Fig. 4.6 a) gave no evidence for residual $ScCl_3$. In the case of $LiSc(BH_4)_4$, the Sc was ultimately decomposed to a species that could not be detected by NMR. If the same is assumed for $NaSc(BH_4)_4$ then decomposition proceeds via a similar route:

$$NaSc(BH_4)_4 \rightarrow NaBH_4 + Sc(BH_4)_3 \rightarrow NaBH_4 + ScB_3 + 6H_2 \quad (4.4)$$

Rehydrogenation of $NaSc(BH_4)_4$ (dehydrogenated at 473 K, 1 day) for 5 days at 523 K under 12 MPa H_2 pressure yielded little change in the ^{45}Sc spectrum (Fig. 4.6 d). In the ^{11}B spectrum, however, new species was present at –12 ppm. Similar to the rehydrogenation of $LiSc(BH_4)_4$, this represented $B_{12}H_{12}^{2-}$ which has not been observed experimentally in dehydrogenation studies of $NaBH_4$. In this case, the counter ion must be Na^+ since no additional resonances appeared in the ^{45}Sc MAS NMR (Fig. 4.6 d). The formation of the species at –12 ppm may have emerged from hydrogenation of trace quantities of a variety of polyboranes at undetectable levels. The absence of $NaSc(BH_4)_4$ in either the ^{11}B or ^{45}Sc spectra verifies that the rehydrogenation pathway, at least under moderate conditions, does not lead to regeneration of the original bimetallic borohydride.

4.3.4 *KBH_4/ $ScCl_3$*

The mixture of $KBH_4/ScCl_3$ after ballmilling consisted primarily of the new species $KSc(BH_4)_4$ at –22 ppm[69] and residual unreacted KBH_4 at –37 ppm as revealed in the ^{11}B MAS NMR data (Fig. 4.7 a). In the ^{45}Sc MAS NMR, two predominant species were present, corresponding to K_3ScCl_6 at 218 ppm and $KSc(BH_4)_4$ at 103 ppm[69] (Fig. 4.8 a). A third and much smaller resonance centered at 165 ppm was unidentified but has been observed in a previous reported synthesis of $KSc(BH_4)_4$.[69] Mechanical milling appeared to have facilitated an analogous reaction to that of the preparation of $NaSc(BH_4)_4$ in spite of the different ratio of the initial Group I borohydride to $ScCl_3$, although for the $KBH_4/ScCl_3$ mixture less $ScCl_3$ may have been more appropriate.

The only change in the ^{11}B MAS NMR spectrum after dehydrogenation at 373 K (Fig. 4.7 b) was a trace signal at 0 ppm, possibly due to exposure to air in either the PCT

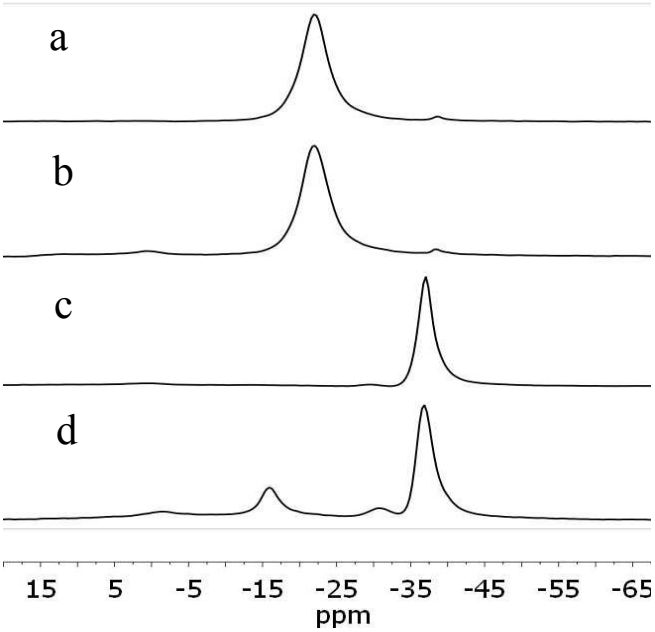

Fig. 4.7 ^{11}B MAS NMR of a) $KSc(BH_4)_4$; (b) after dehydrogenation at 373 K, 1day; (c) after dehydrogenation at 473 K, 1 day; (d) rehydrogenation of powder from (c) at 523 K, 5 days, 12 MPa.

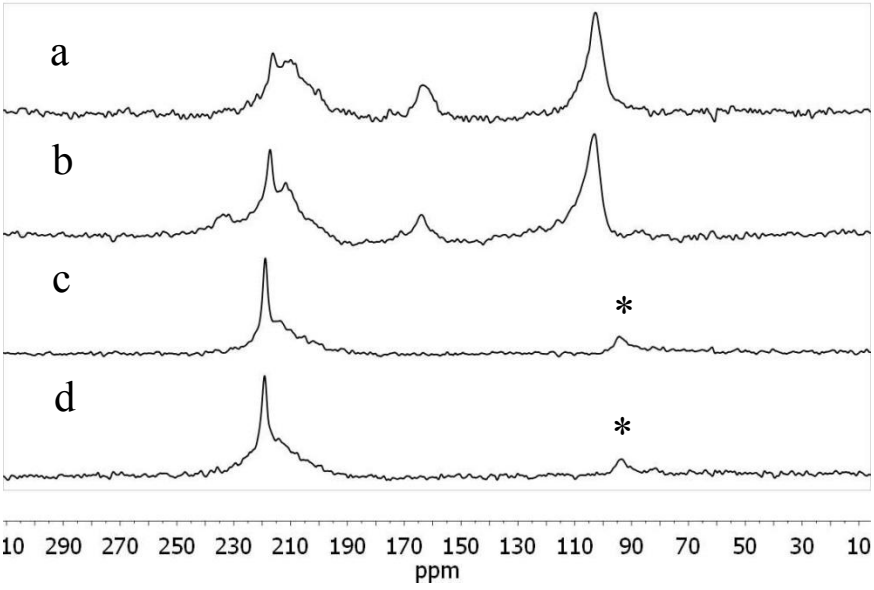

Fig. 4.8 ^{45}Sc MAS NMR of (a) $KSc(BH_4)_4$; (b) after dehydrogenation at 373 K, 1day; (c) after dehydrogenation at 473 K, 1 day; (d) rehydrogenation of powder from (c) at 523 K, 5 days, 12 MPa. Asterisks denote spinning sidebands.

reactor or NMR rotor resulting in the oxidation of a small amount of dehydrogenated $KSc(BH_4)_4$. In the ^{45}Sc MAS NMR, the resonance for K_3ScCl_6 at 218 ppm appeared to resolve into two overlapping peaks (Fig. 4.8 b) attributable to the close chemical shifts of K_3ScCl_6 and residual $ScCl_3$ from an excess in the initial mixture.

After dehydrogenation at 473 K, any evidence of $KSc(BH_4)_4$ (–22 ppm) was absent in the ^{11}B MAS NMR spectrum and only a resonance for KBH_4 (–37 ppm) was seen (Fig. 4.7 c). The $KSc(BH_4)_4$ also disappeared from the ^{45}Sc spectrum (Fig. 4.8 c), leaving K_3ScCl_6 and $ScCl_3$ (as an overlapping shoulder) as the primary Sc species at 218 ppm. Rehydrogenation of the powder did not change the Sc characterization by MAS NMR but a small increase in the shoulder at –33 ppm, downfield from the KBH_4 resonance (Fig. 4.7 d), was observed as well as the appearance of a resonance representative of a polyborane species at –15 ppm. Similar to what was observed from the Li and Na complexes, this new B species most likely corresponded to a $B_{12}H_{12}^{2-}$ salt.

The results of dehydrogenation and rehydrogenation trials on $KSc(BH_4)_4$ resembled those of $NaSc(BH_4)_4$. While dehydrogenation at 373 K caused a colour change from white to orange, little change was seen in the NMR spectra. Heating at 473 K resulted in the complete decomposition of the bimetallic species to KBH_4 and either K_3ScCl_6 or ScB_x. The dehydrogenation process mostly likely involved initial decomposition to KBH_4 and $Sc(BH_4)_3$ followed by formation of ScB_x accompanied by the release of H_2. For this mixture, it is difficult to evaluate from the ^{45}Sc MAS NMR whether the Sc bound in $KSc(BH_4)_4$ formed additional K_3ScCl_6 or if it decomposed to a ScB_x material that could not be detected by either ^{11}B or ^{45}Sc MAS NMR.

Rehydrogenation resulted in the formation of $K_2B_{12}H_{12}$, an indication once again of the lack of reversibility within these bimetallic complexes.

4.3.5 In situ TG-IR of scandium borohydrides

The IR analysis of $LiSc(BH_4)_4$ is plotted as a function of temperature (and therefore time) during ramping to 450 K and given in Fig. 4.9 d. Although only analysis for $LiSc(BH_4)_4$ is shown, similar results were obtained for all three Sc complex borohydrides. Diborane was the only gas phase decomposition species detected in the IR spectra besides impurity levels of CO_2. Bands characteristic of diborane (B_2H_6) appeared at 1174 and 1604 cm^{-1} [100] reaching a maximum in intensity when the temperature reached about 400 K followed by steady decay as the temperature was increased to 450 K.

In Fig. 4.9 a, the diborane signal from IR (solid line) for $LiSc(BH_4)_4$ is presented with the TG mass change data, given as the derivative of mass loss with time/temperature. From this result it is apparent that diborane was released quite early during the dehydrogenation period, beginning at about 350 K for both the IR and TG data. The initial loss of mass in the sample can be attributed to the release of B_2H_6 resulting in a weight loss of up to 0.5 %. Between 400 and 450 K the B_2H_6 IR signal decayed to zero but the TG data reached a maximum within this temperature range.

From Fig. 4.9 a, it is clear that by 450 K B_2H_6 evolution was complete and continued heating was not associated with any B_2H_6 formation. The TG data, however, confirmed that the sample continued to lose mass after 450 K, reaching a second maximum in rate of weight loss at approximately 490 K. The rate of mass loss is still above zero at the cutoff temperature of 573 K, reaching a total mass loss of 4.75 %.

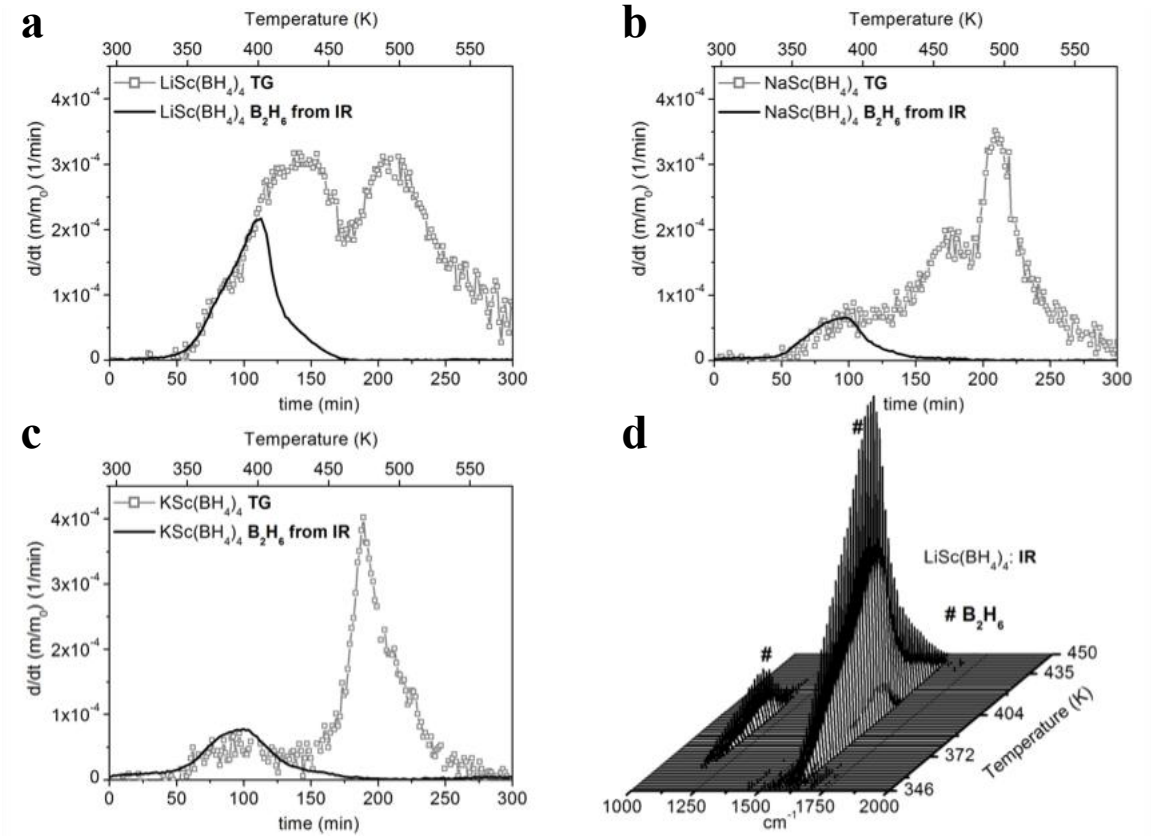

Fig. 4.9 TG data plotted as a function of rate of mass loss vs. time and temperature (open squares) with IR data (solid lines) representing diborane evolution for (a) $LiSc(BH_4)_4$; (b) $NaSc(BH_4)_4$; (c) $KSc(BH_4)_4$. The time evolution of the diborane IR signal for $LiSc(BH_4)_4$ is plotted in (d).

At 373 K the ^{11}B and ^{45}Sc MAS NMR for $LiSc(BH_4)_4$ did not show any change but B_2H_6 evolution had already begun according to Fig. 4.9a. The initial step in decomposition must be representative of a reaction such as

$$LiSc(BH_4)_4 \rightarrow Li^+ + Sc(BH_4)_4^- \rightarrow LiBH_4 + B_2H_6 + ScB_x + 3H_2 \quad (4.5)$$

By 473 K, B_2H_6 was no longer formed and, according to ^{11}B MAS NMR, the primary B species detected was $LiBH_4$ although this result was obtained after 24 hours of dehydrogenation which may have provided sufficient time for kinetically unfavorable processes to complete. Thus, during the TG/IR analysis, during the heat ramp to 573 K, there may have still been intact $LiSc(BH_4)_4$ present at 473 K. We confirmed this by ^{11}B

MAS NMR analysis of $LiSc(BH_4)_4$ decomposed at 473 K and immediately cooled. The data exhibited a distinct resonance remaining for $LiSc(BH_4)_4$. The second step observed between 450 to 573 K (Fig 4.9 a) may simply represent the decomposition of the remaining $LiSc(BH_4)_4$.

Another possible source of mass loss that was not correlated to B_2H_6 release during decomposition of $LiSc(BH_4)_4$ may be due to kinetically fast processes. It was discussed earlier that there may have been an variety of polyborane species observed as a broad feature in the baseline of the ^{11}B MAS NMR spectrum for the decomposed $LiSc(BH_4)_4$ (Fig. 4.4) which, upon rehydrogenation, condensed to form $B_{12}H_{12}^{2-}$ (Fig. 4.3 b). These polyboranes may be a result of the pyrolysis of diborane which is slow below 473 K but becomes faster with higher temperatures.[101] The first step in thermal decomposition is the splitting of B_2H_6 into two BH_3 units[50] followed by the interaction of BH_3 with diborane to condense into larger polyboranes such as B_3H_7, B_4H_{10}, and B_5H_{11}[101] while releasing H_2. These species are all gaseous polyboranes but were not detected by IR analysis because of rapid kinetics in the gas phase, resulting in the condensation of these polyboranes into the solid state species that were detected in the baseline of ^{11}B MAS NMR spectrum (Fig. 4.4) after decomposition at 473 K. This process may also provide an explanation for the second step in the TG data that was not associated with B_2H_6 release.

The TG/IR data for $NaSc(BH_4)_4$ (Fig. 4.9 b) indicated that B_2H_6 was again released early in the decomposition although the intensity of the IR signal was considerably lower than the in the case of $LiSc(BH_4)_4$. The maximum B_2H_6 evolution occurred around 373 K at which an increase in the amount of $NaBH_4$ was observed

relative to $NaSc(BH_4)_4$ in the ^{11}B MAS NMR (Fig. 4.5 b). It is interesting to note that that while the ^{11}B MAS NMR showed more decomposition occurring for $NaSc(BH_4)_4$ than for $LiSc(BH_4)_4$ after dehydrogenation at 373 K, a smaller mass loss was observed for $NaSc(BH_4)_4$. Two subsequent steps occurred after B_2H_6 evolution ceased, both associated with greater rates of mass loss than the initial one.

At temperatures greater than 450 K, B_2H_6 was no longer detected for the decomposition of $NaSc(BH_4)_4$. As discussed for $LiSc(BH_4)_4$, the subsequent change in mass after diborane evolution ceased may result from the decomposition of B_2H_6 that is facilitated by higher temperatures. The two steps that occur between 400-573 K in the TG data probably represent the decomposition (resulting in H_2 release) of different temperature-dependent borane species formed upon condensation.

For $KSc(BH_4)_4$, decomposition occurred over two steps, the initial step being entirely associated with B_2H_6 release, while the subsequent step observed at higher temperature was associated with much higher rates of mass loss. The initial B_2H_6 evolution is very similar to that of $NaSc(BH_4)_4$ with regards to both temperature range, intensity of the IR signal, and rate of mass loss. Overall, $KSc(BH_4)_4$ lost the least mass at 1.9 wt % versus 2.5 wt % and 4.8 wt % for $NaSc(BH_4)_4$ and $LiSc(BH_4)_4$, respectively. This may reflect in part the stabilities of the Group I borohydrides: $LiBH_4$ has the lowest stability of the three complexes and also exhibited the greatest mass loss. The variations seen in the TG data given in Fig. 4.9 may also arise from differences in how the metal cations stabilize polyborane species produced upon decomposition.

The combination of results from NMR, TG and IR experiments confirm that B_2H_6 is formed from all three Sc complexes and decomposition must follow a mechamism

similar to Eq. 4.5 rather than Eqs. 4.2 or 4.4. The B_2H_6 evolution does not necessarily stop at higher temperatures but B_2H_6 may decompose rapidly to form higher boranes, both gas and solid phase, releasing H_2 in the process. Although the amount of mass loss that can be assigned to B_2H_6 versus H_2 was not determined, the low overall weight loss of all three complexes suggests that even if the majority of the loss was due to dehydrogenation, the quantity is insufficient to provide a useful amount of hydrogen for applications where an energy dense fuel source is needed.

4.3.6 *IR characterization of complex manganese borohydrides*

The infrared spectrum for the ballmilled mixture of $LiBH_4/MnCl_2$ (Fig. 4.10) resembled that of $Mn(BH_4)_2$,[70] confirming that this combination does not favor the formation of the anionic Mn borohydride. A broad band was present at 2237 cm^{-1} (B-H stretch) as well as bands at 1114 and 1211 cm^{-1} (deformation).

The IR spectrum for $NaBH_4$ ballmilled with $MnCl_2$ (Fig. 4.11) had significant differences from that of the neutral $Mn(BH_4)_2$. Instead of a single broad band there were two closely overlapping bands at 2249 and 2326 cm^{-1} (B-H stretch), a bridging bending mode band at 1342 cm^{-1}, and bands representing deformation modes at 1134 and 1219 cm^{-1}.[70] This spectrum indicated the presence of $Na_2Mn(BH_4)_4$, the formation of which has been supported by DFT calculations.[70]

The synthesis of $K_2Mn(BH_4)_4$ has also been reported from the mechanical milling of KBH_4 with $MnCl_2$.[96] The IR spectrum for $K_2Mn(BH_4)_4$ was not available however, so our data could not be compared. Inspection of the differences between the IR analysis of the $KBH_4/MnCl_2$ mixture (Fig. 4.12) and Fig. 4.10 confirmed that the ballmilled product

did not contain $Mn(BH_4)_2$. The major bands were similar to those of $Na_2Mn(BH_4)_4$ with 3 bands representing B-H stretches at 2214, 2283, and 2376 cm^{-1}, a more distinct band at 1342 cm^{-1} (bridging bending mode), and deformation modes at 1041 and 1118 cm^{-1}.

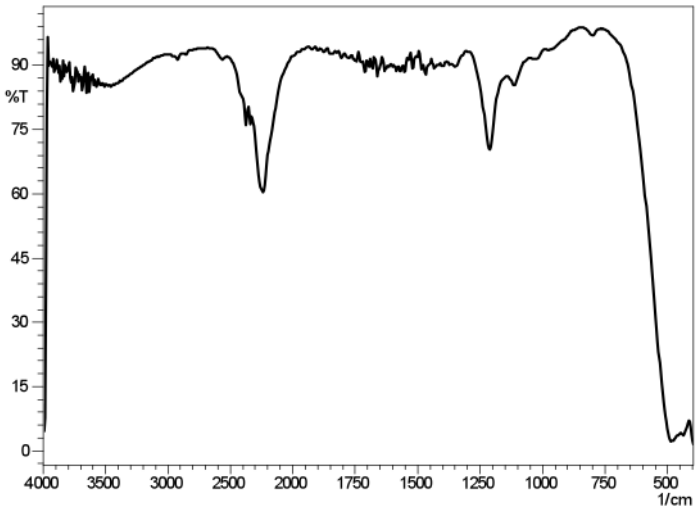

Fig. 4.10 IR spectrum of $Mn(BH_4)_2$.

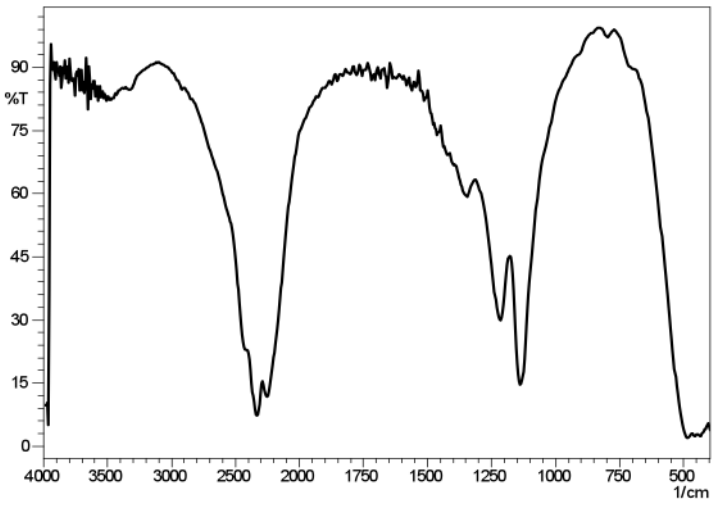

Fig. 4.11 IR spectrum of $Na_2Mn(BH_4)_4$.

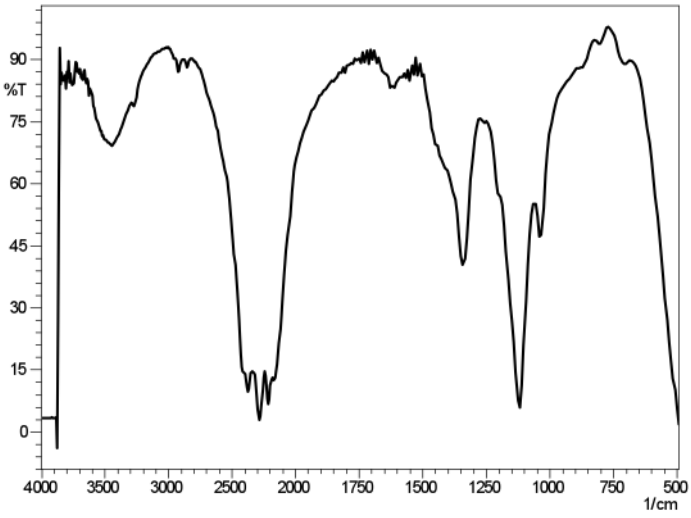

Fig. 12 IR spectrum of $K_2Mn(BH_4)_4$.

4.3.7 *In situ TG-IR of Mn borohydride complexes*

The rates of mass loss based on TG measurements and detection of diborane by IR for the three Mn complexes are given in Fig. 4.13. Note the difference in magnitude in the derivative of mass loss for the Mn vs. Sc complexes: the Mn complexes release B_2H_6 at rates approximately 10 times greater than those of the Sc complex borohydrides. Data is presented for temperature ranges where changes were observed; beyond these temperatures, mass change and B_2H_6 evolution ceased. The time evolution for B_2H_6 production during the decomposition of $KBH_4/MnCl_2$ is given in Fig. 4.13 d and is representative of similar plots for the other two mixtures. B_2H_6 was the primary species detected over the temperature ranges used with only traces of CO_2 as appearing as an impurity.

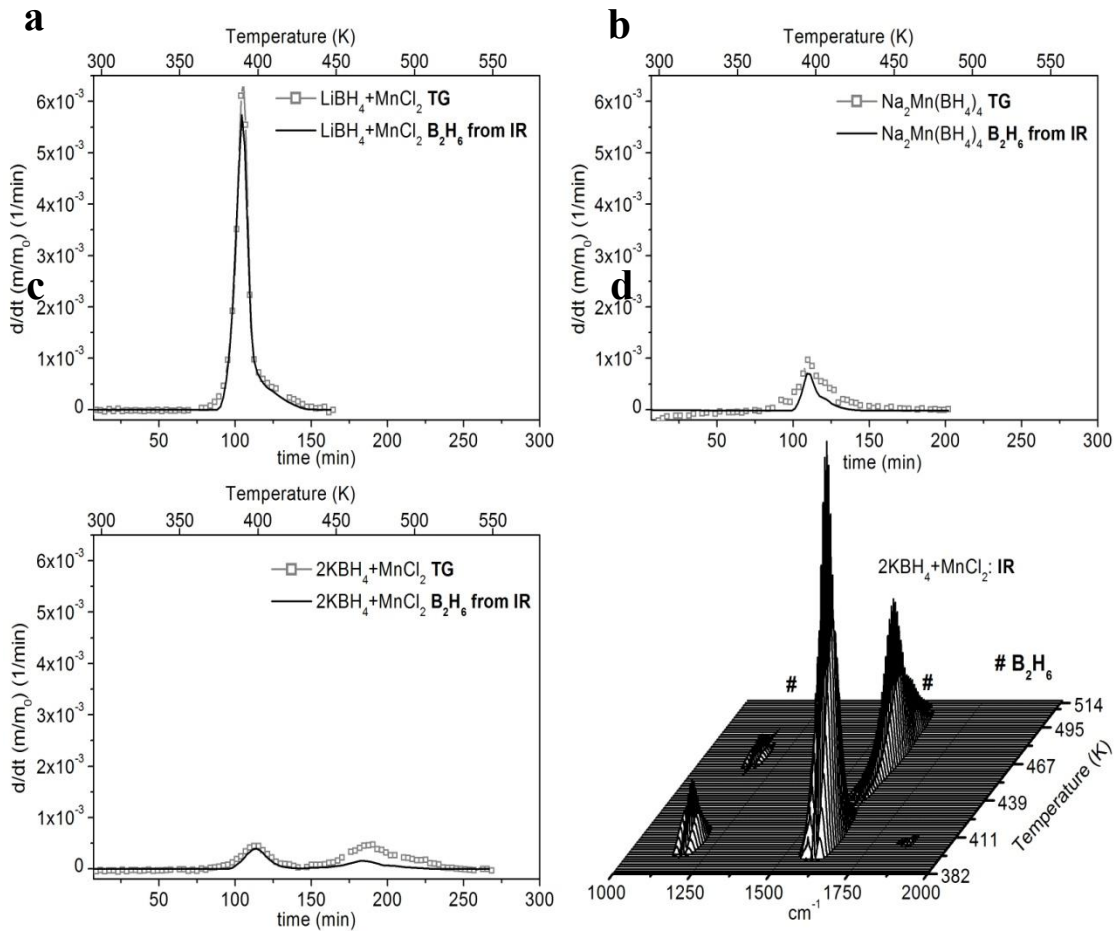

Fig. 13 TG data plotted as a function of rate of mass loss vs. time and temperature (open squares) with IR data (solid lines) representing diborane evolution for (a) $LiBH_4$+$MnCl_2$; (b) $Na_2Mn(BH_4)_4$; (c) KBH_4+$MnCl_2$. The time evolution of the diborane IR signal for the $K_2Mn(BH_4)_4$ is plotted in (d).

Neutral manganese borohydride, formed by ballmilling $LiBH_4$ and $MnCl_2$, released diborane at a higher rate than any of the other Mn or Sc complexes (Fig. 4.13 a). As no other decomposition steps were detected, the reaction must have proceeded via

$$2Mn(BH_4)_2 \rightarrow B_2H_6 + MnB_2 + MnH_2 + 4H_2 \quad (4.6)$$

Although performed under isothermal conditions rather than being subjected to a temperature ramp as in our study, dehydrogenation of $Mn(BH_4)_2$ at 373 K has been found

to occur rapidly, releasing over 3 wt % in about two minutes.[70] This temperature coincides with the maximum in both diborane evolution and rate of mass change in Fig. 4.13 a and corresponds to a total mass loss of 7.5 wt %. These results all confirm that $Mn(BH_4)_2$ is an unstable species which evolves B_2H_6 readily when exposed to dehydrogenating conditions. The large amount of B_2H_6 released early on in the decomposition process indicates that reversibility is very unlikely once this complex begins to decompose.

$Na_2Mn(BH_4)_4$ also decomposed in a single step with B_2H_6 evolution coinciding with maximum rate of mass loss (Fig. 4.13 b). The rate of mass loss was much lower for $Na_2Mn(BH_4)_4$ and the total amount of mass change was only 2 % compared to the 8 % observed for $Mn(BH_4)_2$. The intensity of the diborane IR signal was also significantly lower for $Na_2Mn(BH_4)_4$ hence it can be concluded that the stability of the complex is enhanced by the presence of the Na cation. The stabilization, however, not only suppresses B_2H_6 formation but also slows the reaction kinetics so that H_2 release must also be very slow within the time and temperature range of the experiment.

Of the three Mn complexes, $K_2Mn(BH_4)_4$ was the only sample that exhibited multi-step decomposition and the only complex overall to emit B_2H_6 in more than one step. Decomposition and concomitant B_2H_6 evolution occurred in two steps between 373-433 K and 433-533 K. The maximum rate of mass loss was greater for the first step and the sample lost more mass in total than $Na_2Mn(BH_4)_4$ (~3 wt %). The mixture may have initially decomposed to KBH_4 and $KMn(BH_4)_3$ in the first step[96] although this disproportionation would not be accompanied by the release of any B_2H_6. Perhaps a portion of the $KMn(BH_4)_3$ began decomposing to $Mn(BH_4)_2$ between 373 and 433 K,

evolving some B_2H_6 in the process. Increasing the temperature then decomposed the remaining $KMn(BH_4)_3$ to $Mn(BH_4)_2$ with concurrent release of B_2H_6 from the unstable $Mn(BH_4)_2$. The TG/IR data indicates that only part of the mass loss during the higher temperature step was attributable to diborane, thus hydrogen release also occurred during this step. Unfortunately, the mechanism of the multi-step dehydrogenation route cannot be verified but the release of B_2H_6 associated with both steps indicates that this loss of B again prevents rehydrogenation back to the original borohydride complex.

In general, the formation of B_2H_6 comprises a significant portion of the species produced upon decomposition of the three prepared Mn complexes. B_2H_6 evolution from neutral $Mn(BH_4)_2$ is initiated at <373 K and releases a quantity that may amount to 7.5 wt %. $Na_2Mn(BH_4)_4$ and $K_2Mn(BH_4)_4$ also lose mass as a result of B_2H_6 formation during the initial stages of decomposition. Although characterization of the solid phase products could not be performed, the tendency of these complexes to readily evolve B_2H_6 confirms that rehydrogenation to yield the starting materials is unlikely. $K_2Mn(BH_4)_4$ appears to decompose following a unique pathway that forms B_2H_6 in two steps, eliminating any potential for reversibility.

4.4 *Conclusions*

Recently, the electronegativity of the cation in a complex borohydride was found to dictate charge transfer to the borohydride anion based on vibrational spectroscopy and modeling calculations.[102] This was found to distort the tetrahedral BH_4^-. A degree of distortion above a certain threshold was associated with the release of B_2H_6 and both $LiSc(BH_4)_4$ and $Mn(BH_4)_2$ were found to fall into this category. The well-studied

bimetallic species $LiZn_2(BH_4)_5$ was compared to $LiBH_4$ and two possible reactions were proposed: one that was driven by the formation of a stable binary hydride, i.e. LiH, and the other, in which the hydride formed was unstable, i.e. ZnH_2, resulted in formation of B_2H_6 . This was found to occur through decomposition to $LiBH_4$ and $Zn(BH_4)_2$, accompanied by structural distortion of BH_4^- into $BH_2^{\delta+}$ and $H_2^{\delta-}$, followed by asymmetric assembly with another BH_4^- to yield B_2H_6.

In comparing the three bimetallic Sc complexes examined in our study, $LiSc(BH_4)_4$ released the most B_2H_6 and lost the most mass. This suggests that the Li cation had the least stabilizing effect on $Sc(BH_4)_4^-$ and the complex readily decomposed to $LiBH_4$ and the volatile $Sc(BH_4)_3$ while releasing B_2H_6. The Na and K complexes, both of which form more stable monocation borohyrides than Li, appeared to suppress the emission of B_2H_6 but also lost less mass. As well, all three complexes decomposed to the stable Group I borohydride, the thermodynamic driving force for the reaction, leading to the formation of the tetrahedrally distorted $Sc(BH_4)_3$ and finally B_2H_6.

For the Mn complexes, variations in TG-IR data of $Mn(BH_4)_2$ versus $Na_2Mn(BH_4)_4$ and $K_2Mn(BH_4)_4$ indicated that the incorporation of a Group I metal succeeded in reducing the amount of B_2H_6 released but all three Mn borohydrides evolved significantly more B_2H_6 than the Sc complexes. Furthermore, any mass loss was primarily due to B_2H_6 evolution. The mechanism behind the decomposition route seemed to be unique for each species with the $Mn(BH_4)_2$ and $Na_2Mn(BH_4)_4$ decomposing in a single step associated with the loss of B_2H_6, while $K_2Mn(BH_4)_4$ differed by following a two-step decomposition pathway, where both steps corresponded to B_2H_6 release.

While the bimetallic Sc and Mn complexes all demonstrated onset decomposition temperatures that fell between that of the parent Group I and transition metal borohydrides, B_2H_6 was consistently released within the initial period of decomposition, eliminating any chance of reversibility. The formation of B_2H_6 is a critical factor in determining whether reversible dehydrogenation is a possibility and our results confirm that this species is a major component of the decomposition products. In addition, the formation of stable alkali metal borohydrides and transition metal borides make rehydrogenation improbable, at least within the limits of practical application. Evidently these combinations of stable/unstable metals are not ideal for hydrogen storage purposes and examination of different metal mixtures is necessary.

In Chapter 2 TG-IR data was presented for the decomposition of $Mg(BH_4)_2$. For this complex, no B_2H_6 was detected beyond impurity levels. Furthermore, low temperature cycling of H_2 was successfully demonstrated, reinforcing the assertion that B_2H_6 release is a major barrier to reversibility. This also suggests that of the classes of monocation borohydrides, the Group II complexes may be the ideal compromise between the high stability of Group I and volatility of the transition metals. Bimetallic complexes involving thermodynamic tuning with Group II and transition metals may lead to the discovery of more appropriate materials for hydrogen storage.

CHAPTER 5 CONCLUSIONS AND FUTURE DIRECTIONS

5.1 *Borohydride complexes as hydrogen storage materials*

In the search for a lightweight material with high hydrogen cycling capacity the complex borohydrides have come forth as an attractive class of compounds. Ideally, pairing the borohydride anion with an alkali metal forms complexes with maximum gravimetric hydrogen content but their use is hindered by the ionic interaction of these metals, resulting in exceptionally stable salts. The Group II metals and Al, in comparison, are still light elements and have the additional benefit of forming less stable complexes. Within the Group II elements, Mg is the most attractive due to its potential for reversible storage based on its thermodynamic properties as well as for health (toxicity of Be) and practical ($AlBH_4$ is a pyrophoric liquid) reasons. The decomposition and subsequent hydrogenation of $Mg(BH_4)_2$ was studied rigorously to evaluate its potential for hydrogen storage.

5.2 *The role of intermediate boron species in the $Mg(BH_4)_2$ system*

The low temperature dehydrogenation of $Mg(BH_4)_2$ was explored in an effort to avoid the formation of the highly stable $MgB_{12}H_{12}$ species and elucidate the solid state decomposition pathway. The overlying goal was to evaluate whether other, less stable polyborane intermediates could regenerate $Mg(BH_4)_2$ upon hydrogenation, and also under moderate conditions. These trials revealed the preference of the $Mg(BH_4)_2$ system to decompose to $Mg(B_3H_8)_2$. The formation of this intermediate during dehydrogenation

preceded the formation of $MgB_{12}H_{12}$ and rehydrogenation successfully yielded $Mg(BH_4)_2$.

We proposed that rehydrogenation is dependent on the presence of MgH_2 and its persistence in the solid state reaction presents a very different situation from that available in solution chemistry where MgH_2 would be hydrolyzed. The thermodynamic stability of MgH_2 must play an active role in dictating the conditions under which hydrogenation of the dehydrogenated products can occur. In other words, the ease at which Mg-H bonds can be broken so that hydrides can be donated to $Mg(B_3H_8)_2$ will determine the temperature and pressure needed to form $Mg(BH_4)_2$.

This theory was tested in Chapter 3 by preparing $Mg(B_3H_8)_2{\cdot}x$THF and hydrogenating the powder with different metal hydrides (LiH, NaH, and MgH_2). The results of these experiments confirmed that regardless of the metal cation, hydrogenation of $Mg(B_3H_8)_2$ to $Mg(BH_4)_2$ occurred without the formation of $MgB_{12}H_{12}$ as long as a metal hydride was present. The hydrogenation mechanisms exhibited distinct differences between the three metal hydrides indicating that the stability of the metal hydride does play an active role in the hydrogenation process with the least stable hydride, MgH_2, allowing selective hydrogenation to $Mg(BH_4)_2$ in a single exothermic step.

The results of these trials, and of the many other studies attempting to exploit the favorable properties of $Mg(BH_4)_2$ for hydrogen storage, highlight the major challenges associated with any potential solid state storage material. There are both kinetic and thermodynamic barriers to overcome and improving conditions in the dehydrogenation direction does not necessarily have a beneficial effect in the reverse reaction. Here, we have found that reversibility under mild conditions is possible in the $Mg(BH_4)_2$ system by

avoiding the formation of $MgB_{12}H_{12}$. Unfortunately, the slow kinetics of mild temperature dehydrogenation and the low hydrogen cycling capacity of the $Mg(B_3H_8)_2$ (2.5 wt%) is too low to be of practical use. There have been many successful examples of kinetic and thermodynamic adjustment and these may be effective ways to alleviate such issues. These findings provide a new outlook on how to evaluate materials by probing the mechanism behind the decomposition path. By understanding the steps involved in the pathway and how stability within the system varies according to the step, the potential for reversibility and hydrogen release can be maximized.

5.3 *Bimetallic complex hydrides*

One of the major issues associated with the use of borohydride complexes for hydrogen storage is the thermodynamic stability of these materials, with the complexes possessing the highest gravimetic hydrogen capacity also requiring the most demanding temperatures to facilitate dehydrogenation. In recent years, the idea of modulating thermodynamic properties by combining metals with different stabilities (as monocation borohydrides) has come to light. By incorporating a cation with ionic bonding characteristics, it has been proposed that volatile transition metal borohydrides, and particularly those which form anionic complexes, can be stabilized to an extent that the release of diborane is prevented. The formation of diborane is an irrevocable barrier to reversibility and whether or not it is evolved during dehydrogenation is a critical factor in evaluating the suitability of a material for hydrogen cycling.

Following previously published methods, we prepared mixtures of $LiBH_4$, $NaBH_4$, or KBH_4 with $ScCl_3$ or $MnCl_2$ and examined the low temperature

dehydrogenation of the resulting bimetallic complexes. All complexes were not only found to release diborane but did so during the early stages of decomposition. This result, along with the formation of scandium boride and the corresponding Group I borohydride, fully prevents regeneration of the original complex.

Our findings confirm that mixing Group I metals with anionic transition metals does effectively adjust the onset decomposition temperatures to a value in between those of the individual metal borohydrides. The decomposition path, however, follows a mechanism that evolves significant quantities of diborane and does not allow for reversible dehydrogenation. These results support the conclusions obtained from the $Mg(BH_4)_2$ studies that the Group II borohydrides appear to be the most promising complexes for reversible hydrogen storage.

5.4 *Future work*

Further studies to find other borane intermediates with higher hydrogen gravimetric content, particularly boranes with a 1:1 ratio of B:H, ie. $B_{10}H_{10}^{2-}$, should be conducted. We have shown that the addition of LiH to $Mg(BH_4)_2$ favors the formation of $B_{10}H_{10}^{2-}$. The cycling capacity of $B_{10}H_{10}^{2-}$ is an appealing 7.4 wt %, making this borane species worthy of continued investigation. The exact role of LiH in this reaction should be clarified as well as the identification of the products formed upon decomposition. Isolation of $B_{10}H_{10}^{2-}$ and subsequent trials to understand the mechanism behind its formation may represent a significant step forward towards development of an ideal hydrogen storage material.

With regards to the bimetallic borohydrides, our work demonstrated the unsuitability of the alkali/transition metal pairs for avoiding diborane evolution. By pairing two metals that have less disparity between their electronegativity and ΔH_f values, the interaction between the two cations will change sufficiently to result in a material that follows a different decomposition route. New composites should focus on incorporating the Group II metals, which show more favorable enthalpy values for reversible dehydrogenation.

APPENDIX A

Nanoconfinement of MgH_2 and AlH_3 in γ-$Mg(BH_4)_2$

A stainless steel autoclave (Parr, 170 mL capacity) was charged with 0.50 g of γ-$Mg(BH_4)_2$ and dibutylmagnesium (10 mL). The autoclave was flushed with H_2 for 30 min and subsequent hydrogenation of the dibutylmagnesium proceeded as outlined in a study by Zhang et al.[103] The autoclave was pressurized to 40 bar under H_2, heated to 135ºC and then the pressure was adjusted to 55 bar. The mixture was hydrogenated for 24 h, allowed to cool, and then filtered through a sintered glass crucible. After drying at 90ºC under vacuum, the final product was a light gray powder.

Similarly, triethylaluminum (Aldrich, 93%, 5 mL) was combined in the autoclave with 1 g of γ-$Mg(BH_4)_2$ and pressurized to 40 bar. The autoclave was heated, after flushing with H_2, to 130ºC for 24 h under 55 bar H_2. The resulting white powder was washed with pentane, filtered and then dried under vacuum at room temperature.

The powders were dehydrogenated at 473 K on the PCT for 1 day. $^{11}B\{^1H\}$ NMR are given below along with $Mg(BH_4)_2$ (dehydrogenated under the same conditions) for comparison.

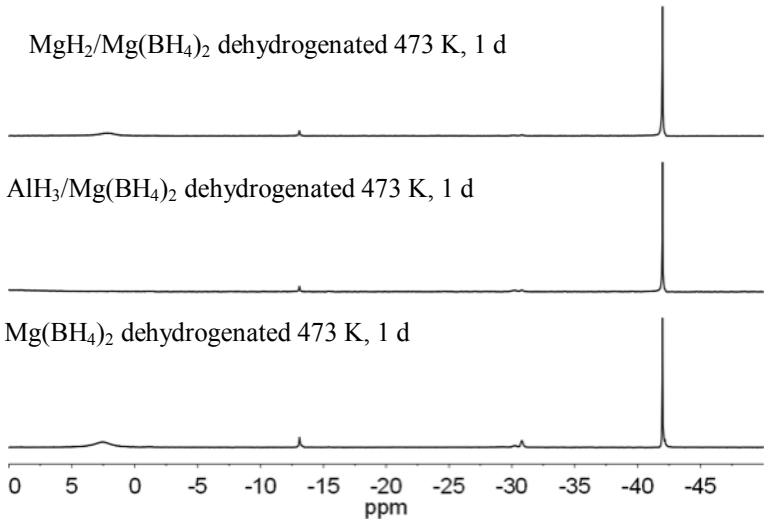

The attempted nanoconfinement of both MgH_2 and AlH_3 did not improve the kinetics of dehydrogenation at low temperature. On the contrary, less $Mg(B_3H_8)_2$ (–31 ppm) formed after decomposition of these two samples than in the pure $Mg(BH_4)_2$.

REFERENCES

(1) Züttel, A. *Naturwissenschaften* **2004**, *91*, 157–172.

(2) International Energy Outlook 2011 http://www.eia.gov/forecasts/ieo/index.cfm.

(3) Jochem, E. *Energy and Environment* **1991**, *2*, 31–44.

(4) Watson, R. T. *Climate Change 2001; Synthesis Report*; 2001.

(5) Greg Fiske http://polardiscovery.whoi.edu/poles/climate.html.

(6) Demirbas, A. *Energy Sources, Part A: Recovery, Utilization, and Environmental Effects* **2007**, *30*, 101–109.

(7) Demirbas, A. *Energy Sources, Part A: Recovery, Utilization, and Environmental Effects* **2007**, *30*, 170–178.

(8) Hordeski, M. F. *Aternative Fuels -The Future of Hydrogen*; The Fairmont Press, Inc.: Lilburn, GA, 2007.

(9) Furimsky, E. *Energy Sources, Part A: Recovery, Utilization, and Environmental Effects* **2007**, *30*, 119–131.

(10) *The Hydrogen Energy Transition*; Sperling, D.; Cannon, J. S., Eds.; Elsevier: Amsterdam, 2004.

(11) Schlapbach, L.; Züttel, A. *Nature* **2001**, *414*, 353–358.

(12) Porterfield, W. W. *Inorganic Chemistry*; 2nd ed.; Academic press, Inc.: San Diego, CA, 1993.

(13) Dickson, E. M.; Ryan, J. W.; Smulyan, M. H. *The Hydrogen Energy Economy*; Praeger Publishers: New York, NY, 1977.

(14) U.S. Department of Energy: Hydrogen Storage http://www1.eere.energy.gov/hydrogenandfuelcells/storage/current_technology.html .

(15) Chen, P.; Wu, X.; Lin, J.; Tan, K. *Science (New York, N.Y.)* **1999**, *285*, 91–93.

(16) Hirscher, M.; Becher, M.; Haluska, M.; Quintel, A; Skakalova, V.; Choi, Y.-M.; Dettlaff-Weglikowska, U.; Roth, S.; Stepanek, I.; Bernier, P.; Leonhardt, A; Fink, J. *Journal of Alloys and Compounds* **2002**, *330-332*, 654–658.

(17) Van den Berg, A. W. C.; Areán, C. O. *Chemical Communications* **2008**, 668.

(18) *Metal Hydrides*; Sastri, M. V. C.; Viswanathan, B.; Srinivasa Murthy, S., Eds.; Narosa Publishing House: New Delhi, 1998.

(19) Dornheim, M.; Doppiu, S.; Barkhordarian, G.; Boesenberg, U.; Klassen, T.; Gutfleisch, O.; Bormann, R. *Scripta Materialia* **2007**, *56*, 841–846.

(20) *Metal Hydrides*; Mueller, W. M.; Blackledge, J. P.; Libowitz, G. G., Eds.; Academic Press, Inc.: New York, NY, 1968.

(21) Suryanarayana, C. *Progress in Materials Science* **2001**, *46*, 1–184.

(22) Huot, J.; Liang, G.; Schulz, R. *Applied Physics A* **2001**, *19571*, 187–195.

(23) Barkhordarian, G.; Klassen, T.; Bormann, R. *Scripta Materialia* **2003**, *49*, 213–217.

(24) Gutfleisch, O.; Dal Toè, S.; Herrich, M.; Handstein, A.; Pratt, A. *Journal of Alloys and Compounds* **2005**, *404-406*, 413–416.

(25) Bogdanovic, B.; Schwickardi, M. *Journal of Alloys and Compounds* **1997**, *253*, 1–9.

(26) Løvvik, O. M.; Molin, P. N. *AIP Conf. Proc.* **2006**, *837*, 85.

(27) Løvvik, O. M.; Swang, O.; Opalka, S. M. *Journal of Materials Research* **2005**, *20*, 3199.

(28) Jacobs, H. Z. *Zeitschrift Fur Anorganische Und Allgemeine Chemie,* **1976**, *427*, 8.

(29) Jacobs, H.; Von Osten, E. Z. *Zeitschrift für Naturforschung B. A Journal of Chemical Sciences.* **1976**, 385.

(30) *CRC Handbook of Chemistry and Physics, 83rd Ed.*; CRC Press: Boca Raton, FL, 2002.

(31) SCI Finder Scholar: "Hazardous Substances Data Bank" data are provided by the National Library of Medicine (U.S.).

(32) Orimo, S.-I.; Nakamori, Y.; Eliseo, J. R.; Züttel, A.; Jensen, C. M. *Chemical Reviews* **2007**, *107*, 4111–4132.

(33) Luo, W. F.; Wang, J.; Stewart, K.; Clift, M.; Gross, K. *Journal of Alloys and Compounds* **2007**, *447-448*, 336–341.

(34) Luo, W. F.; Stewart, K. *Journal of Alloys and Compounds* **2007**, *440*, 357-361.

(35) Orimo, S.; Nakamori, Y.; Kitahara, G.; Miwa, K.; Ohba, N.; Noritake, T.; Towata, S. *Applied Physics A* **2004**, *79*, 1765-1767.

(36) Schlesinger, H. I.; Brown, H. C. *Journal of the American Chemical Society* **1940**, *62*, 3429–3434.

(37) Fedneva, E. M.; Alpatova, V. L.; Mikheeva, V. I. *Russian Journal of Inorganic Chemistry* **1964**, *9*, 826–827.

(38) Stasinevich, D. S.; Egorenko, G. A. *Russian Journal of Inorganic Chemistry* **1968**, *13*, 341–343.

(39) Züttel, A.; Rentsch, S.; Fischer, P.; Wenger, P.; Sudan, P.; Mauron, P.; Emmenegger, C. *Journal of Alloys and Compounds* **2003**, *356-357*, 515–520.

(40) Orimo, S.; Nakamori, Y.; Kitahara, G.; Miwa, K.; Ohba, N.; Towata, S.; Züttel, a. *Journal of Alloys and Compounds* **2005**, *404-406*, 427–430.

(41) Nakamori, Y.; Miwa, K.; Ninomiya, A.; Li, H.; Ohba, N.; Towata, S.; Züttel, A.; Orimo, S. *Physical Review B* **2006**, *74*, 1–9.

(42) Rönnebro, E.; Majzoub, E. H. *The Journal of Physical Chemistry. B* **2007**, *111*, 12045–12047.

(43) Kim, Y.; Reed, D.; Lee, Y.-S.; Lee, J. Y.; Shim, J.-H.; Book, D.; Cho, Y. W. *The Journal of Physical Chemistry C* **2009**, *113*, 5865–5871.

(44) Li, H.-W.; Kikuchi, K.; Sato, T.; Nakamori, Y.; Ohba, N.; Aoki, M.; Miwa, K.; Towata, S.; Orimo, S.-I. *Materials Transactions* **2008**, *49*, 2224–2228.

(45) Davis, W. D.; Mason, L. S.; G., S. *Journal of the American Chemical Society* **1949**, *71*, 2775–2781.

(46) Li, H.-W.; Kikuchi, K.; Nakamori, Y.; Ohba, N.; Miwa, K.; Towata, S.; Orimo, S.-I. *Acta Materialia* **2008**, *56*, 1342–1347.

(47) Matsunaga, T.; Buchter, F.; Mauron, P.; Bielman, M.; Nakamori, Y.; Orimo, S.; Ohba, N.; Miwa, K.; Towata, S.; Züttel, A. *Journal of Alloys and Compounds* **2008**, *459*, 583–588.

(48) Matsunaga, T.; Buchter, F.; Miwa, K.; Towata, S.; Orimo, S.; Züttel, A. *Renewable Energy* **2008**, *33*, 193–196.

(49) Soloveichik, G.; Gao, Y.; Rijssenbeek, J.; Andrus, M.; Kniajanski, S.; Bowmanjr, R.; Hwang, S.; Zhao, J. *International Journal of Hydrogen Energy* **2009**, *34*, 916–928.

(50) Muetterties, E. L.; Knoth, W. H. *Polyhedral Boranes*; M. Dekker: New York, 1968; p. 197.

(51) Muetterties, E. L.; Balthis, J. H.; Chia, Y. T.; Knoth, W. H.; Miller, H. C. *Inorganic Chemistry* **1964**, *3*, 444–451.

(52) Ohba, N.; Miwa, K.; Aoki, M.; Noritake, T.; Towata, S.; Züttel, A. *Physical Review B* **2006**, *74*, 075110.

(53) Li, H.-W.; Miwa, K.; Ohba, N.; Fujita, T.; Sato, T.; Yan, Y.; Towata, S.; Chen, M. W.; Orimo, S. *Nanotechnology* **2009**, *20*, 204013.

(54) Ozolins, V.; Majzoub, E. H.; Wolverton, C. *Journal of the American Chemical Society* **2009**, *131*, 230–7.

(55) Hwang, S.; Bowman, R. C.; Reiter, J. J. W.; Rijssenbeek, J.; Soloveichik, G. L.; Zhao, J.; Kabbour, H.; Ahn, C. C. *Journal of Physical Chemistry C Letters* **2008**, 3164–3169.

(56) Jeon, E.; Cho, Y. *Journal of Alloys and Compounds* **2006**, *422*, 273–275.

(57) - ttel, A. *Journal of Physical Chemistry C* **2011**, *115*, 17220–17226.

(58) Severa, G.; Rönnebro, E.; Jensen, C. M. *Chemical Communications* **2010**, *46*, 421–423.

(59) Vajo, J. J.; Skeith, S. L.; Mertens, F. *Journal of Physical Chemistry B* **2005**, *109*, 3719–3722.

(60) Vajo, J. J.; Salguero, T. T.; Gross, A. F.; Skeith, S. L.; Olson, G. L. *Journal of Alloys and Compounds* **2007**, *446-447*, 409–414.

(61) Alapati, S. V.; Johnson, J. K.; Sholl, D. S. *Journal of Physical Chemistry C* **2008**, *112*, 5258–5262.

(62) Alapati, S. V; Karl Johnson, J.; Sholl, D. S. *Physical Chemistry Chemical Physics* **2007**, *9*, 1438–52.

(63) Alapati, S. V; Johnson, J. K.; Sholl, D. S. *Journal of Physical Chemistry. B* **2006**, *110*, 8769–8776.

(64) Li, H.-W.; Orimo, S.; Nakamori, Y.; Miwa, K.; Ohba, N.; Towata, S.; Züttel, A. *Journal of Alloys and Compounds* **2007**, *446-447*, 315–318.

(65) Ravnsbaek, D.; Filinchuk, Y.; Cerenius, Y.; Jakobsen, H. J.; Besenbacher, F.; Skibsted, J.; Jensen, T. R. *Angewandte Chemie* **2009**, *48*, 6659–63.

(66) Jensen, C. M.; Sulic, M.; Kuba, M.; Brown, C.; Langley, W.; Dalton, T.; Culnane, L.; Severa, G.; Eliseo, J.; Ayabe, R.; Zhang, S. In *Proceedings of the U.S. DOE Hydrogen and Fuel Cells Annual Program/ Lab R&D Review*; Arlington, VA, 2007.

(67) Cerny, R.; Severa, G.; Ravnsbæk, D. B.; Filinchuk, Y.; Anna, V. D.; Hagemann, H.; Jensen, C. M.; Jensen, T. R. *Journal of Physical Chemistry C* **2010**, *114*, 1357–1364.

(68) Hagemann, H.; Longhini, M.; Kaminski, J. W.; Wesolowski, T. A.; Cerný, R.; Penin, N.; Sørby, M. H.; Hauback, B. C.; Severa, G.; Jensen, C. M. *Journal of Physical Chemistry A* **2008**, *112*, 7551–7555.

(69) Cerny, R.; Ravnsbæk, D. B.; Severa, G.; Filinchuk, Y.; Anna, V. D.; Hagemann, H.; Skibsted, J.; Jensen, C. M.; Jensen, T. R. *Journal of Physical Chemistry C* **2010**, *114*, 19540–19549.

(70) Severa, G.; Hagemann, H.; Kaminski, J. W.; Wesolowski, T. A.; Jensen, C. M. *Journal of Physical Chemistry C* **2010**, *114*, 15516–15521.

(71) Kim, C.; Hwang, S.; Bowman, R. C.; Reiter, J. W.; Zan, J. A.; Kulleck, J. G.; Kabbour, H.; Majzoub, E. H.; Ozolins, V. *Journal of Physical Chemistry C* **2009**, *113*, 9956–9968.

(72) Chłopek, K.; Frommen, C.; Léon, A.; Zabara, O.; Fichtner, M. *Journal of Materials Chemistry* **2007**, *17*, 3496-3503.

(73) Her, J. H.; Stephens, P. W.; Gao, Y.; Soloveichik, G. L.; Rijssenbeek, J.; Andrus, M.; Zhao, J. C. *Acta crystallographica. Section B, Structural science* **2007**, *63*, 561–568.

(74) Filinchuk, Y.; Richter, B.; Jensen, T. R.; Dmitriev, V.; Chernyshov, D.; Hagemann, H. *Angewandte Chemie* **2011**, *50*, 11162–11166.

(75) Huang, Z.; Eagles, M.; Porter, S.; Sorte, E. G.; Billet, B.; Corey, R. L.; Conradi, M. S.; Zhao, J.-C. *Dalton Transactions* **2013**, *42*, 701–708.

(76) Gurvich, L. V.; Veyts, I. V.; Alcock, C. B.; Iorish, V. S. *Thermodynamic Properties of Individual Substances, 4th ed.*; Vol. 2.; Hemisphere: New York, NY, 1991.

(77) Cottrell, T. L. *The Strengths of Chemical Bonds*; 2nd ed.; Butterworths Scientific Publications: London, 1958.

(78) Humphries, T. pers.comm.

(79) Yang, J.; Fu, H.; Song, P.; Zheng, J.; Li, X. *International Journal of Hydrogen Energy* **2012**, *37*, 6776–6783.

(80) Chong, M.; Karkamkar, A.; Autrey, T.; Orimo, S.; Jalisatgi, S.; Jensen, C. M. *Chemical Communications* **2011**, *47*, 1330–1332.

(81) Hoy, J. M. *Syntheses of Aluminum Amidotrihydroborate Compounds and Ammonia Triborane as Potential Hydrogen Storage Materials*, Ohio State University, 2010.

(82) Hill, T. G.; Godfroid, R. A.; White III, J. P.; Shore, S. G. *Inorganic Chemistry* **1991**, *30*, 2952–2954.

(83) Kim, D. Y.; Yang, Y.; Abelson, J. R.; Girolami, G. S. *Inorganic Chemistry* **2007**, *46*, 9060–9066.

(84) Olson, J. K.; Boldyrev, A. I. *Computational and Theoretical Chemistry* **2011**, *967*, 1–4.

(85) Newhouse, R. J.; Stavila, V.; Hwang, S.-J.; Klebanoff, L. E.; Zhang, J. Z. *Journal of Physical Chemistry C* **2010**, *114*, 5224–5232.

(86) Zeng, K.; Klassen, T.; Oelerich, W.; Bormann, R. *International Journal of Hydrogen Energy* **1999**, *24*, 989–1004.

(87) Au, M.; Jurgensen, A. R.; Spencer, W. A.; Anton, D. L.; Pinkerton, F. E.; Hwang, S.-J.; Kim, C.; Bowman, R. C. *Journal of Physical Chemistry C* **2008**, *112*, 18661–18671.

(88) Gross, A. F.; Vajo, J. J.; Atta, S. L. Van; Olson, G. L. *Journal of Physical Chemistry C* **2008**, *112*, 5651–5657.

(89) Fang, Z. Z.; Wang, P.; Rufford, T. E.; Kang, X. D.; Lu, G. Q.; Cheng, H. M. *Acta Materialia* **2008**, *56*, 6257–6263.

(90) Cahen, S.; Eymery, J.-B.; Janot, R.; Tarascon, J.-M. *Journal of Power Sources* **2009**, *189*, 902–908.

(91) Hoekstra, H. R.; Katz, J. J. *Journal of the American Chemical Society* **1949**, *71*, 2488–2492.

(92) Marks, T. J.; Kolb, J. R. *Chemical Reviews* **1977**, *77*, 263–293.

(93) Schrauzer, G. N. *Naturwissenschaften* **1955**, *42*, 438.

(94) Nickels, E. A.; Jones, M. O.; David, W. I. F.; Johnson, S. R.; Lowton, R. L.; Sommariva, M.; Edwards, P. P. *Angewandte Chemie* **2008**, *47*, 2817–2819.

(95) Eliseo, J. R. *Synthesis and Characterization of Novel Anionic Transition Metal Borohydrides*, University of Hawaii, 2007, p. 92.

(96) Schouwink, P.; Anna, V. D.; Ley, M. B.; Lawson, M.; Richter, B.; Jensen, T. R.; Hagemann, H.; Radovan, C. *Journal of Physical Chemistry C* **2012**, *116*, 10829-10840.

(97) Tanaka, T.; Okada, S.; Gurin, V. N. *Journal of Alloys and Compounds* **1998**, *267*, 211–214.

(98) Orimo, S.-I.; Nakamori, Y.; Ohba, N.; Miwa, K.; Aoki, M.; Towata, S.; Zuttel, A. *Applied Physics Letters* **2006**, *89*, 021920.

(99) Züttel, A.; Borgschulte, A.; Orimo, S.-I. *Scripta Materialia* **2007**, *56*, 823–828.

(100) Anderson, W. E.; Barker, E. F. *Journal of Chemical Physics* **1950**, *18*, 698–705.

(101) Söderlund, M.; Mäki-Arvela, P.; Eränen, K.; Salmi, T.; Rahkola, R.; Murzin, D. Y. *Catalysis Letters* **2005**, *105*, 191–202.

(102) Callini, E.; Borgschulte, A.; Ramirez-Cuesta, A. J.; Züttel, A. *Dalton Transactions* **2013**, *42*, 719–725.

(103) Zhang, S.; Gross, A. F.; Van Atta, S. L.; Lopez, M.; Liu, P.; Ahn, C. C.; Vajo, J. J.; Jensen, C. M. *Nanotechnology* **2009**, *20*, 204027.